

add #23677

U.S. DEPARTMENT OF COMMERCE
National Technical Information Service

DTIC
S ELECTED D
NOV 24 1995
F

N77-23211

ANALYSIS OF SHEAR TEST METHOD FOR COMPOSITE
LAMINATES

HENRY W. BERGNER, ET AL

VIRGINIA POLYTECHNIC INSTITUTE AND STATE
UNIVERSITY
BLACKSBURG, VIRGINIA

APRIL 1977

DISTRIBUTION STATEMENT A
Approved for public release
Distribution Unlimited

19951121 002

DTIC QUALITY INSPECTED 8

PLASTIC 27433

AN77-23211

College of Engineering
Virginia Polytechnic Institute and State University
Blacksburg, VA. 24061

VPI-E-77-14

April, 1977

Analysis of Shear Test Method
for Composite Laminates

Henry W. Bergner, Jr.¹
John G. Davis, Jr.²
Carl T. Herakovich³

Accession For	
NTIS CRA&I	<input checked="" type="checkbox"/>
DTIC TAB	<input type="checkbox"/>
Unannounced	<input type="checkbox"/>
Justification	
By	
Distribution/	
Availability Codes	
Dist	Avail and/or Special
A-1	

Department of Engineering Science and Mechanics

Interim Report Number 6
NASA-VPI&SU Cooperative Program in Composite
Materials Research and Education

NASA Grant NGR 47-004-129

Prepared for: Materials Application Branch
National Aeronautics & Space Administration
Langley Research Center
Hampton, VA. 23665

- 1 Graduate Student
- 2 Materials Engineer - NASA-Langley
- 3 Professor

Approved for public release, distribution unlimited.

BIBLIOGRAPHIC DATA SHEET		1. Report No. VPI-E-77-14	2.	3. Recipient's Accession No.
4. Title and Subtitle ANALYSIS OF SHEAR TEST METHOD FOR COMPOSITE LAMINATES			5. Report Date May, 1977	6.
7. Author(s) Henry W. Bergner, Jr., John G. Davis, Jr. Carl T. Herakovich			8. Performing Organization Rept. No. VPI-E-77-14	
9. Performing Organization Name and Address Virginia Polytechnic Institute and State University Engineering Science and Mechanics Blacksburg, Virginia 24061			10. Project/Task/Work Unit No.	
			11. Contract/Grant No. NASA NGR-47-004-129	
12. Sponsoring Organization Name and Address National Aeronautics & Space Administration Langley Research Center Hampton, Virginia 23665			13. Type of Report & Period Covered	
			14.	
15. Supplementary Notes				
16. Abstracts see page ii				
17. Key Words and Document Analysis. 17a. Descriptors Composites, In-plane Shear, Finite Elements, Rail Shear, Iosipescu, Cross Beam, Slotted Coupon, Elastic Fixtures, Thermal Stresses, Graphite-epoxy, Graphite-polyimide				
17b. Identifiers/Open-Ended Terms				
17c. COSATI Field/Group				
18. Availability Statement Distribution unlimited			19. Security Class (This Report) UNCLASSIFIED	21. No. of Pages
			20. Security Class (This Page) UNCLASSIFIED	22. Price

FOREWORD

This report documents a portion of the work accomplished under NASA Grant NGR-47-004-129 during the period September, 1975 through April, 1977. Mr. Bergner was in residence at NASA-Langley during the period September 1976 - February, 1977.

The authors are grateful to Mr. Donald J. Baker of the U. S. Army Air Mobility Research and Development Laboratory at NASA's Langley Research Center, and Mr. Edward A. Humphreys and Ms. Frances Carter of Virginia Polytechnic Institute and State University for their contributions to this work.

ANALYSIS OF SHEAR TEST METHODS FOR COMPOSITE LAMINATES

ABSTRACT

An elastic plane stress finite element analysis of the stress distributions in four flat test specimens for in-plane shear response of composite materials subjected to mechanical or thermal loads is presented. The shear test specimens investigated include: slotted coupon, cross beam, Iosipescu, and rail shear. Results are presented in the form of normalized stress contour plots for all three in-plane stress components.

The slotted specimen is studied for three graphite-epoxy laminates ($[0]$, $[90]$, $[\pm 45]_S$); the cross beam is studied for two graphite-epoxy laminates ($[0/90]_S$, $[\pm 45]_S$); the Iosipescu and rail shear specimens are studied with several materials (steel, graphite-epoxy, and graphite-polyimide) and several laminates ($[0]$, $[90]$, $[0/90]_S$, $[\pm 45]_S$, $[0/90/\pm 45]_S$) with rigid and elastic fixtures loaded mechanically or thermally. Geometric alterations are also investigated.

The study shows that the cross beam, Iosipescu, and rail shear specimens have stress distributions which are more than adequate for determining linear shear behavior of composite materials. Laminate properties, core effects, and fixture configurations are among the factors which were found to influence the stress distributions.

TABLE OF CONTENTS

	<u>Page</u>
FOREWORD	ii
LIST OF SYMBOLS	vi
LIST OF TABLES	viii
LIST OF FIGURES	ix
1. INTRODUCTION	1
2. LITERATURE REVIEW	3
2.1 The Slotted Shear Specimen	3
2.2 The Cross Beam Shear Specimen	3
2.3 The Iosipescu Shear Specimen	5
2.4 The Rail Shear Specimen	7
2.5 The Picture Frame Shear Specimen	9
2.6 The $[\pm 45]_S$ Tension Coupon	9
2.7 The Off-axis Unidirectional Tension Coupon	10
2.8 The Torsion Tube	11
2.9 Other Shear Test Methods	12
2.10 Summary	12
3. THEORETICAL CONSIDERATIONS	13
3.1 Lamination Theory	13
3.2 The Finite Element Formulation	18
4. THE SLOTTED SHEAR SPECIMEN	23
4.1 General	23
4.2 The $[0]$ Laminate	25
4.3 The $[90]$ and $[\pm 45]_S$ Laminates	25
4.4 Summary	29
5. THE CROSS BEAM SHEAR SPECIMEN	30
5.1 General	30
5.2 The $[\pm 45]_S$ Laminate	32
5.3 The $[0/90]_S$ Laminate	36
5.4 Summary	39

	<u>Page</u>
6. IOSIPESCU SPECIMEN	41
6.1 General	41
6.2 Rigid Fixture Results	41
6.2.1 General	41
6.2.2 Isotropic and Quasi-isotropic Materials	43
6.2.3 The [0] Laminate	43
6.2.4 The [90] _s Laminate	46
6.2.5 The [0/90] _s Laminate	46
6.2.6 The [±45] _s Laminate	46
6.3 Elastic Fixture Results	52
6.3.1 Mechanical Loading	52
6.3.1.1 Isotropic Material	54
6.3.1.2 The [0] Laminate	54
6.3.2 Thermal Loading.	56
6.4 Other Results	59
6.4.1 Doubler Effects	59
6.4.2 Aspect Ratio Effects	59
6.4.3 Rounded Notch Effects	62
6.5 Summary	66
7. THE RAIL SHEAR SPECIMEN	67
7.1 General	67
7.2 Rigid Rail Solutions	67
7.2.1 Fourier Series Representation	67
7.2.2 Comparison of Fourier Series and Finite Element Results	69
7.3 Elastic Rails	72
7.3.1 Effects of Offset Loading and Tapered Rails	72
7.3.2 Thermal Load Effects	82
7.3.3 Other Mechanically Loaded Laminates	85
7.3.3.1 The [90] Laminate	85
7.3.3.2 The [±45] _s Laminate	85
7.4 Summary	88
8. CONCLUSIONS	89
BIBLIOGRAPHY	91
APPENDICES	
A. COMPUTER PROGRAMS	94
A.1 Introduction	95

	<u>Page</u>
A.2 The Finite Element Program	96
A.2.1 General	96
A.2.2 Input Description	97
A.3 The Mesh Generation Program	100
A.3.1 General	100
A.3.2 Generation Initialization and Termination Data Input	102
A.3.3 Element Generation Input	105
A.3.4 Reference Frame Alteration Data Sets	113
A.3.5 Node Repositioning Data Sets	116
A.4 The Plotting Program	118
A.4.1 General	118
A.4.2 Input Description	118
B. PROGRAM LISTINGS	127
B.1 The Finite Element Program	127
B.2 The Mesh Generation Program	127
B.3 The Plotting Program	127
C. MATERIAL PROPERTIES	128

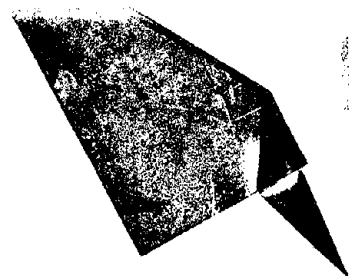
LIST OF SYMBOLS

[a]	Orthotropic elastic constant matrix (3x3)
[A]	Laminate extensional stiffness matrix (3x3)
[B]	Elemental strain-displacement matrix (6x3)
E_i	Moduli of elasticity
G_i	Moduli of rigidity
h	Lamina thickness
H	Laminate half thickness
[k]	Elemental stiffness matrix (6x6 or 8x8)
[K]	Finite element global stiffness matrix (variable size)
n	Total number of plies or lamina in a laminate
{N}	Inplane forces per unit length in laminate X-Y coordinates (1x3)
{Q}, {Q ^T }	Elemental mechanical and thermal load vectors, respectively (1x6 or 1x8)
[Q], [Q̄]	Lamina stiffness matrix in natural 1-2 coordinates and laminate X-Y coordinates, respectively (3x3)
{R}	Global load vector for finite element model (variable size)
[T]	Tensor transformation matrix (3x3)
u, v	Displacements in X and Y directions, respectively
{u}	Nodal displacement vector for an element (1x6 or 1x8)

U, W, Π	Strain energy, potential energy of external loads, and total potential energy, respectively
X, Y, Z	Global or laminate $X, Y,$ and Z coordinates, respectively
$\{\alpha\}, \{\bar{\alpha}\}$	Lamina and average laminate coefficient of thermal expansion matrix (1x3), respectively
B_i	Generalized coordinate coefficients ($i=1,2,3,\dots,6$)
δ	Applied displacement
ΔT	Uniform laminate temperature change
$\{\epsilon\}, \{\epsilon^t\}, \{\epsilon^o\}$	Total, thermal, and mechanical laminate midplane strains, respectively
γ	Engineering shear strain
$\bar{\sigma}, \bar{\tau}$	Average laminate normal and shear stress, respectively
$\{\sigma\}, \{\bar{\sigma}\}$	Lamina and average laminate stresses in natural 1-2 and laminate X - Y coordinates, respectively
θ	Angle of rotation from laminate coordinate system to lamina coordinate system
Subscripts	
1, 2	Natural lamina coordinate system
k	k^{th} ply of lamina
x, y	Laminate coordinate system

LIST OF TABLES

<u>Table</u>	<u>Page</u>
1. Normalized Stresses for Graphite-polyimide and Steel Iosipescu Specimen with Rigid Fixtures	51
2. Effects of Doublers and Aspect Ratios for the Iosipescu Specimen	60
3. Graphite-epoxy and Graphite-polyimide Normalized Stresses for Iosipescu Specimen with Rigid Fixtures (R = 2.5)	61
4. Normalized Stresses for V-notch and Rounded Notch Iosipescu Specimens with Rigid Fixtures	65
5. Normalized Stresses for Graphite-polyimide Rail Shear Specimens with Elastic Rails	80



LIST OF FIGURES

<u>Figure</u>	<u>Page</u>
1. Slotted Shear Specimens	4
2. Various Shear Specimens	6
3. Rail Shear Specimen Geometries	8
4. Lamina and Laminate Coordinates	14
5. Finite Element Representation of Slotted Shear Specimen .	24
6. Normalized Stress Contours for [0] Slotted Shear Specimen, $S = 0.6 W$, $D = 0.5 W$, $T = 0.0625 W$	26
7. Normalized Stress Contours for [90] Slotted Shear Specimen, $S = 0.6 W$, $D = 0.5 W$, $T = 0.0625 W$	27
8. Normalized Stress Contours for $[\pm 45]_S$ Slotted Shear Specimen, $S = 0.6 W$, $D = 0.5 W$, $T = 0.0625 W$	28
9. Finite Element Representation of Cross Beam Shear Specimen	31
10. Normalized σ'_x Contours for $[\pm 45]_S$ Cross Beam	33
11. Normalized σ'_y Contours for $[\pm 45]_S$ Cross Beam	34
12. Normalized τ'_{xy} Contours for $[\pm 45]_S$ Cross Beam	35
13. Normalized σ'_x and σ'_y Contours for $[0/90]_S$ Cross Beam . .	37
14. Normalized τ'_{xy} Contours for $[0/90]_S$ Cross Beam	38
15. Finite Element Model for Iosipescu Specimen with Rigid Fixtures	42
16. Normalized Stress Contours for Iosipescu Specimen with Isotropic Material and Rigid Fixtures	44
17. Normalized Stress Contours for $[0/90/\pm 45]_S$ Graphite-polyimide Iosipescu Specimen with Rigid Fixtures	45
18. Normalized Stress Contours for [0] Graphite-polyimide Iosipescu Specimen with Rigid Fixtures	47

<u>Figure</u>	<u>Page</u>
19. Normalized Stress Contours for [90] Graphite-polyimide Iosipescu Specimen with Rigid Fixtures	48
20. Normalized Stress Contours for [0/90] _s Graphite-polyimide Iosipescu Specimen with Rigid Fixtures	49
21. Normalized Stress Contours for [±45] _s Graphite-polyimide Iosipescu Specimen with Rigid Fixtures	50
22. Finite Element Model for Iosipescu Specimen with Elastic Fixtures	53
23. Normalized Stress Contours for Iosipescu Specimen with Isotropic Material and Elastic Fixtures	55
24. Normalized Stress Contours for [0] Graphite-polyimide Iosipescu Specimen with Elastic Fixtures	57
25. Normalized Stress Contours for Thermally Loaded [0] Graphite-polyimide Iosipescu Specimen with Elastic Fixtures	58
26. Rounded Notch Effects for the [0] Iosipescu Specimen Along $Y = 0$	63
27. Rounded Notch Effects for the [90] Iosipescu Specimen Along $Y = 0$	64
28. Comparison of Rigid Rail Solutions for Thorne1 50 Graphite-epoxy at $Y = b/2$	70
29. Finite Element Models for Rail Shear Specimen with Rigid Rails	71
30. Axially Loaded Rail Shear Specimen	73
31. Tapered Rail Shear Specimen	74
32. Offset Loaded Rail Shear Specimen	75
33. Normalized Stress Contours for [0] Graphite-polyimide Rail Shear Specimen with Nontapered Elastic Rails	77
34. Normalized Stress Contours for [0] Graphite-polyimide Rail Shear Specimen with Tapered Elastic Rails	78
35. Normalized Stress Contours for [0] Graphite-polyimide Rail Shear Specimen with Offset Loaded Elastic Rails	79

<u>Figure</u>	<u>Page</u>
36. Normalized Stress Contours for Thermally Loaded [0] Graphite-polyimide Rail Shear Specimen with Non-tapered Rails	83
37. Normalized Stress Contours for Thermally Loaded [0] Graphite-polyimide Rail Shear Specimen with Tapered Rails	84
38. Normalized Stress Contours for [90] Graphite-polyimide Rail Shear Specimen with Tapered Rails	86
39. Normalized Stress Contours for [± 45] _s Graphite-polyimide Rail Shear Specimen with Tapered Rails	87
A.1 Element Groups	108

2. LITERATURE REVIEW

2.1 The Slotted Shear Specimen

The slotted shear specimen has been used to measure shear properties of both metals and composites. Fenn and Clapper [1] used the geometry of Fig. 1a for their studies on metals. Breindel et al [2] suggested a standardized metal specimen thickness, width, and length of shear path (Fig. 1a). Iosipescu's photoelastic study [3] of this specimen indicated that the state of stress for a slotted specimen is generally unacceptable for quantitative shear behavior due to the lack of pure uniform shear stress in the test area.

Elkin et al [4] used the slotted specimen in Fig. 1b for shear tests on three unidirectional graphite-epoxies. They reported low strength values which were attributed to the stress concentrations at the edges of the holes. Their finite element analysis indicated a maximum stress concentration of 1.57 at the edge of the holes. Other variations of the slotted shear specimen shown in Figs. 1c and 1d have been used for composite materials [5].

2.2 The Cross Beam Shear Specimen

The cross beam shear specimen has been used for determining linear and nonlinear shear stress-strain response as well as ultimate shear strength values for graphite-epoxy and boron-epoxy laminates. As shown in Fig. 2a, the cross beam shear specimen is loaded in positive and negative bending to produce a biaxial state of tension and compression over the test area at the center of the specimen. Stresses on 45°

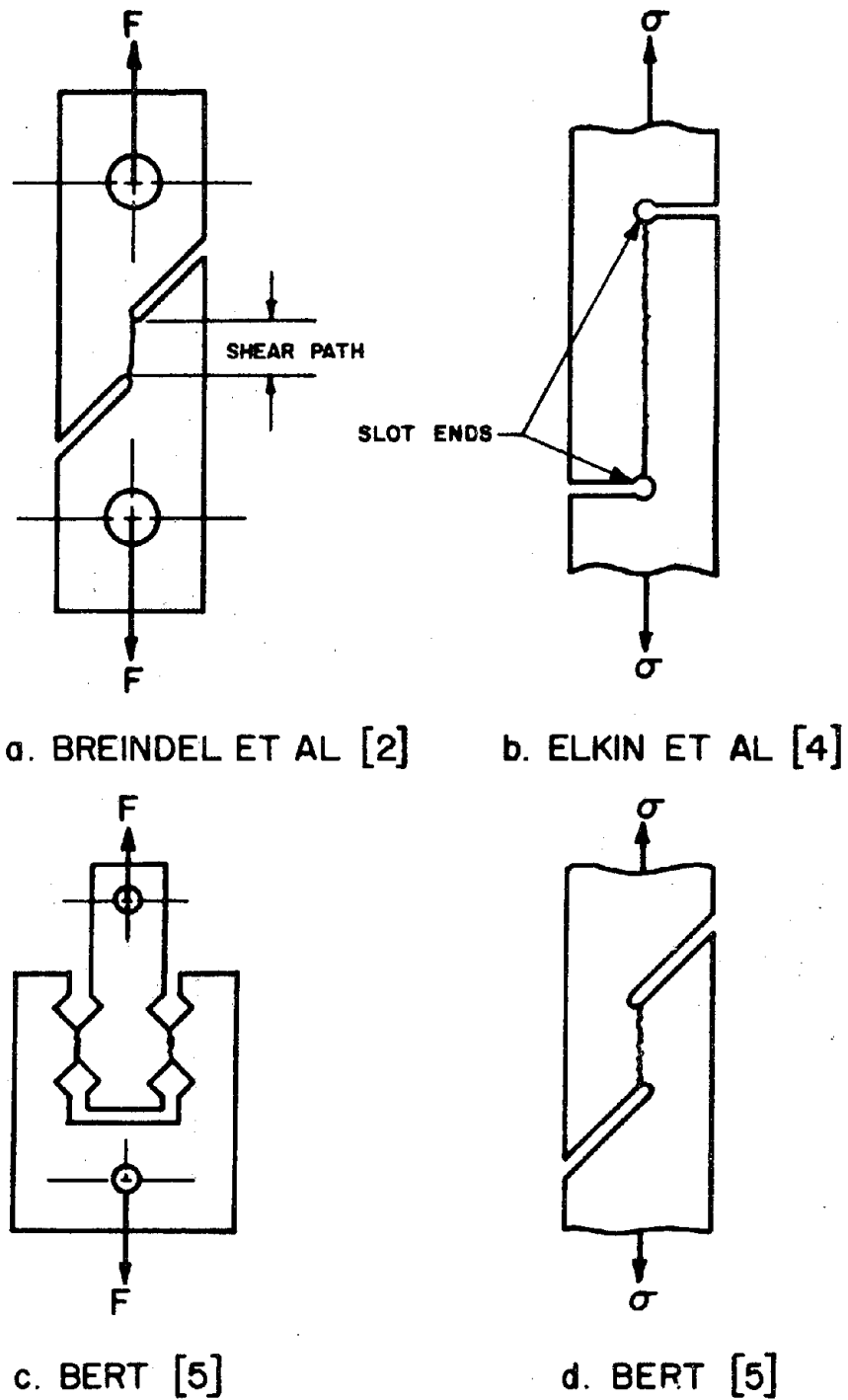


FIGURE 1. SLOTTED SHEAR SPECIMENS

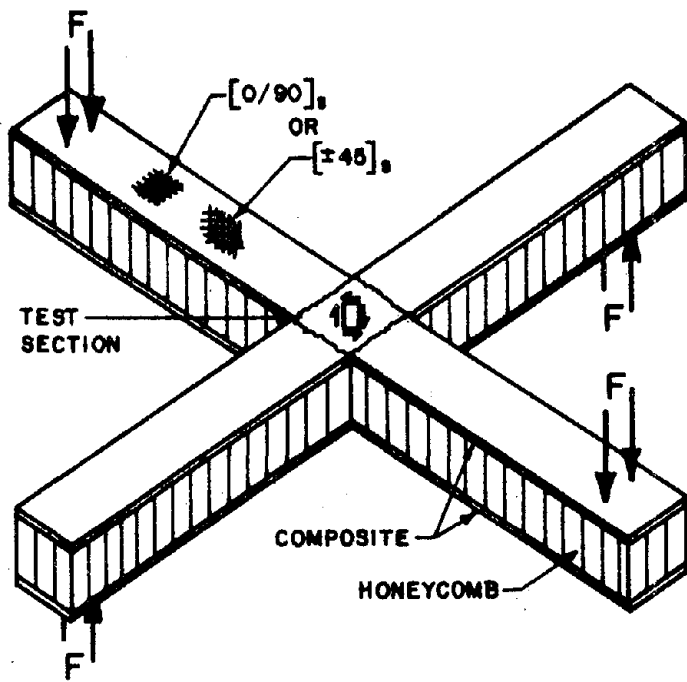
planes are presumed to be pure, uniform shear over the test section. Laminates commonly used with the cross beam are $[0/90]_s$ and $[\pm 45]_s$.

Petit [6] compared experimental results of this test method to those of the $[\pm 45]_s$ tension coupon and found good agreement for both linear and nonlinear shear stress-strain response of unidirectional laminates. Waddoups [7] compared experimental ultimate shear strength values obtained by this method to those of the short beam shear test and reported that the cross beam specimen produced considerably higher ultimate shear strength values than those of the short beam shear test.

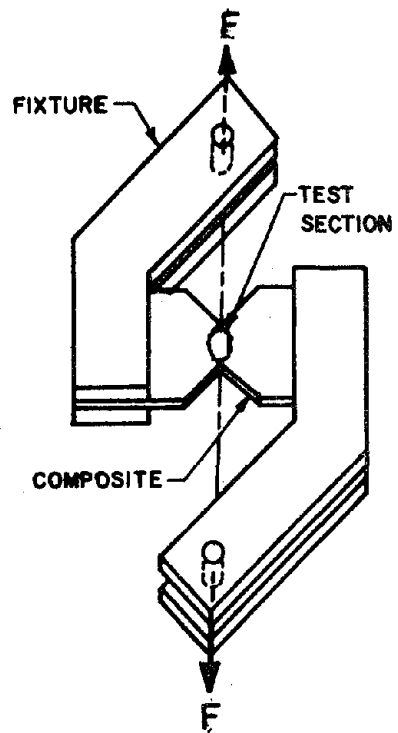
2.3 The Iosipescu Shear Specimen

As mentioned previously, an extensive photoelastic study was conducted by Iosipescu [3] on some of the slotted shear specimens that had been used for shear testing. The results of this study generally indicated a need for a more precise shear test method. A new specimen (the Iosipescu specimen) was consequently developed as a test method for shear strength of metals.

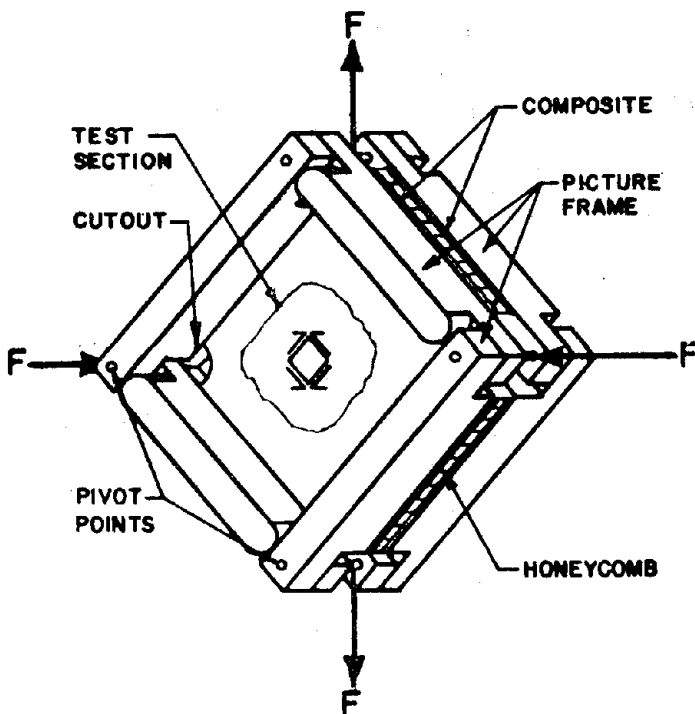
Although the Iosipescu shear specimen has not been used extensively for shear testing of composite materials, the encouraging results from metals indicate that this specimen should be analyzed for composite materials to evaluate any potential for use as a test method. The effects of several modifications to the original Iosipescu specimen are studied for use with composite materials. While metal Iosipescu specimens are normally notched in two directions, the specimen in the present study is notched in only one direction (Fig. 2b) so that the laminate



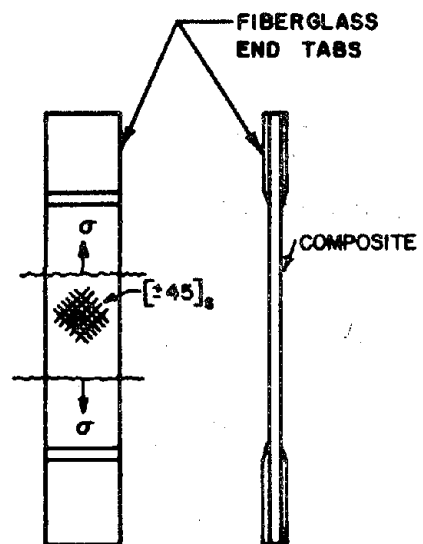
a. CROSS BEAM SHEAR



b. IOSIPESCU SHEAR



c. PICTURE FRAME



d. $[\pm 45]_s$ TENSION COUPON

FIGURE 2. VARIOUS SHEAR SPECIMENS

stiffness in the test section is uniform and strain measurements may be taken at the center. The specimen is loaded to produce a shear stress acting between the notch ends with zero bending moment and zero normal stress. The reduced specimen area between the notch ends ensures failure in this region.

2.4 The Rail Shear Specimen

The rail shear specimen has been used quite often for composites with various laminate configurations and at elevated temperatures as well as room temperature. As shown in (Fig. 3) and in studies by Whitney et al [8], Rutherford et al [9], and The Advanced Composites Design Guide [10], this test method consists of bolting or bonding stiff rails to a composite plate to form a long, narrow test area between the rails. The load is introduced at the ends of the rails to displace the rails essentially parallel to one another.

A Fourier series plate solution and parametric study of this specimen was conducted by Whitney et al [8]. The study indicated that specimen dimensions can be standardized to produce an acceptable area of shear stress for most laminates. The only exceptions are laminates with a high Poisson's ratio (≈ 1.0). Experimental results presented in this study showed excellent agreement with lamination theory for in-plane shear modulus. A double rail shear test procedure was investigated by Sims [11] who found good agreement with both the $[\pm 45]_S$ tension coupon and the torsion tube for linear and nonlinear shear stress-strain response. Bert [5] pointed out that the rail shear specimen may be readily sized

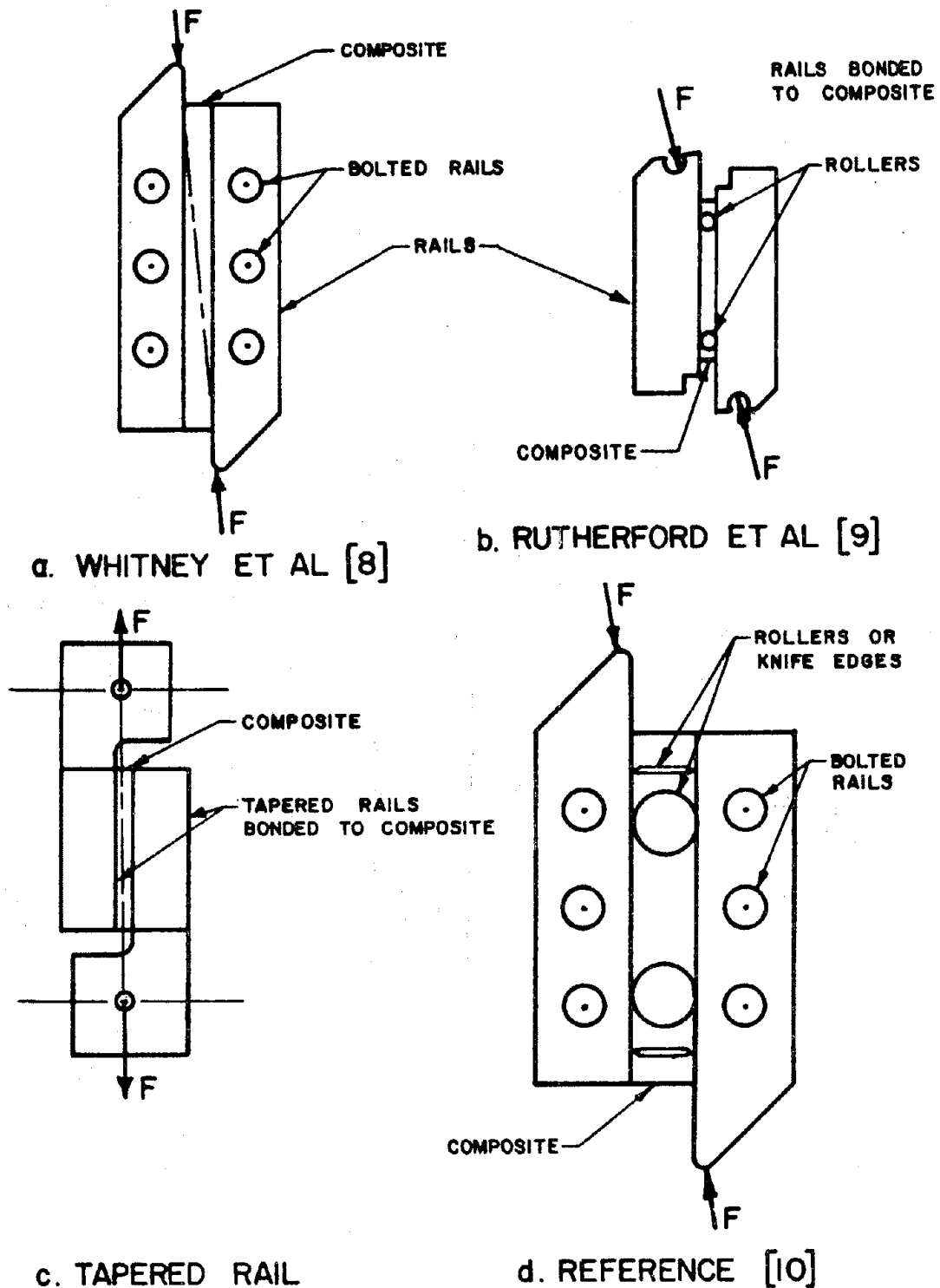


FIGURE 3. RAIL SHEAR SPECIMEN GEOMETRIES

to avoid buckling.

2.5 The Picture Frame Shear Specimen

The picture frame specimen shown in Fig. 2c consists of two thin square composite laminates bonded to a honeycomb core material for stability. A rigid four bar linkage frame is then bolted over the sandwiched composite for load introduction. In order to reduce high corner stresses these areas usually are cutout and have doublers bonded on near the resulting free edge. The load is introduced by a combination of tension and/or compression forces in pairs on opposite corners. Thus, the specimen is subjected to shear loading along planes at 45° to the diagonals.

A state of pure shear was not observed in a photoelastic study of this specimen by Bryan [12]. Dastin et al [13], Hyer and Douglas [14], and Hadcock and Whiteside [15] tested boron-epoxy and borsic-aluminum picture frame specimens with cutouts and/or doublers at the corners. Hadcock and Whiteside [15] and Douglas et al [16] reported that the corner stress concentrations nevertheless remained significantly high in both experiments and in the finite element analysis that included frame and nonlinear effects. However, Dastin et al [13] reported that reliable initial shear modulus and ultimate strength values could be obtained from the picture frame specimen for $[0/90]_s$ laminates.

2.6 The $[\pm 45]_s$ Tension Coupon

The $[\pm 45]_s$ tension coupon is a simple test for obtaining linear and nonlinear shear stress-strain response in the natural lamina coordinates.

As shown in figure 2d, the specimen is simply a $[\pm 45]_s$ tension coupon, usually with tabs. During loading, incremental values of axial force and axial and transverse strain are recorded. Various transformation laws as employed by Petit [6], Adams and Thomas [17], Rosen [18], and Hahn [19] may be used to obtain the piecewise linear modulus of rigidity, G_{12} , in the natural lamina coordinates.

Petit compared test results of the $[\pm 45]_s$ tension coupon to those of the cross beam and found close agreement with the exception of the highly nonlinear portion of the shear stress-strain curve. He also pointed out that the laminate Poisson's ratio must be exactly 1.0 in order to have a state of pure shear in the $[\pm 45]_s$ tensile coupon. The measured value of Poisson's ratio for his tests was 0.85. The study also reported that specimen delamination may take place due to edge effects at high strain values.

2.7 The Off-axis Unidirectional Tension Coupon

The off-axis unidirectional tension coupon is a simple specimen similar in geometry to the $[\pm 45]_s$ tension coupon shown in figure 2d. The laminate is unidirectional with fibers oriented at an angle usually between 10 and 75 degrees to the axis of loading. This specimen has been used to measure linear and nonlinear shear response in the natural lamina coordinates (with the aid of transformation equations).

The state of stress in the off-axis unidirectional tension coupon has been determined by several methods. Rizzo [20] and Richards et al [21] analyzed this specimen by means of anisotropic finite elements;

geometry, boundary conditions, and influence of material properties were among the parameters studied. Pagano and Halpin [22] described the stress state by means of an elasticity solution supplemented with anisotropic rubber specimens subjected to large deformations.

Pipes and Cole [23] showed good agreement between the shear responses as obtained from 15°, 30°, 45°, and 60° off-axis coupons when corrections for Poisson effect are included. Richards et al [21] obtained good agreement between experiment and their finite element solution using long narrow 45° boron-epoxy coupons. Wu and Thomas [24] developed grips that allowed in-plane rotations of the anisotropic off-axis tension coupon. Chamis and Sinclair [25] suggested an optimum fiber orientation of 10° to minimize the effects of the biaxial state of stress present in the off-axis coupon.

2.8 The Torsion Tube

A desirable specimen for determining shear stress-strain response is the torsion tube (Bert [5,26]). In this test a thin-walled circular tube is subjected to pure torque resulting in a state of uniform pure shear away from the ends. The torsion tube has a very desirable shear stress distribution with minimal normal stresses in the test section. Torsion tubes have been successfully used to obtain both linear and nonlinear shear stress-strain response, however, Rizzo and Vicario [27] reported that strength values may be influenced by gripping the ends of the tube. The main drawback to this specimen is the difficulty associated with fabricating and testing tubular specimens.

2.9 Other Shear Test Methods

Various other test methods have been used to measure in-plane shear response of composite materials. See Bert [5], Adams and Thomas [17], Hancox [28], Greszczuk [29], Sattar and Kellogg [30], and Berg et al [31] for a description of these methods. These other methods generally provide qualitative data rather than accurate, quantitative shear stress-strain response.

2.10 Summary

While this literature review has discussed many test methods for the determination of in-plane shear response of composite laminates, it is evident that complete analyses including effects of specimen geometry and grips, laminate configuration, high temperature test requirements, and nonlinear behavior are lacking. This study will attempt to resolve some of these deficiencies for flat specimens.

3. THEORETICAL CONSIDERATIONS

3.1 Lamination Theory

This study is limited to linear, elastic, orthotropic laminates in plane stress due to mechanical and thermal loads. For such material behavior, the laminate moduli of elasticity (E_x, E_y), Poisson's ratios (ν_{xy}, ν_{yx}) modulus of rigidity (G_{xy}), and the coefficients of thermal expansion ($\bar{\alpha}_x, \bar{\alpha}_y$) referenced to the laminate x-y coordinate system (Fig. 4) are the only material properties required for a finite element analysis. Experimental results have shown that these elastic and thermal constants of the laminate can be predicted given the lamina properties. The accepted method for doing this is called lamination theory [32].

The lamina, or individual ply, is the basis upon which the laminate is built. It is an orthotropic ply in a state of plane stress and is characterized by the constitutive relationship:

$$\begin{Bmatrix} \sigma_1 \\ \sigma_2 \\ \sigma_{12} \end{Bmatrix} = \begin{bmatrix} Q_{11} & Q_{12} & 0 \\ Q_{12} & Q_{22} & 0 \\ 0 & 0 & Q_{66} \end{bmatrix} \begin{Bmatrix} \epsilon_1 \\ \epsilon_2 \\ \gamma_{12} \end{Bmatrix} \quad (3.1)$$

where the stresses $\sigma_1, \sigma_2, \tau_{12}$ and strains $\epsilon_1, \epsilon_2, \gamma_{12}$ are referred to the 1-2 natural (or principal) lamina coordinate system shown in Fig. 4. The terms of the lamina stiffness matrix, $[Q]$, can be expressed in terms of the engineering constants as follows:

$$Q_{11} = E_{11}/(1-\nu_{12}\nu_{21})$$

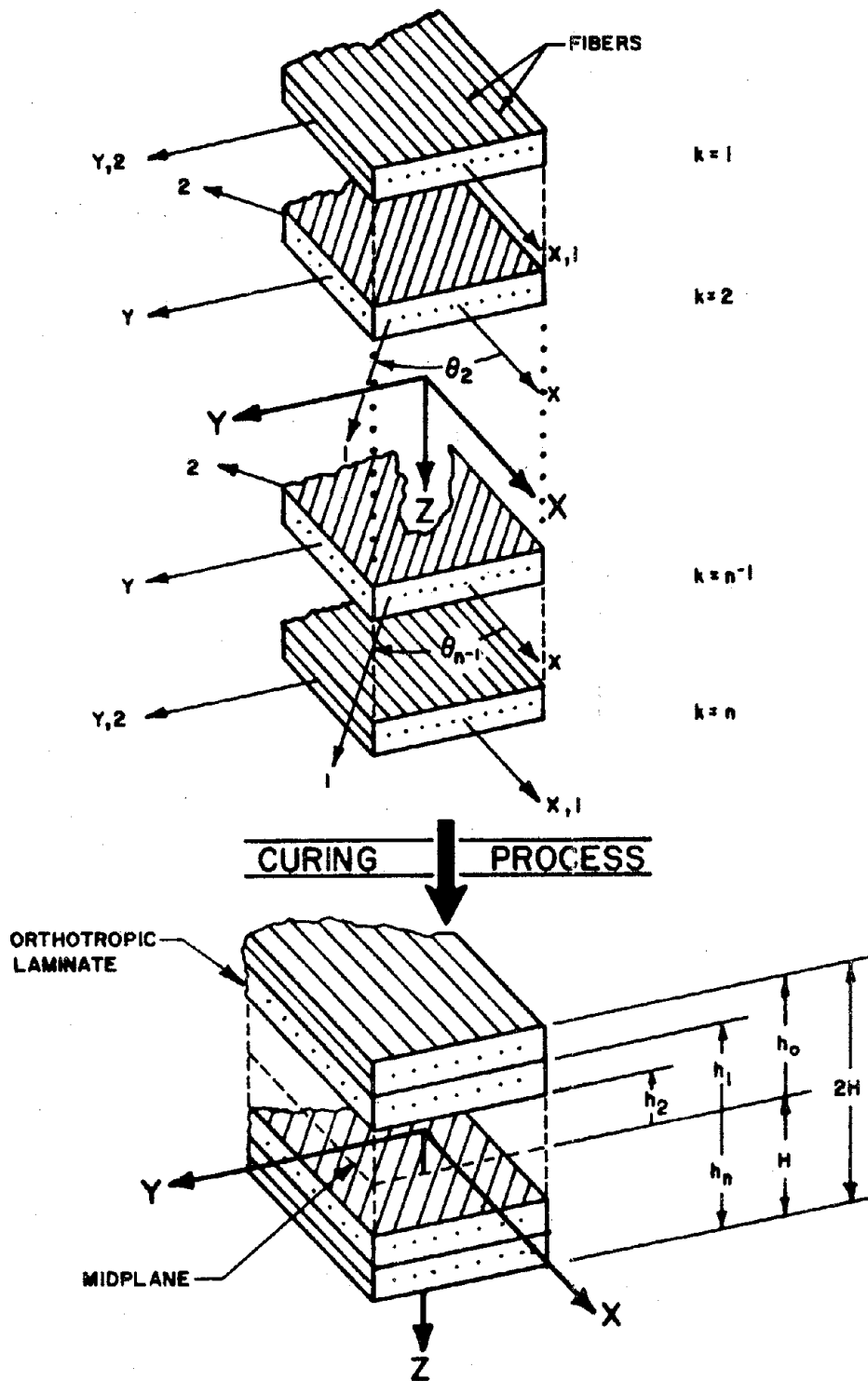


FIGURE 4. LAMINA & LAMINATE COORDINATES

$$\begin{aligned}
 Q_{22} &= E_{22}/(1-\nu_{12}\nu_{21}) \\
 Q_{12} &= \nu_{21}E_{11}/(1-\nu_{12}\nu_{21}) = \nu_{12}E_{22}/(1-\nu_{12}\nu_{21}) \\
 Q_{66} &= G_{12} \\
 Q_{16} &= Q_{26} = 0,
 \end{aligned}
 \tag{3.2}$$

where all material properties are referred to the lamina principal directions. When the principal material directions of any lamina are not coincident with the laminate x-y coordinate system, the constitutive relations for each lamina must be referred to the laminate x-y coordinate system. This is accomplished using the transformation matrix [T], defined as

$$[T] = \begin{bmatrix} m^2 & n^2 & 2mn \\ n^2 & m^2 & -2mn \\ -mn & mn & m^2 - n^2 \end{bmatrix}$$

and the inverse $[T]^{-1}$ defined as

$$[T]^{-1} = \begin{bmatrix} m^2 & n^2 & -2mn \\ n^2 & m^2 & 2mn \\ mn & -mn & m^2 - n^2 \end{bmatrix}
 \tag{3.3}$$

where

$$m = \cos\theta$$

$$n = \sin\theta.$$

Theta (θ), the angle between the lamina natural coordinate system and

the laminate x-y coordinate system, is shown in Fig. 4. Using the transformation matrix to relate the stresses and strains in the natural coordinate system to those in the x-y coordinate system leads to the relationship

$$\{\sigma_x\}_k = [\bar{Q}]_k \{\epsilon_x\}_k. \quad (3.4)$$

Thus, for the k^{th} lamina, the stresses, $\{\sigma_x\}_k$, are related to the strains, $\{\epsilon_x\}_k$, in the x-y coordinate system by the transformed lamina stiffness matrix, $[\bar{Q}]_k$, defined as

$$[\bar{Q}]_k = [T]_k^{-1} [Q] [T]_k. \quad (3.5)$$

For symmetric laminates subjected to in-plane loading only, strains in each lamina are equal to the laminate midplane strain, $\{\epsilon^0\}$:

$$\{\epsilon_x\}_k = \{\epsilon^0\}. \quad (3.6)$$

The stress resultants per unit length, $\{N\}$, are defined in terms of the stresses by the relationship

$$\begin{Bmatrix} N_x \\ N_y \\ N_{xy} \end{Bmatrix} = \int_{-H}^H \begin{Bmatrix} \sigma_x \\ \sigma_y \\ \tau_{xy} \end{Bmatrix} dz, \quad (3.7)$$

where $2H$ is the total laminate thickness. Combining equations (3.4), (3.6), and (3.7) and rewriting the integral in terms of a summation over all n plies, the force resultants are

$$\{N\} = \left(\sum_{k=1}^n [\bar{Q}]_k (h_k - h_{k-1}) \right) \{\epsilon^0\}. \quad (3.8)$$

From equation (3.8), the extensional stiffness matrix A_{ij} is defined

$$A_{ij} = \sum_{k=1}^n (\bar{Q}_{ij})_k (h_k - h_{k-1}), \quad (3.9)$$

so that the force resultant relationship can be written

$$\{N\} = [A]\{\epsilon^o\}. \quad (3.10)$$

The average laminate stresses, $\{\bar{\sigma}\}$, are defined

$$\{\bar{\sigma}\} = \frac{1}{2H} \{N\}. \quad (3.11)$$

Combining equations (3.10) and (3.11) and considering appropriate non-zero $\{\bar{\sigma}\}$ terms, the effective laminate engineering constants are:

$$\begin{aligned} E_x &= \frac{A_{11}A_{22} - A_{12}^2}{2HA_{22}} \\ E_y &= \frac{A_{11}A_{22} - A_{12}^2}{2HA_{11}} \\ \nu_{xy} &= -\frac{A_{12}}{A_{22}} \\ \nu_{yx} &= -\frac{A_{12}}{A_{11}} \\ G_{xy} &= \frac{A_{66}}{2H}. \end{aligned} \quad (3.12)$$

The laminate thermal coefficients of expansion, $\{\bar{\alpha}\}$, are derived in a similar manner. When the lamina thermal strains, $\{\epsilon_x^T\}_k$, are included the lamina constitutive equation (3.4) becomes

$$\{\sigma_x\}_k = [\bar{Q}]_k (\{\epsilon^o\} - \{\epsilon_x^T\}) \quad (3.13)$$

and with zero force resultants, equation (3.8) becomes

$$0 = \sum_{k=1}^n [\bar{Q}]_k (\{\epsilon^o\} - \{\epsilon_X^T\}_k) (h_k - h_{k-1}). \quad (3.14)$$

Solving (3.14) for the laminate thermal strains $\{\epsilon^i\}$ results in

$$\{\epsilon^i\} = [A]^{-1} \sum_{k=1}^n [\bar{Q}]_k \{\epsilon_X^T\}_k (h_k - h_{k-1}) \quad (3.15)$$

and for uniform temperature change ΔT , the lamina thermal strains are

$$\{\epsilon_X^T\}_k = \{\alpha_X\}_k \Delta T. \quad (3.16)$$

Now defining the laminate thermal coefficients $\{\bar{\alpha}\}$ as

$$\{\bar{\alpha}\} = \frac{1}{\Delta T} \{\epsilon^i\} \quad (3.17)$$

and combining (3.15), (3.16), and (3.17) gives the relationship

$$\{\bar{\alpha}\} = [A]^{-1} \sum_{k=1}^n [\bar{Q}]_k \{\alpha_X\}_k (h_k - h_{k-1}). \quad (3.18)$$

3.2 The Finite Element Formulation

The finite element method is a versatile technique for obtaining approximate solutions for structures subjected to loads. Text book accounts can be found in Desai and Abel [33] and Zienkiewicz [34], among others. This section describes the theory of the two-dimensional finite element program used in this study. The analysis considers orthotropic materials in plane stress due to mechanical and thermal loading.

The program uses both triangular and quadrilateral elements with the quadrilateral elements being composed of four triangles. All

triangles are constant strain elements. Convergence requirements for the finite element solution are satisfied by using a linear displacement model for the in-plane displacements u and v in the x and y directions, respectively;

$$\begin{aligned} u &= \beta_1 + \beta_2 x + \beta_3 y \\ v &= \beta_4 + \beta_5 x + \beta_6 y, \end{aligned} \quad (3.19)$$

where the generalized coordinate coefficients, β_i , are functions of the initial location of generic nodes 1, 2, and 3 and are given by

$$\begin{aligned} \begin{Bmatrix} \beta_1 \\ \beta_2 \\ \beta_3 \end{Bmatrix} &= \frac{1}{D} \begin{bmatrix} x_2 y_3 - x_3 y_2 & y_3 - y_2 & x_3 - x_2 \\ x_1 y_3 - x_3 y_1 & y_3 - y_1 & x_3 - x_1 \\ x_1 y_2 - x_2 y_1 & y_2 - y_1 & x_2 - x_1 \end{bmatrix} \begin{Bmatrix} u_1 \\ u_2 \\ u_3 \end{Bmatrix} \\ \begin{Bmatrix} \beta_4 \\ \beta_5 \\ \beta_6 \end{Bmatrix} &= \frac{1}{D} \begin{bmatrix} x_2 y_3 - x_3 y_2 & y_3 - y_2 & x_3 - x_2 \\ x_1 y_3 - x_3 y_1 & y_3 - y_1 & x_3 - x_1 \\ x_1 y_2 - x_2 y_1 & y_2 - y_1 & x_2 - x_1 \end{bmatrix} \begin{Bmatrix} v_1 \\ v_2 \\ v_3 \end{Bmatrix} \end{aligned} \quad (3.20)$$

where

$$D = \begin{vmatrix} 1 & x_1 & y_1 \\ 1 & x_2 & y_2 \\ 1 & x_3 & y_3 \end{vmatrix}.$$

The general strain-displacement relationships are

$$\epsilon_x = \frac{\partial u}{\partial x}$$

$$\epsilon_y = \frac{\partial v}{\partial y} \quad (3.21)$$

$$\gamma_{xy} = \frac{\partial u}{\partial y} + \frac{\partial v}{\partial x}$$

and combining equations (3.20) and (3.21) leads to the specific strain-displacement relationship

$$\{\epsilon\} = [B]\{u\} \quad (3.22)$$

where the strain-displacement matrix, $[B]$, and the transposed nodal displacement matrix, $\{u\}^T$, are defined

$$[B] = \frac{1}{2A} \begin{bmatrix} y_2 - y_3 & y_3 - y_1 & y_1 - y_2 & 0 & 0 & 0 \\ 0 & 0 & 0 & x_3 - x_2 & x_1 - x_3 & x_2 - x_1 \\ x_3 - x_2 & x_1 - x_3 & x_2 - x_1 & y_2 - y_3 & y_3 - y_1 & y_1 - y_2 \end{bmatrix} \quad (3.23)$$

and

$$\{u\}^T = [u_1 \quad u_2 \quad u_3 \quad v_1 \quad v_2 \quad v_3], \quad (3.24)$$

where A is the area of the element.

The thermoelastic constitutive relationship for an orthotropic laminate is

$$\{\bar{\sigma}\} = [a]\{\{\epsilon\} - \{\epsilon^i\}\}, \quad (3.25)$$

where the strain that contributes to the laminate stress is the difference between the total midplane strain, $\{\epsilon\}$, and the strain caused

only by initial (free thermal) strains, $\{\epsilon^i\}$ (eq. 3.15). The terms of the orthotropic laminate stiffness matrix, $[a]$, referenced to the x-y coordinate system, are defined

$$\begin{aligned} a_{11} &= E_x / (1 - \nu_{xy} \nu_{yx}) \\ a_{22} &= E_y / (1 - \nu_{xy} \nu_{yx}) \\ a_{12} &= \nu_{yx} E_x / (1 - \nu_{xy} \nu_{yx}) = \nu_{xy} E_y / (1 - \nu_{xy} \nu_{yx}) \\ a_{66} &= G_{xy} \\ a_{16} &= a_{26} = 0. \end{aligned} \quad (3.26)$$

The total potential energy, Π , of a system is the sum of the strain energy, U , and the potential energy of the external loads, W :

$$\Pi = U + W. \quad (3.27)$$

Considering equations (3.22-3.25), U and W are, respectively

$$\begin{aligned} U &= \frac{1}{2} \iiint_V \{\epsilon\}^T [a] \{\epsilon\} dv - \iiint_V \{\epsilon\}^T [a] \{\epsilon^i\} dv \\ &\quad + \frac{1}{2} \iiint_V \{\epsilon^i\}^T [a] \{\epsilon^i\} dv \end{aligned} \quad (3.28)$$

$$W = - \{u\}^T \{Q\}$$

where V is the elemental volume and the transposed mechanical nodal load vector, $\{Q\}^T$, is defined as

$$\{Q\}^T = [q_1 \quad q_2 \quad q_3 \quad p_1 \quad p_2 \quad p_3]. \quad (3.29)$$

The variables q_i and p_i are mechanical loads applied in the x and y directions, respectively, at the i^{th} node of the element. Minimization of the total potential energy of an element (eq. 3.27) leads to the equilibrium equations

$$[k]\{u\} = \{Q\} + \{Q^i\} \quad (3.30)$$

where the relationships for the elemental stiffness matrix, $[k]$, and the initial load vector, $\{Q^i\}$, are

$$[k] = \iiint_V [B]^T [a] [B] dv \quad (3.31)$$

$$\{Q^i\} = \iiint_V [B]^T [a] \{\epsilon^i\} dv \quad (3.32)$$

The total stiffness matrix $[K]$ and the total load vector $\{R\}$ for the entire structure is formed by combining the elemental stiffness matrices and the total load vector ($\{Q\} + \{Q^i\}$) for all the elements resulting in the system of linear equations

$$[K]\{X\} = \{R\}. \quad (3.33)$$

For N number of nodes the total stiffness matrix will be $2N \times 2N$ and the total load vector and node displacement vector $\{X\}$ will be $2N$. These equations relate the stiffnesses and nodal displacements of the entire structure to the applied loads and hence this formulation is called the direct stiffness method. Geometric boundary conditions are then imposed and a solution is obtained for the node displacement vector, $\{X\}$.

4. THE SLOTTED SHEAR SPECIMEN

4.1 General

The slotted shear specimen was analyzed using the basic finite element representation shown in Fig. 5. The specimen was always loaded to simulate uniform axial and zero lateral displacement at the ends of the specimen. These boundary conditions are idealizations of machine grips loading a flat coupon specimen in tension. The effects of laminate properties were studied for three graphite-epoxy laminates. The [0], [90], and [± 45]_s laminates were chosen because they offer substantial variations in orthotropic properties. The [0] laminate exhibits a low E_x/E_y value; the [90] laminate exhibits a high E_x/E_y value; and the [± 45]_s laminate exhibits a high G_{xy}/E_y value.

Elementary rigid body statics assumes the shear stress distribution in the test section between the ends of the slots to be pure, uniform, and maximum and independent of the laminate properties. Actual stress contour plots for the laminates studied are shown in Figs. 6-8. All stresses have been normalized with respect to the average axial stress away from the test section. Since a limited parametric study on the slot spacing, S (ranging from $0.2W$ to W), and slot depth, D (ranging from $0.25W$ to $0.75W$), showed no significant changes in the stress distributions, the slot spacing, slot depth, and slot width (T) were standardized to $S = 0.6W$, $D = 0.5W$, and $T = 0.0625W$ for all subsequent studies. As indicated in the figures, the finite element results did exhibit the expected symmetries.

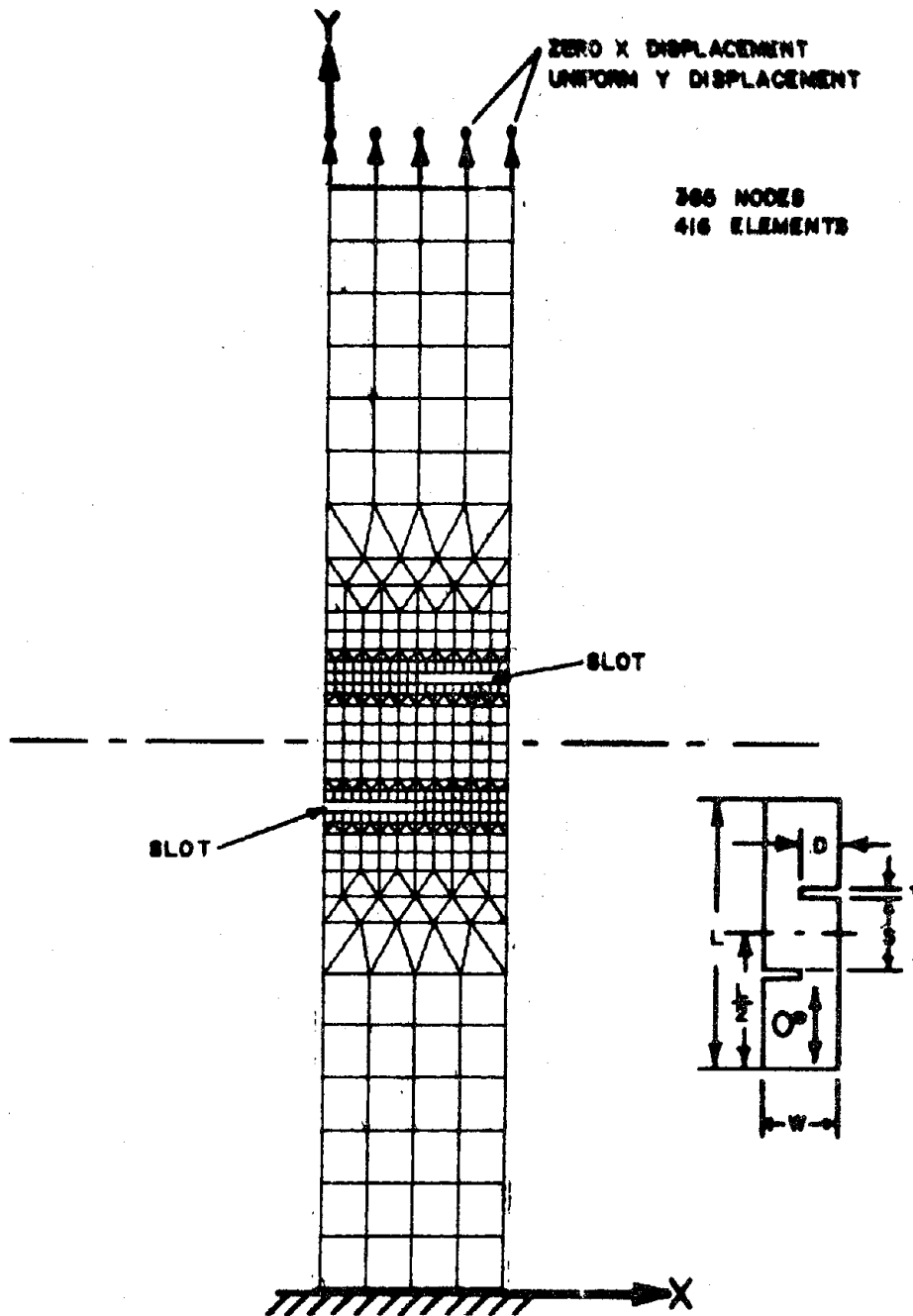


FIGURE 5. FINITE ELEMENT REPRESENTATION
OF SLOTTED SHEAR SPECIMEN

4.2 [0] Laminate

The normalized stress contours for the [0] slotted shear specimen are shown in Fig. 6. The $\sigma_x/\bar{\sigma}$ and $\sigma_y/\bar{\sigma}$ contour plots clearly indicate stress concentrations at the slot ends ($\sigma_x/\bar{\sigma} = 0.4$ and $\sigma_y/\bar{\sigma} = 8.0$) with the $\sigma_y/\bar{\sigma}$ stress remaining at 4.0 along the centerline of the test section. The $\sigma_x/\bar{\sigma}$ stress is insignificant ($\sigma_x/\bar{\sigma} = -0.065$) at the center of the specimen. The normalized shear stress remains essentially constant throughout the test section at -0.6; the maximum magnitude is -0.8 near the slot ends. Although this stress distribution is acceptable in principle, this region may be too narrow for practical strain measurements.

Since a region of uniform shear stress occurs in the test section, the [0] slotted specimen may be used for qualitative shear measurements. However, stress concentrations at the slot ends and a rather small area of uniform shear stress make this specimen unacceptable for quantitative shear measurements.

4.3 [90] and [± 45]_s Laminates

The contour plots for [90] and [± 45]_s graphite-epoxy laminates are shown in Figs. 7 and 8. The stress distributions for these laminates are clearly unacceptable for a shear specimen. As well as having $\sigma_x/\bar{\sigma}$ and $\sigma_y/\bar{\sigma}$ stress concentrations at or near the slot ends, the $\tau_{xy}/\bar{\sigma}$ contour plots indicate that the state of shear is not maximum or uniform (for the [90] laminate, $\tau_{xy}/\bar{\sigma}$ ranges from -2.0 to 0.25 and for the [± 45]_s laminate, $\tau_{xy}/\bar{\sigma}$ ranges from -1.0 to -0.4).

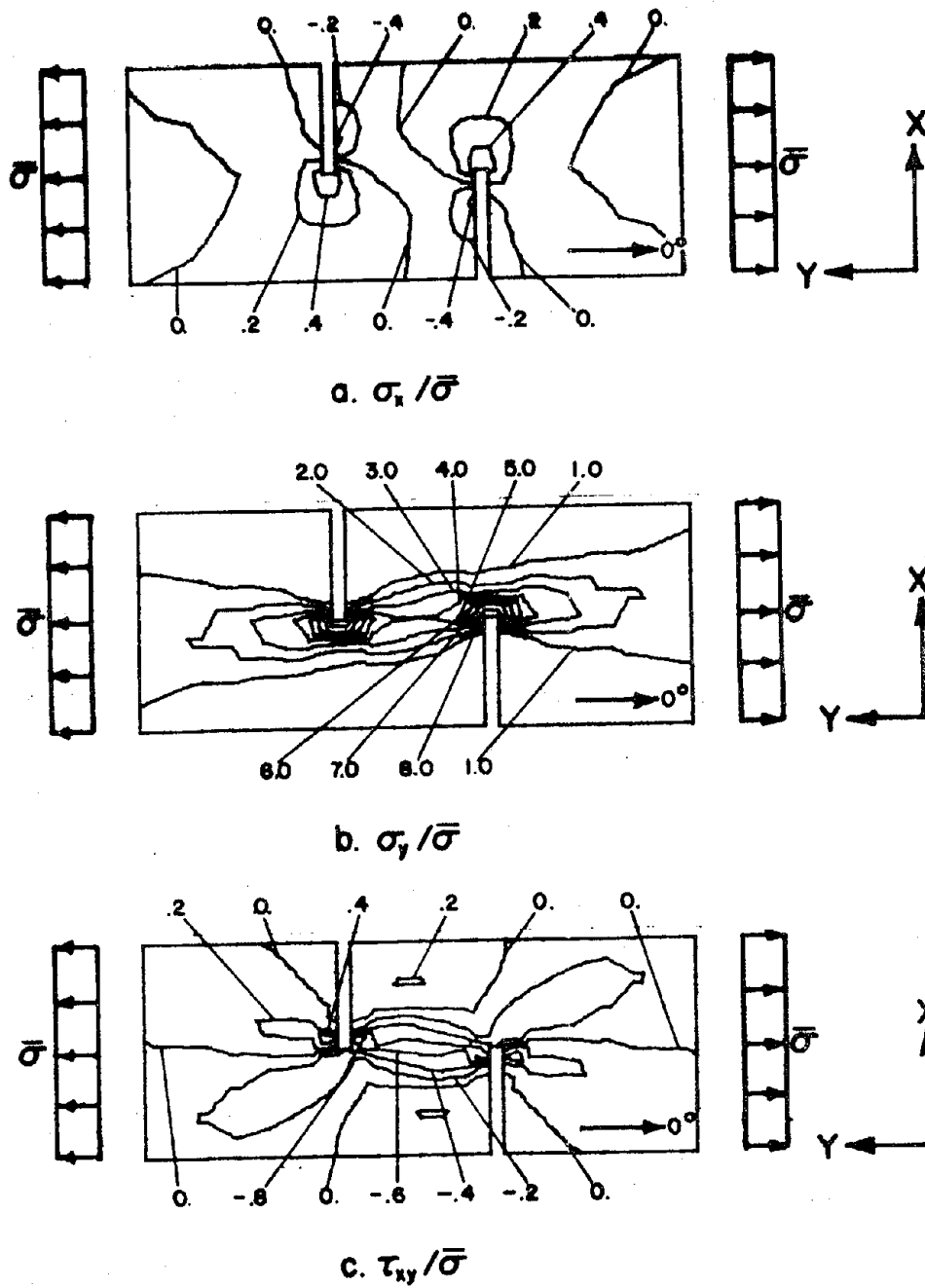
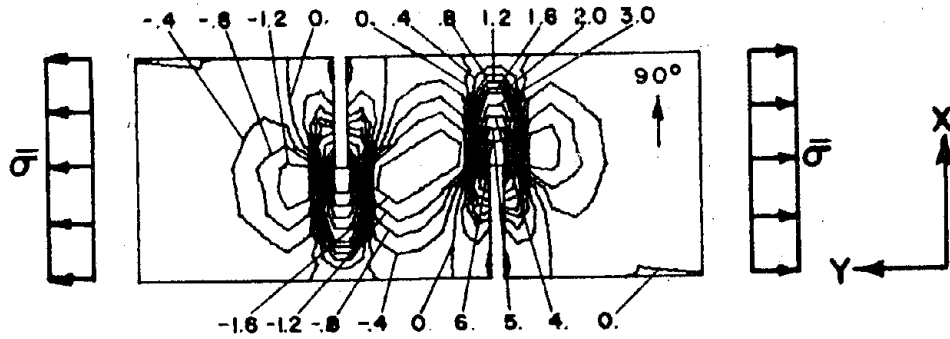
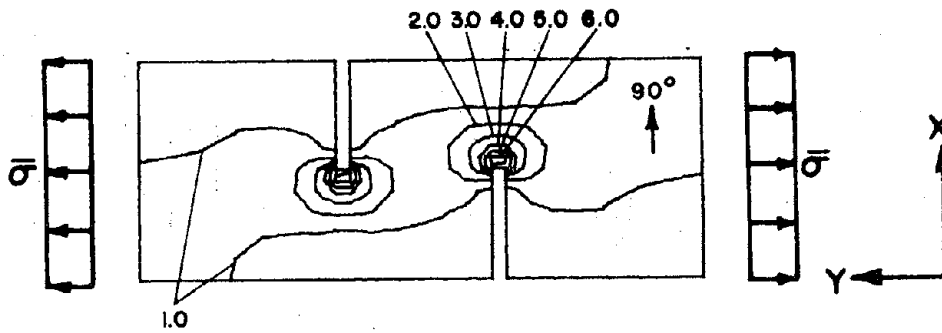


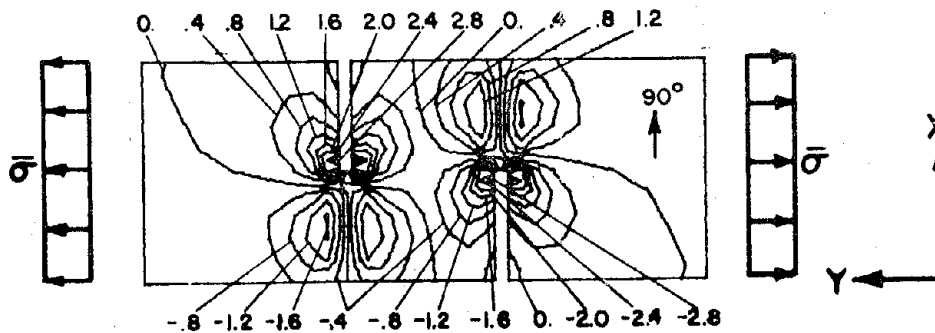
FIGURE 6. NORMALIZED STRESS CONTOURS FOR [0] SLOTTED SHEAR SPECIMEN, $S=0.6W$, $D=0.5W$, $T=0.0625W$



a. $\sigma_x / \bar{\sigma}$

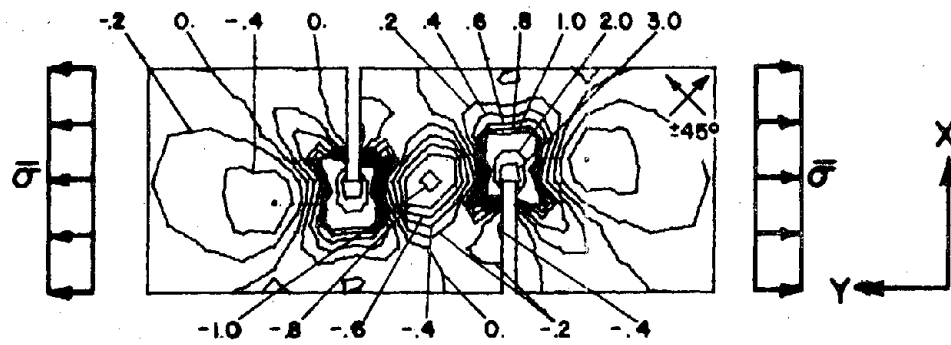


b. $\sigma_y / \bar{\sigma}$

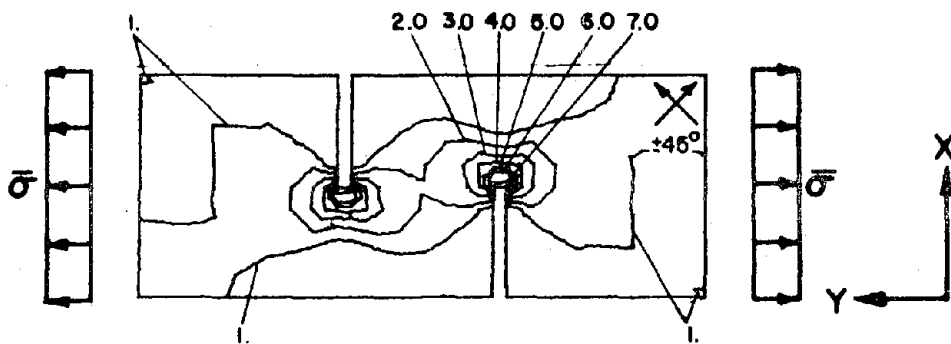


c. $\tau_{xy} / \bar{\sigma}$

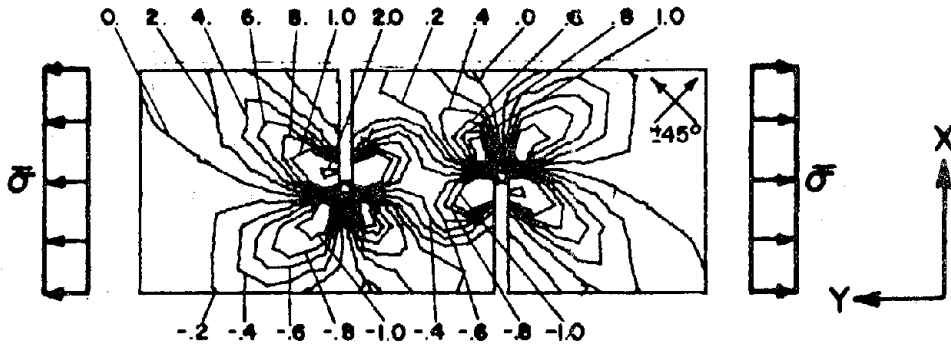
FIGURE 7. NORMALIZED STRESS CONTOURS FOR [90] SLOTTED SHEAR SPECIMEN, $S=0.6W$, $D=0.5W$, $T=0.0625W$



a. $\sigma_x / \bar{\sigma}$



b. $\sigma_y / \bar{\sigma}$



c. $\tau_{xy} / \bar{\sigma}$

FIGURE 8. NORMALIZED STRESS CONTOURS FOR $[\pm 45]_s$ SLOTTED SHEAR SPECIMEN, $S=0.6W$, $D=0.5W$, $T=0.0625W$

4.4 Summary

For the [0], [90], and [± 45]_s laminates, the slotted shear specimen exhibits σ_x , σ_y , and τ_{xy} stress concentrations in the vicinity of the slot ends as expected. As a result of such stress concentrations, high normal stresses were often found in the test section. For the [90] and [± 45]_s laminates, $\tau_{xy}/\bar{\sigma}$ is very low in magnitude (for the [90] laminate $\tau_{xy}/\bar{\sigma} = 0.25$ and for the [± 45]_s laminate $\tau_{xy}/\bar{\sigma} = -0.4$) and nonuniform in the test section. Obviously this slotted specimen does not provide acceptable shear data for these laminates. The normalized shear stress in the test section of the [0] laminate is somewhat uniform (with the exception of a small area in the vicinity of each slot end), however, this area of high shear stress is rather narrow for strain measurements. Also, the normalized σ_y is significant in the test section for the [0] laminate. In conclusion, the stress distributions of the slotted shear specimens analyzed were significantly influenced by laminate properties and none of the laminates studied were found to be acceptable for providing reliable quantitative shear data.

5. THE CROSS BEAM SHEAR SPECIMEN

5.1 General

As mentioned previously, the cross beam shear specimen shown in Fig. 2a has been used to obtain shear stress-strain response for both $[\pm 45]_S$ and $[0/90]_S$ laminates. When analyzing the results from such a test it is assumed that the test section is subjected to uniform biaxial normal stresses of equal magnitude and opposite sign resulting from the application of positive and negative bending moments to the cross beam. For this state of biaxial stress, stresses on 45° planes are pure shear and equal to the magnitude of the applied average normal stresses. The purpose of this analysis is to study the influence of corner effects, laminate properties, and, to a limited extent, core materials on the stress distribution in the test section.

The elastic analysis of the cross beam shear specimen involved the following assumptions. The composite material was assumed to be in a state of plane stress. This neglected any transverse stress components associated with the application of loads near the ends of the beam (Fig. 2a) and also interlaminar effects from the core in the test section. Loading and geometric symmetry allowed the analysis to be applied to only one quarter of the central portion of the specimen. These symmetry conditions were simulated by imposing zero x displacement along the y axis and zero y displacement along the x axis shown in Fig. 9.

Cross beam specimens usually are designed with two types of honeycomb core. Stiff, heavyweight core material is sandwiched between the

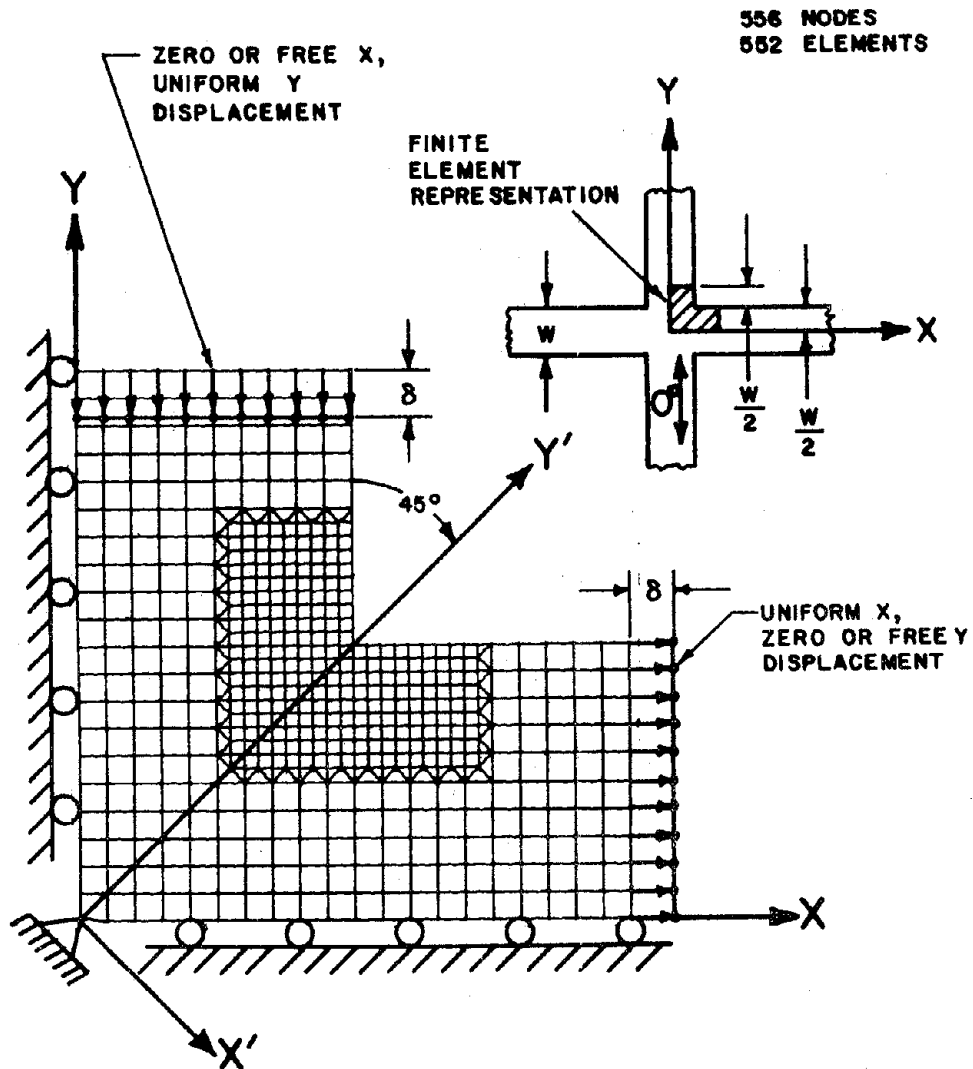


FIGURE 9. FINITE ELEMENT REPRESENTATION
OF CROSS BEAM SHEAR SPECIMEN

composite material away from the central portion of the specimen (x and $y \geq W$) to preclude local failure at the points of load application, while a more flexible, relatively light weight core material is used in the central portion (x and $y < W$). Because of the unknown net stiffening effects of core, displacements rather than forces were imposed as boundary conditions at $x = W$ and $y = W$ to represent the loading introduced by the bending moments. In order to study core stiffness effects away from the test section, two sets of lateral displacement boundary conditions were considered at $x = W$ and $y = W$. "Rigid" core for x and y greater than W was simulated by fixing lateral displacements to zero across the width of the beam. "Flexible" core was simulated by allowing free lateral displacements across the width of the beam. The stiffness of the core material in the test section and all other core influences were always neglected.

Contour plots of the stresses on a 45° plane (x',y'), normalized with respect to the magnitude of the applied average normal stress, $\bar{\sigma}$, are shown in Figs. 10-14. These plots reflect the symmetric loading and geometry.

5.2 The $[\pm 45]_S$ Laminate

A cross beam with fibers at $\pm 45^\circ$ is used to determine shear stress-strain response of $[0/90]_S$ laminates. Such response is equivalent to the shear response of a lamina referenced to its natural coordinates. Figures 10-12 compare the rigid core results to the flexible core results for normalized σ'_x , σ'_y and τ'_{xy} stress distributions.

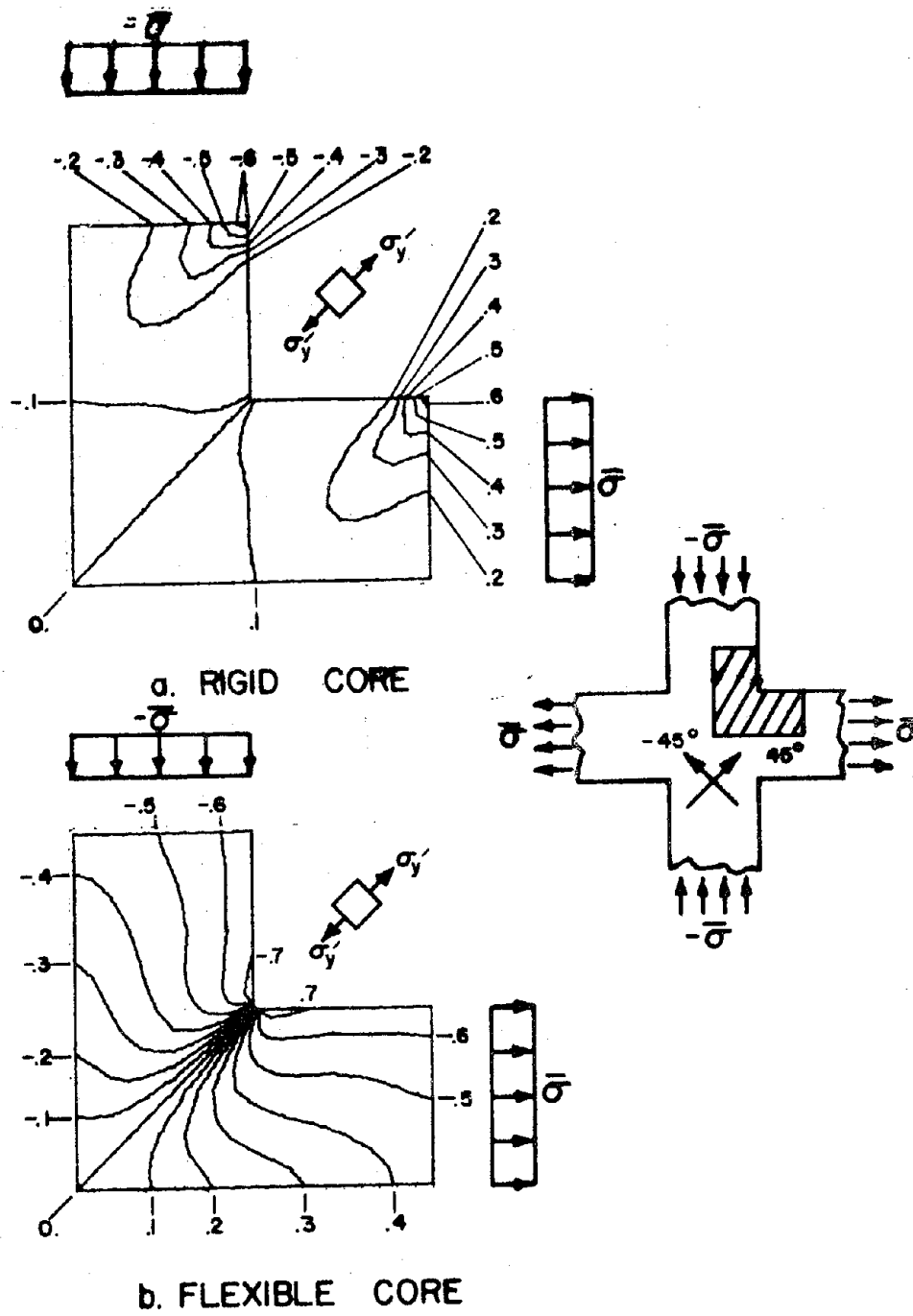


FIGURE 11. NORMALIZED σ_y' CONTOURS FOR $[\pm 45]_s$ CROSS BEAM

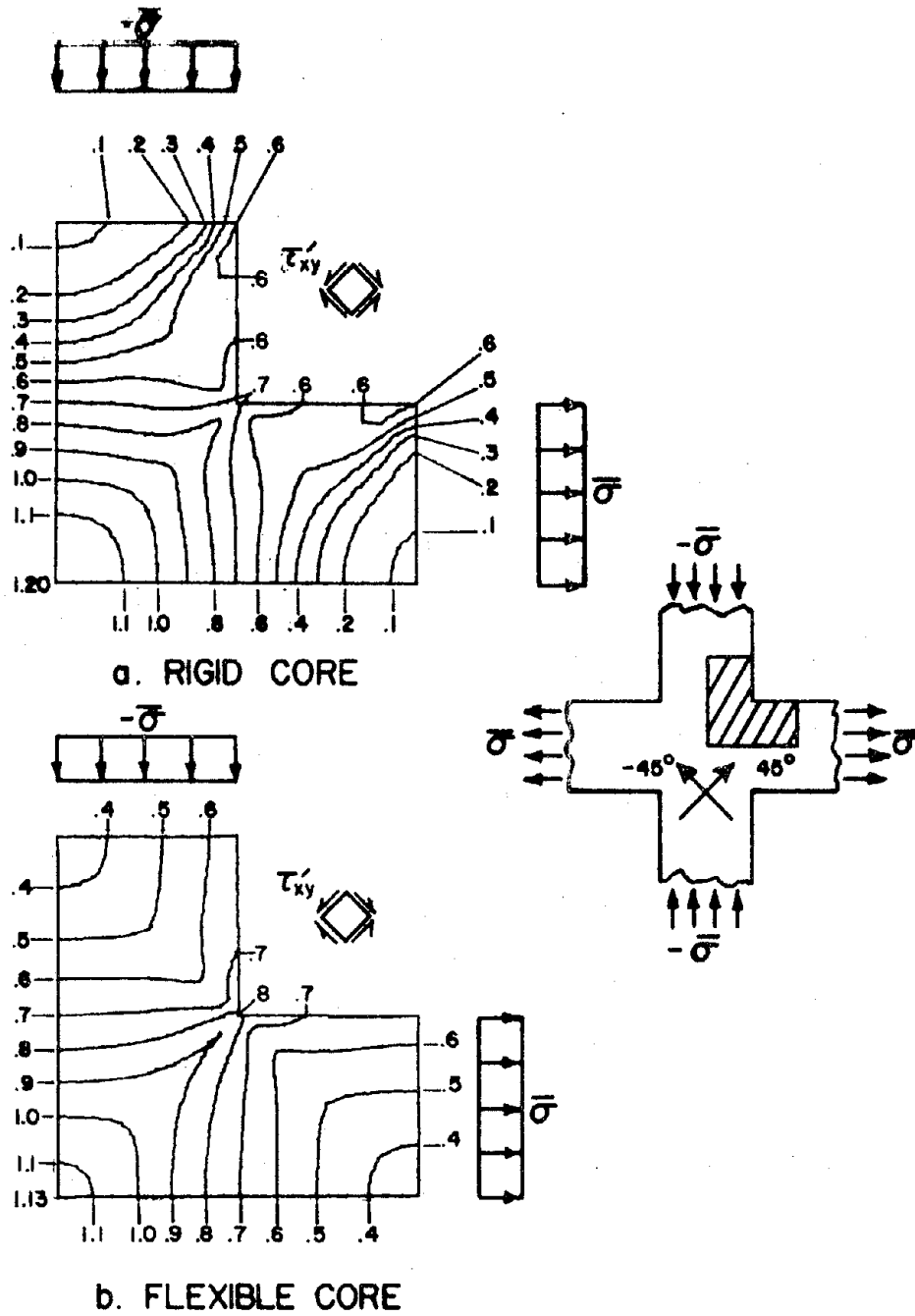


FIGURE 12. NORMALIZED τ'_{xy} CONTOURS FOR $[\pm 45]_s$ CROSS BEAM

For both cases the shear stress is maximum and pure over a finite region in the center of the specimen. This region is large enough for a strain gage to be used for accurate strain measurements. Although these are excellent features of the cross beam, the magnitude of $\tau'_{xy}/\bar{\sigma}$ at the center is significantly different from 1.0 because of the corner effects. Specifically, values of $\tau'_{xy}/\bar{\sigma}$ were found to be 1.20 and 1.13 for the rigid and flexible core boundary conditions, respectively.

Corner stresses for the rigid core boundary conditions were lower than those of the flexible core boundary conditions, especially for the $\sigma_y/\bar{\sigma}$ stress. With one exception (Fig. 11a), all normalized stress components are greater than 0.6 in the vicinity of the corner. This is significant and may contribute to premature failure in a mode different from pure shear.

In general the stress distributions in the $[\pm 45]_s$ cross beam are significantly more complex than those of the "ideal" cross beam. The magnitude of the shear stress in the test section is higher than 1.0 due to corner effects and stress concentrations at the corners undoubtedly contribute to any failures. However, this analysis indicates that the stress distribution in the center section is uniform pure shear. Thus, the elastic shear modulus may be determined knowing the magnitude of the shear stress in this region.

5.3 The $[0/90]_s$ Laminate

A cross beam with fibers at 0° and 90° is used to determine shear stress-strain response of a $[\pm 45]_s$ laminate. Finite element results for

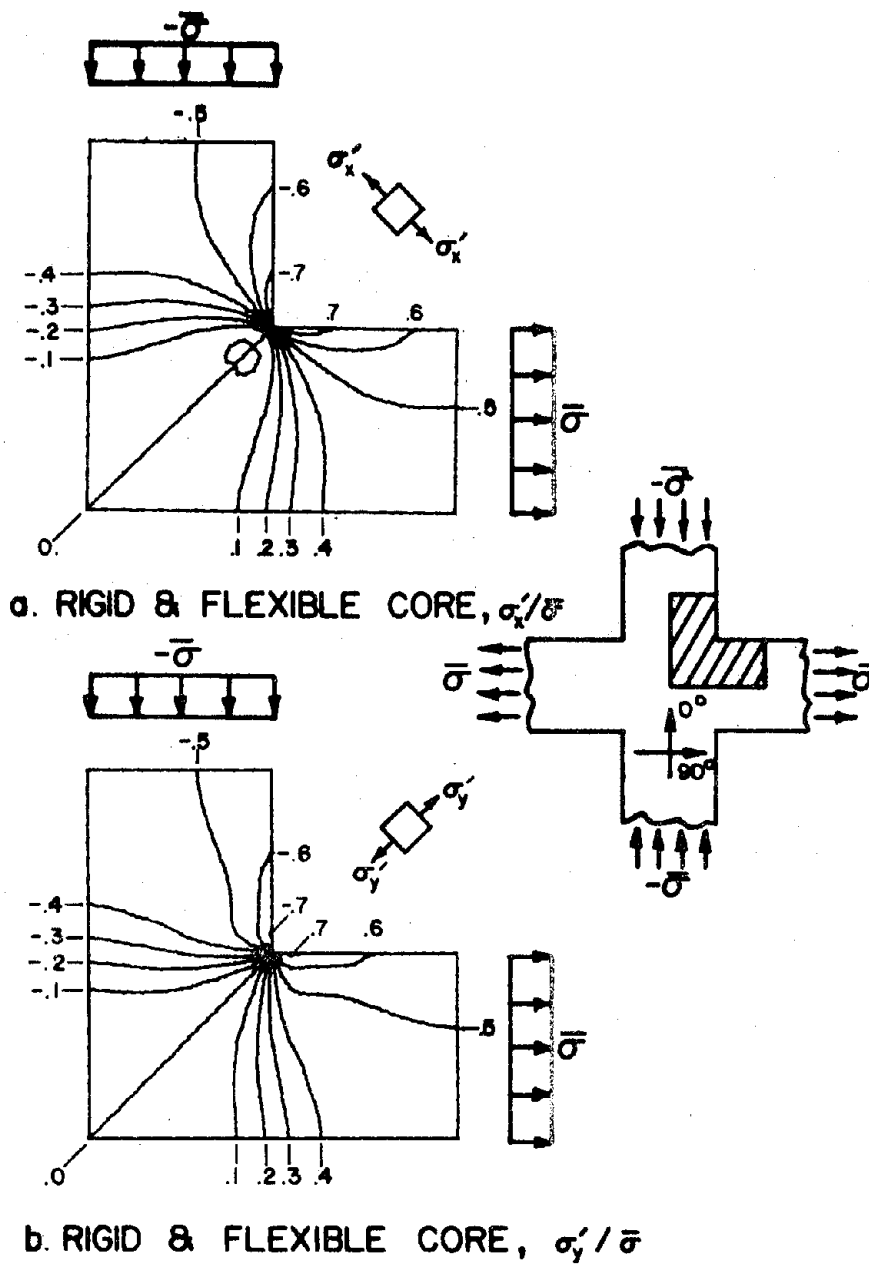


FIGURE 13. NORMALIZED σ'_x & σ'_y CONTOURS FOR $[0/90]_s$ CROSS BEAM

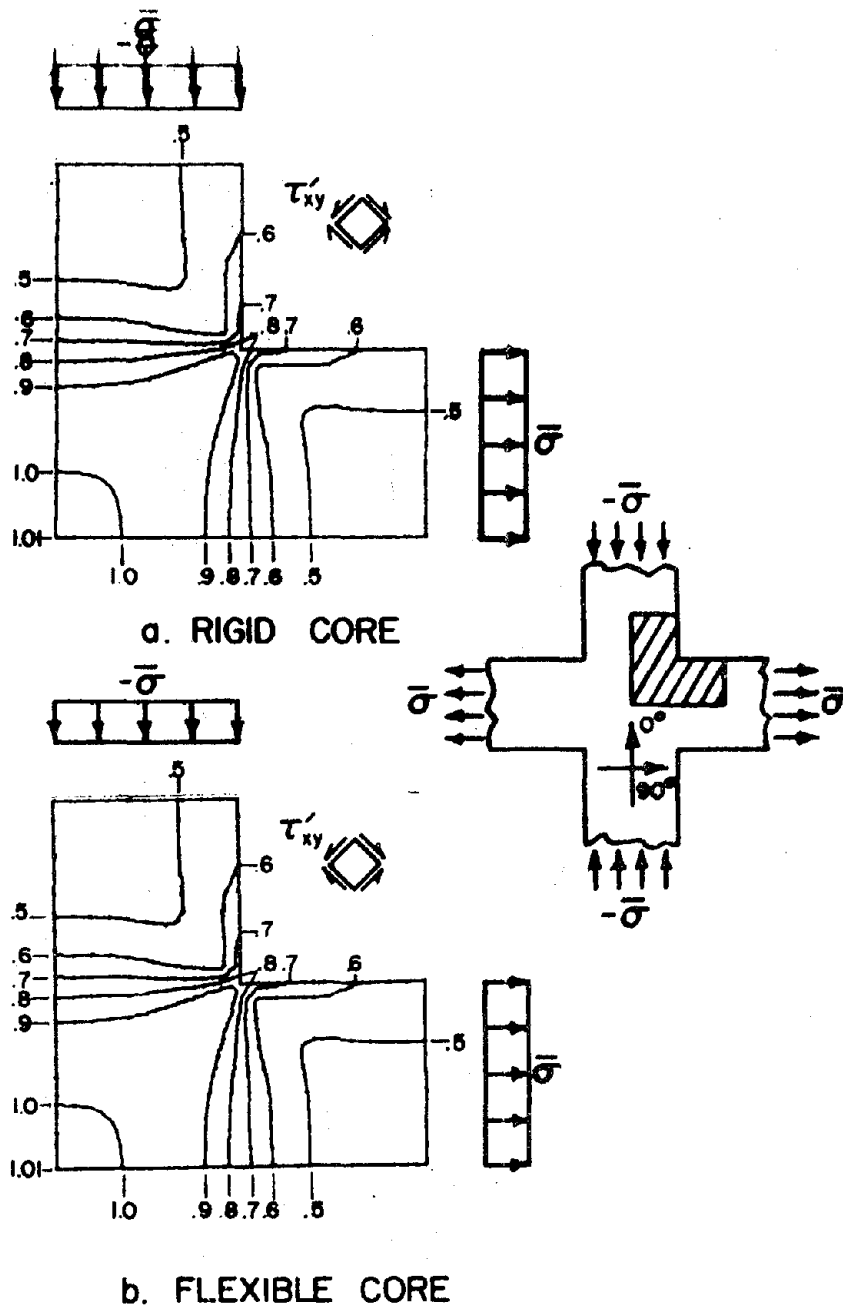


FIGURE 14. NORMALIZED τ'_{xy} CONTOURS FOR $[0/90]_s$ CROSS BEAM

both the rigid and flexible core boundary conditions were similar and thus specific results for both core types are shown only for the normalized τ'_{xy} stresses. The results are not affected appreciably by the lateral displacement boundary condition because the high lateral stiffness of the specimen results in very small lateral displacements.

As in the $[\pm 45]_S$ laminate, the $[0/90]_S$ laminate produces a maximum, pure shear region in the center of the specimen. This shear region has more characteristics of the "ideal" shear specimen. An area of maximum, uniform shear stress is present over nearly the entire test section and the maximum $\tau'_{xy}/\bar{\sigma}$ is very close to 1.00 (exactly 1.01). In the vicinity of the corner of the specimen all the normalized components of stress remain above 0.6, however.

The finite element analysis indicates that the $[0/90]_S$ laminate should provide reliable stress-strain response to a high degree of accuracy in the linear portion of the shear stress-strain curve. Although failures may initiate due to corner stresses, the core effects are minimal with the $[0/90]_S$ laminate.

5.4 Summary

For both the $[\pm 45]_S$ and the $[0/90]_S$ cross beam shear specimens, the maximum value of $\tau'_{xy}/\bar{\sigma}$ occurs at the center of the specimen and is suitable for strain measurements. However, the magnitude of $\tau'_{xy}/\bar{\sigma}$ at the center is dependent on the laminate properties, and for the $[\pm 45]_S$ laminate, $\tau'_{xy}/\bar{\sigma}$ is significantly higher than 1.0. For laminates that are relatively stiff across the width of the beam compared to their

shear stiffness, the honeycomb core effects were shown to be minimal with this plane stress analysis.

Finite element results indicate the cross beam may be used with a $[0/90]_s$ laminate for linear response since its stress distribution is nearly "ideal" (with the exception of high corner stresses). The state of shear stress at the center of the $[\pm 45]_s$ laminate is influenced by the core stiffness and is significantly greater than 1.0 because of a low shear stress away from the center. Thus, the applied normal stress in the $[\pm 45]_s$ laminate is not simply related to the shear stress at the center of the specimen. However, initial shear modulus values may be determined if this relationship is known from a numerical study such as this one.

6. THE IOSIPESCU SPECIMEN

6.1 General

The specimen analyzed in this study is a modified Iosipescu specimen [3] in that the specimen is a flat laminate notched on two sides with the load introduced through fixtures bonded to the specimen. Iosipescu's original specimen was a bar notched on four sides and loads were applied directly to the specimen. This modified specimen was studied with both isotropic and orthotropic materials. In addition, several minor variations in the specimen configuration were studied as were the influence of elastic fixtures and thermal loads.

6.2 Rigid Fixture Results

6.2.1 General

Several laminates were studied assuming that the fixtures are rigid (Fig. 2b). The finite element mesh used to represent these specimens is shown in Fig. 15. Because a finite element analysis of the entire specimen indicated quarter symmetry of stresses and displacements, only one quarter of the specimen was modeled in subsequent studies. This was accomplished by applying uniform u and zero v displacements along the line $y = L/2$, and constraining the v displacements along $x = 0$ and u displacements along $y = 0$ as indicated in Fig. 15. The dimensions of the specimen were standardized to: notch depth, $A = 0.225W$; notch angle, $\theta = 90^\circ$; and specimen length, $L = W$, where W is the width. Normalized stress contour plots for the rigid fixture assumption are shown in Figs. 16-21 and results are tabulated in Table 1. All stresses are normalized

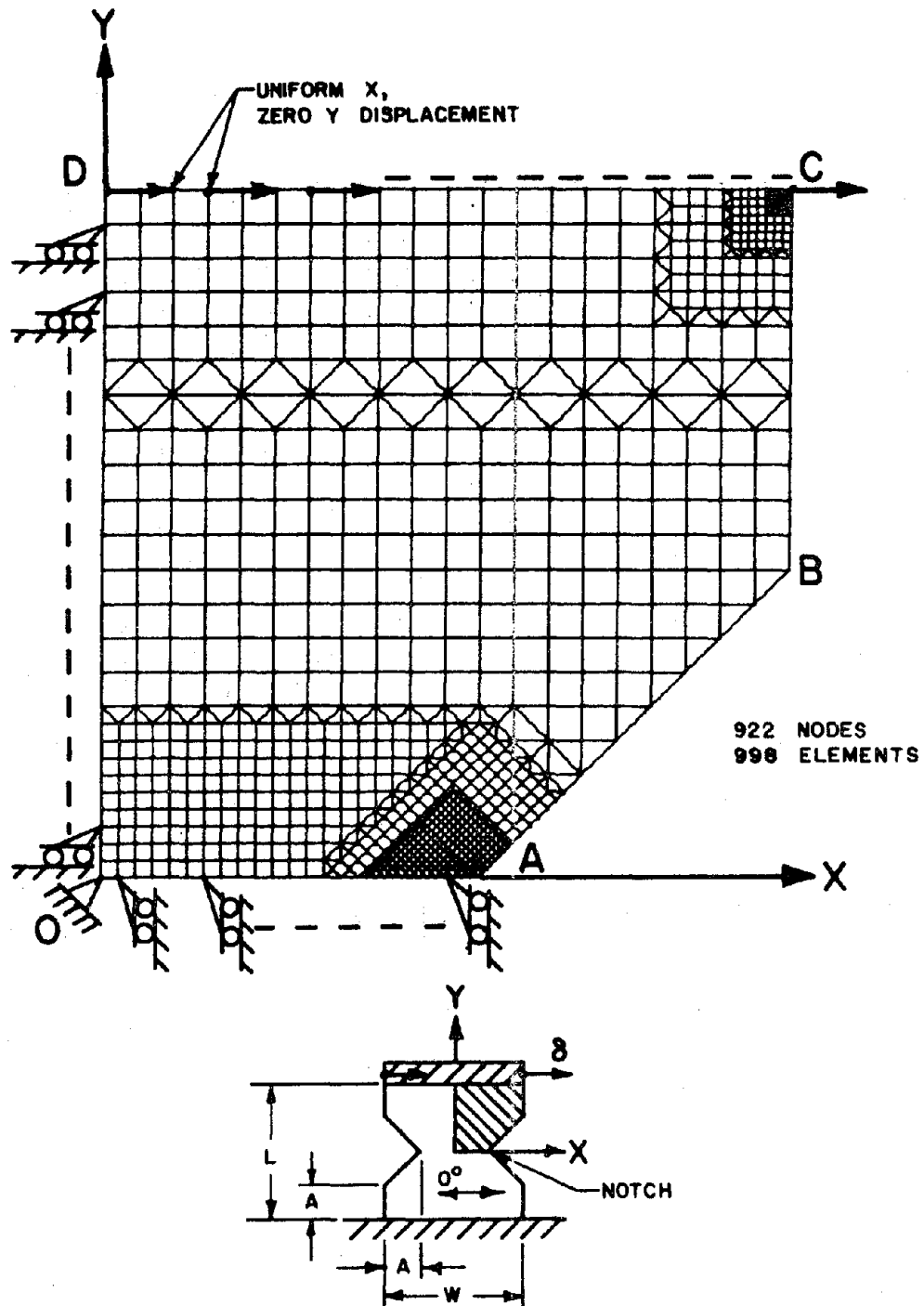


FIGURE 15. FINITE ELEMENT MODEL FOR IOSIPESCU SPECIMEN WITH RIGID FIXTURES

with respect to $\bar{\tau}$, the average shear stress along the line OA between the notches (Fig. 15).

6.2.2 Isotropic and Quasi-isotropic Materials

Normalized stress contours for an isotropic material (steel) and a quasi-isotropic material ($[0/90/\pm 45]_s$ graphite-polyimide) are shown in Figs. 16 and 17, respectively. The two stress distributions are nearly identical exhibiting essentially uniform pure shear in the test section. The normalized shear stress along the centerline OA ranges from 0.97 at the center O to 1.12 in the vicinity of the notch tip A (Table 1). As expected, stress concentrations are present at the corner C. These linear elastic results indicate that this specimen produces a very satisfactory stress distribution for determining the linear shear response of isotropic and quasi-isotropic materials. They are in agreement with the photoelastic results obtained by Iosipescu. It is also evident from these results that failure will initiate at the notch tip A or the corner C due to the stress concentrations in these regions.

6.2.3 The [0] Laminate

Normalized stress contours for a [0] laminate are shown in Fig. 18. The shear stress is pure, uniform, and maximum at the center of the specimen (point O), but is not uniform along the centerline OA, ranging from 1.10 at the center O to 0.48 at the notch tip. Stress concentrations are again present at the corner C. These linear elastic results indicate that the stress distribution at the center of the [0] specimen is suitable for linear shear response, however, the magnitude of this normalized shear stress is greater than 1.0 due to the nonuniform shear

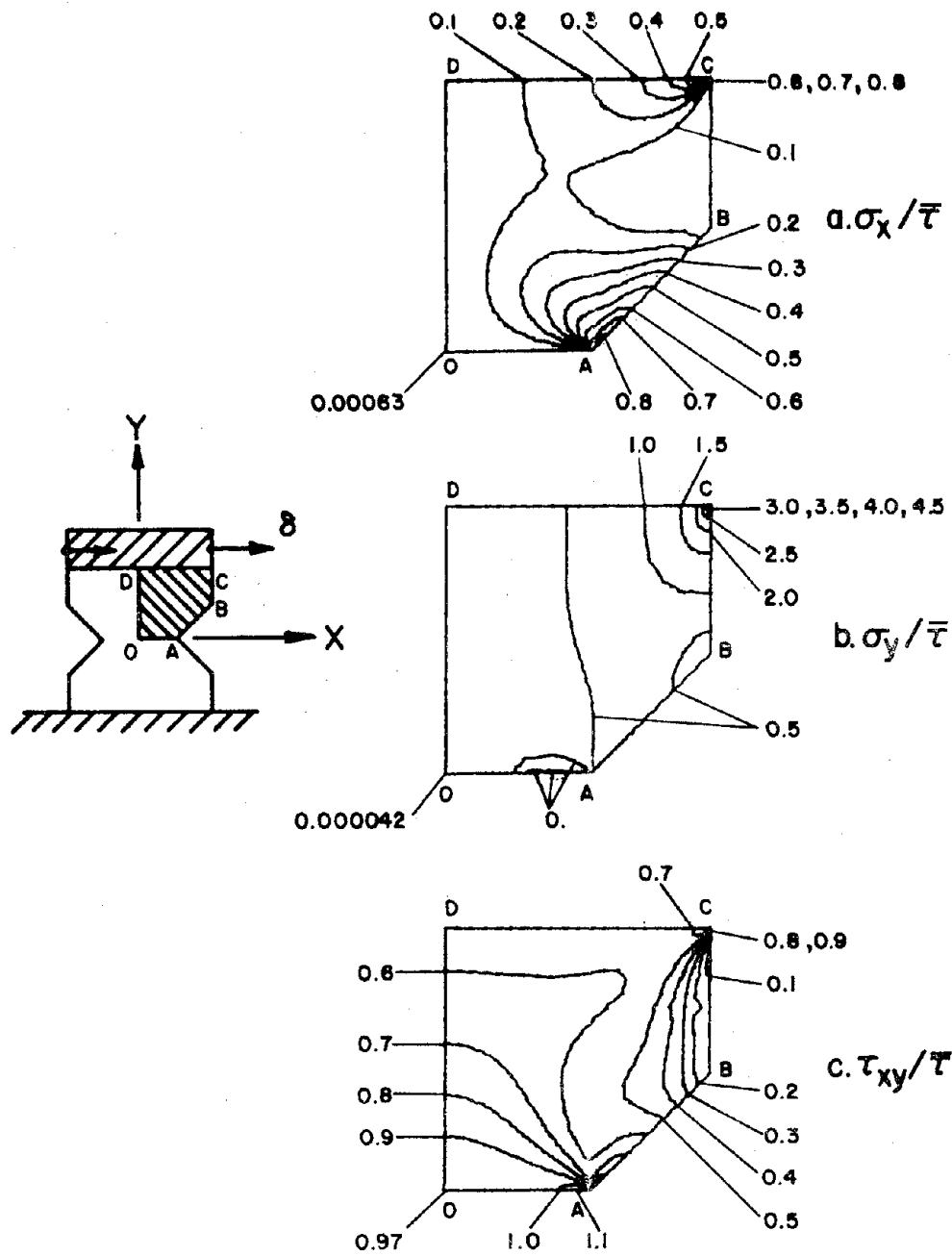


FIGURE 16. NORMALIZED STRESS CONTOURS FOR IOSIPESCU SPECIMEN WITH ISOTROPIC MATERIAL AND RIGID FIXTURES

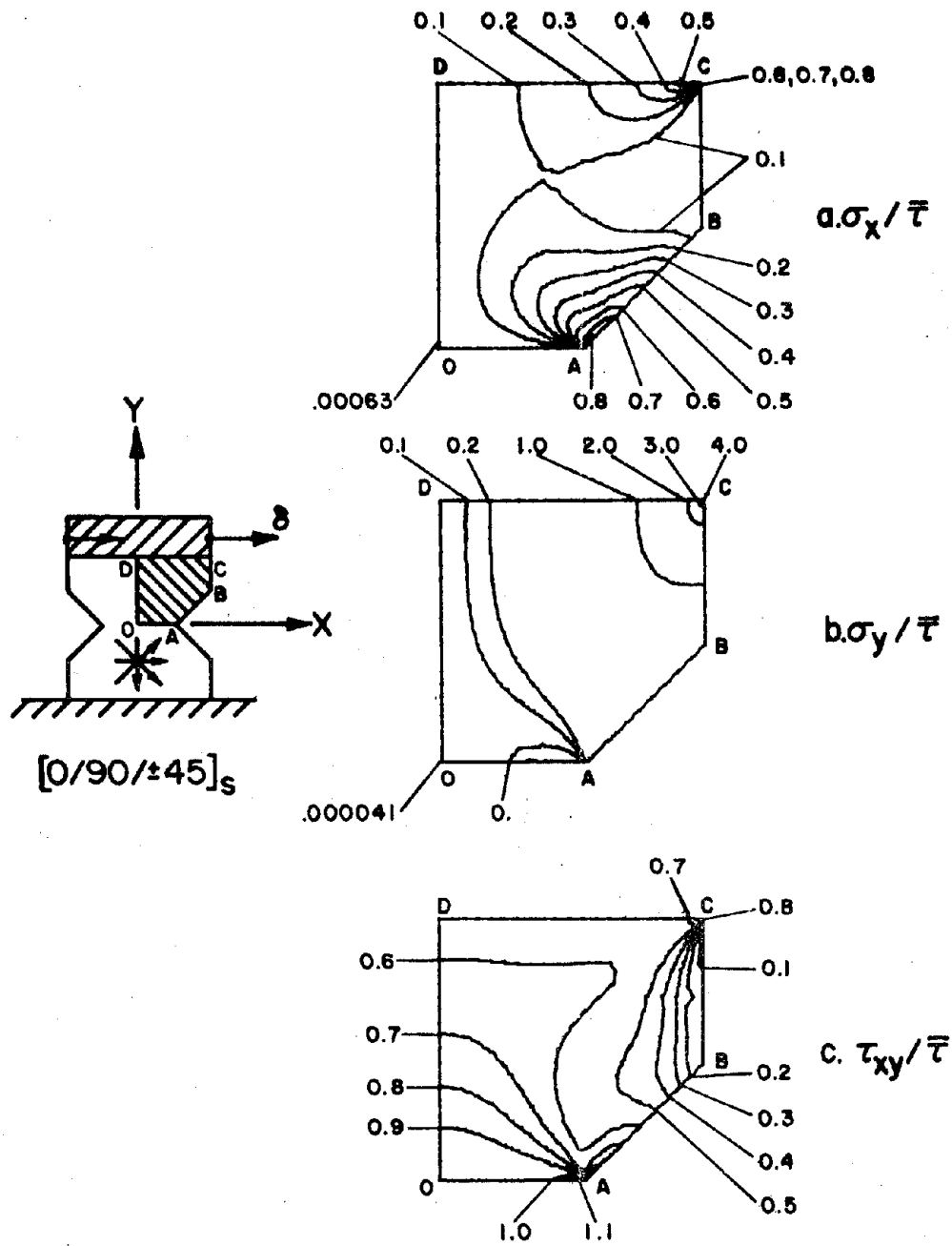


FIGURE 17. NORMALIZED STRESS CONTOURS FOR $[0/90/\pm 45]_s$ GRAPHITE-POLYIMIDE IOSIPESCU SPECIMEN WITH RIGID FIXTURES

stress distribution along the centerline OA. Since all stresses were rather low in magnitude at the notch tip, failure is expected at the corner C.

6.2.4 The $[90]_S$ Laminate

Normalized stress contours for a $[90]_S$ laminate are shown in Fig. 19. Although a pure, uniform shear stress at the center O is present, the distribution is very nonuniform along the centerline OA with normalized shear stress values ranging from 0.84 at the center to 1.94 at the notch tip A. Because this laminate exhibits a nonuniform shear stress distribution along OA, a stress factor relating the shear stress at the center of the specimen to the applied load (0.84) must be used in order to obtain accurate initial shear response. In addition, stress concentrations at the notch tip A will contribute to any failures.

6.2.5 The $[0/90]_S$ Laminate

Normalized stress contours for a $[0/90]_S$ laminate are shown in Fig. 20. The normalized shear stress along the centerline OA ranges from a maximum of 1.09 near the notch tip to a value of 0.96 at the center. As expected, stress concentrations are again present at the corner C. Since this laminate produces a very uniform region of pure shear in the test section, it will provide accurate linear shear response. These results also show that failure may initiate at the notch tip A or at the corner C due to the stress concentrations in these regions.

6.2.6 The $[\pm 45]_S$ Laminate

Normalized stress contours for a $[\pm 45]_S$ laminate are shown in Fig.

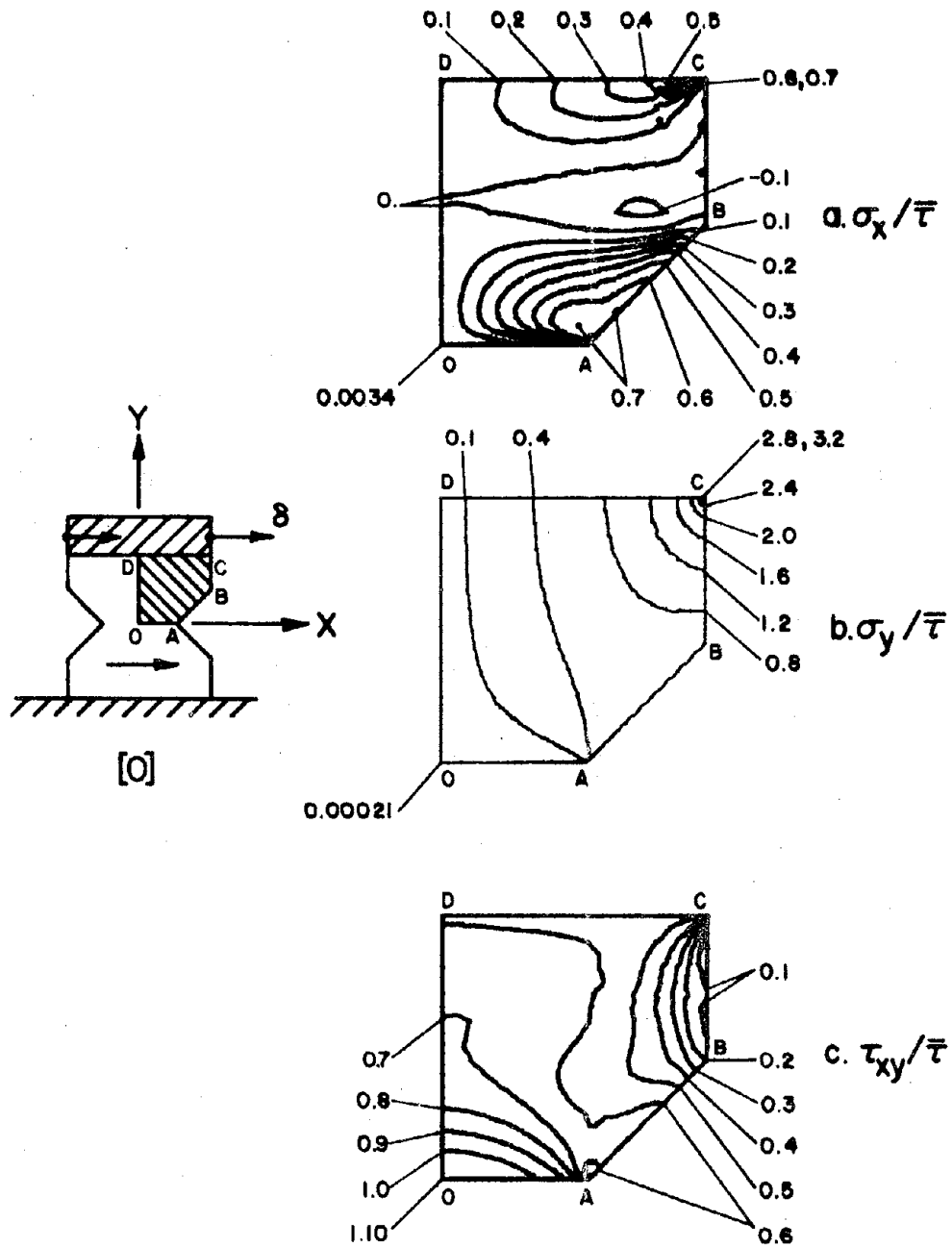


FIGURE 18. NORMALIZED STRESS CONTOURS FOR [0] GRAPHITE-POLYIMIDE IOSIPESCU SPECIMEN WITH RIGID FIXTURES

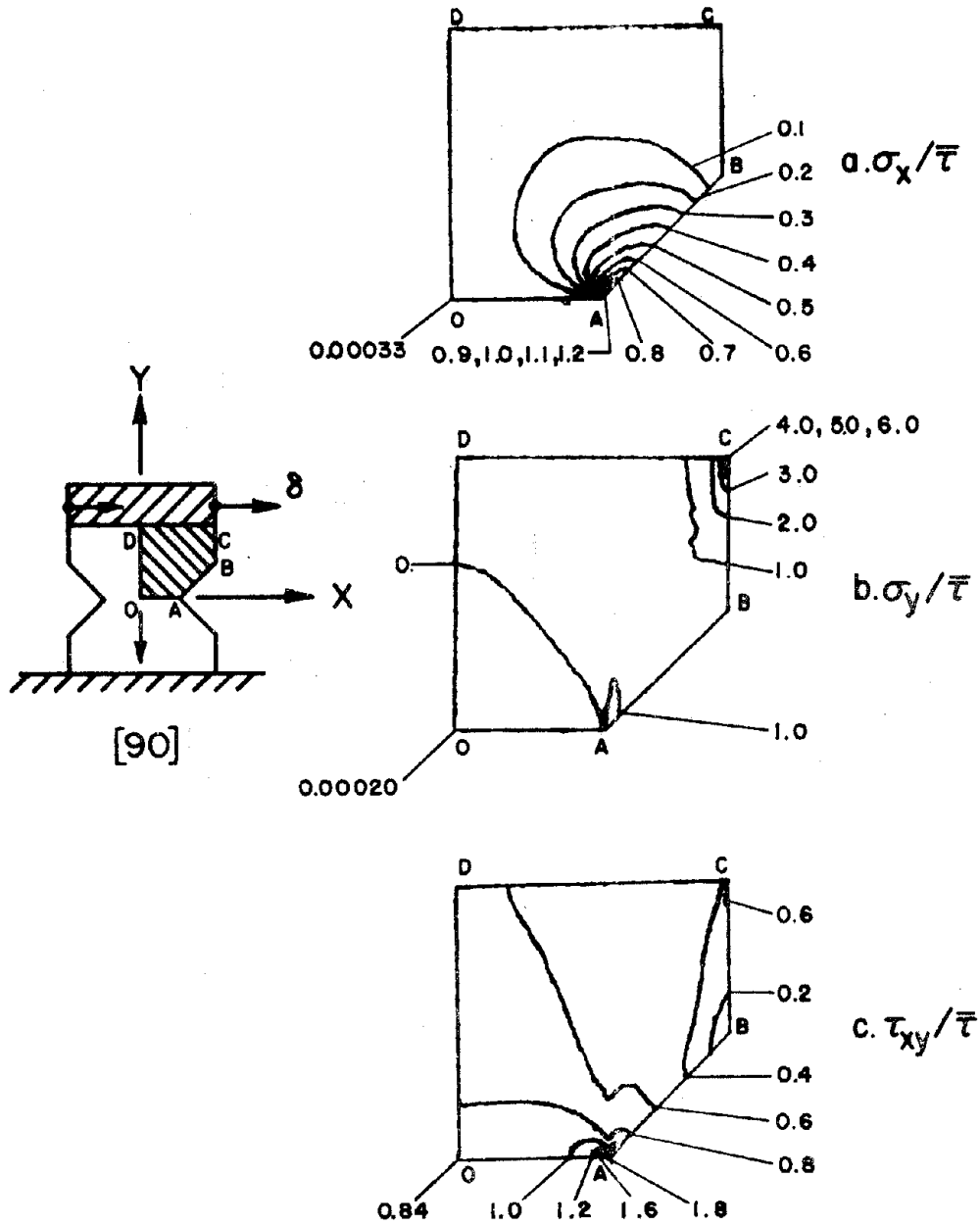


FIGURE 19. NORMALIZED STRESS CONTOURS FOR [90] GRAPHITE-POLYIMIDE IOSIPESCU SPECIMEN WITH RIGID FIXTURES

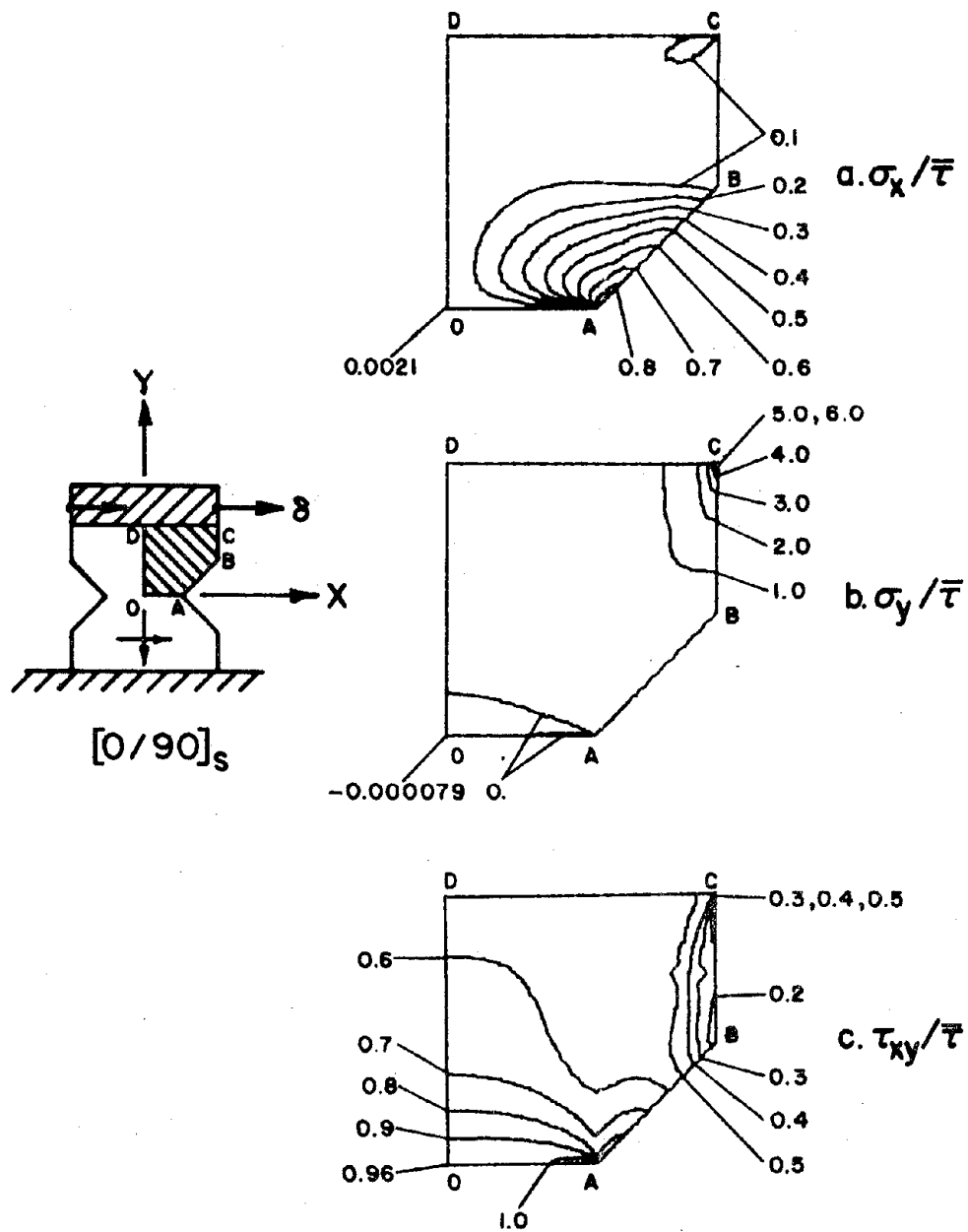


FIGURE 20. NORMALIZED STRESS CONTOURS FOR $[0/90]_s$ GRAPHITE-POLYIMIDE IOSIPESCU SPECIMEN WITH RIGID FIXTURES

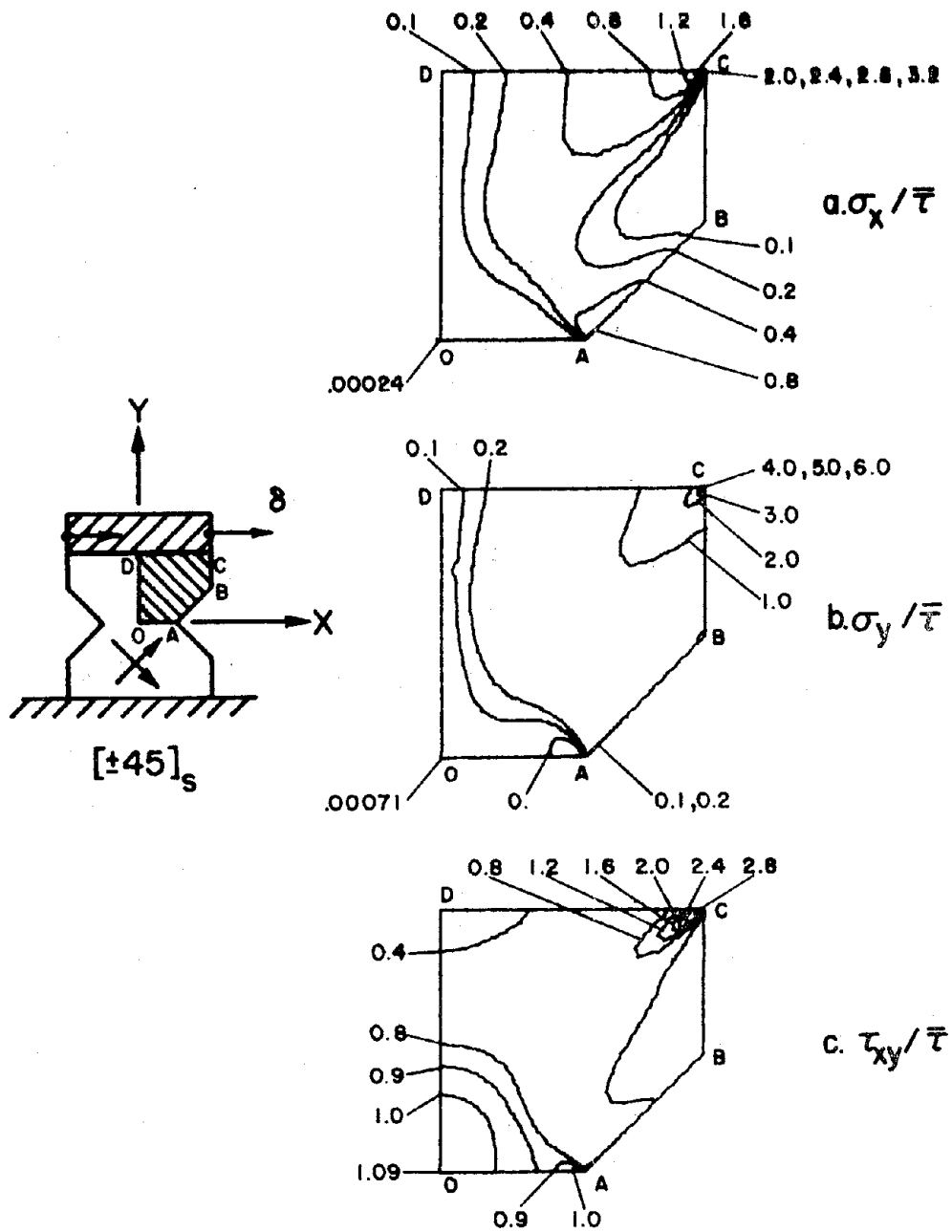


FIGURE 21. NORMALIZED STRESS CONTOURS FOR $[\pm 45]_s$ GRAPHITE-POLYIMIDE IOSIPESCU SPECIMEN WITH RIGID FIXTURES

TABLE 1. Normalized Stresses for Graphite-polyimide and Steel
Iosipescu Specimen with Rigid Fixtures.

		0 ¹	A ¹	C ¹
Steel	$\sigma_x/\bar{\tau}$	6.27×10^{-4}	0.42	0.89
	$\sigma_y/\bar{\tau}$	4.18×10^{-5}	0.35	4.70
	$\tau_{xy}/\bar{\tau}$	0.97	1.05	0.94
[0/90/±45] _s Gr/Pi	$\sigma_x/\bar{\tau}$	6.28×10^{-4}	0.42	0.82
	$\sigma_y/\bar{\tau}$	4.08×10^{-5}	0.35	4.61
	$\tau_{xy}/\bar{\tau}$	0.97	1.05	0.88
[0] Gr/Pi	$\sigma_x/\bar{\tau}$	3.41×10^{-3}	0.25	0.57
	$\sigma_y/\bar{\tau}$	2.12×10^{-4}	0.18	3.26
	$\tau_{xy}/\bar{\tau}$	1.10	0.48	0.43
[90] Gr/Pi	$\sigma_x/\bar{\tau}$	3.34×10^{-4}	0.56	8.46×10^{-2}
	$\sigma_y/\bar{\tau}$	-2.02×10^{-4}	0.62	6.91
	$\tau_{xy}/\bar{\tau}$	0.84	1.95	0.38
[0/90] _s Gr/Pi	$\sigma_x/\bar{\tau}$	2.06×10^{-3}	0.43	0.13
	$\sigma_y/\bar{\tau}$	-7.92×10^{-5}	0.34	6.26
	$\tau_{xy}/\bar{\tau}$	0.96	1.02	0.40
[±45] _s Gr/Pi	$\sigma_x/\bar{\tau}$	2.38×10^{-4}	0.41	3.32
	$\sigma_y/\bar{\tau}$	7.18×10^{-4}	0.33	6.38
	$\tau_{xy}/\bar{\tau}$	1.09	1.06	3.17

¹See Figure 15.

21. The shear stress distribution in the vicinity of the center of the specimen is essentially pure and uniform. The normalized shear stress along the centerline OA ranges from a maximum of 1.10 near the notch tip to a minimum of 0.89 between O and A. The value at the center of the specimen is 1.09. All stress components are unusually high at the corner C. These linear elastic results indicate that this specimen produces a very satisfactory stress distribution for determining the linear shear response of a $[\pm 45]_S$ laminate. It is also evident that failure will initiate at the corner C due to the stress concentrations in this region.

6.3 Elastic Fixture Results

6.3.1 Mechanical Loading

The finite element representation for the specimen with elastic fixtures is shown in Fig. 22. This finite element representation is a two-dimensional elastic model of a specimen with four steel fixtures (each with a thickness $T_f = 0.25W$) bonded to the test material. Lamination theory was used to predict the elastic properties of the fixture - composite laminate. All dimensions were the same as those used in section 6.2 and in addition: $A = 0.25W$; fixture dimensions, $F_1 = 0.65W$, $F_2 = 0.25W$, $F_3 = 0.1W$; fixture angle, $\theta_f = 45^\circ$; and specimen thickness, $T_C = 0.0384W$ (10 plies of graphite-polyimide, 0.00768"/ply). The stresses were normalized with respect to the average shear stress determined from the given applied load and the area of the specimen between the notch tips A and B.

419 NODES
434 ELEMENTS

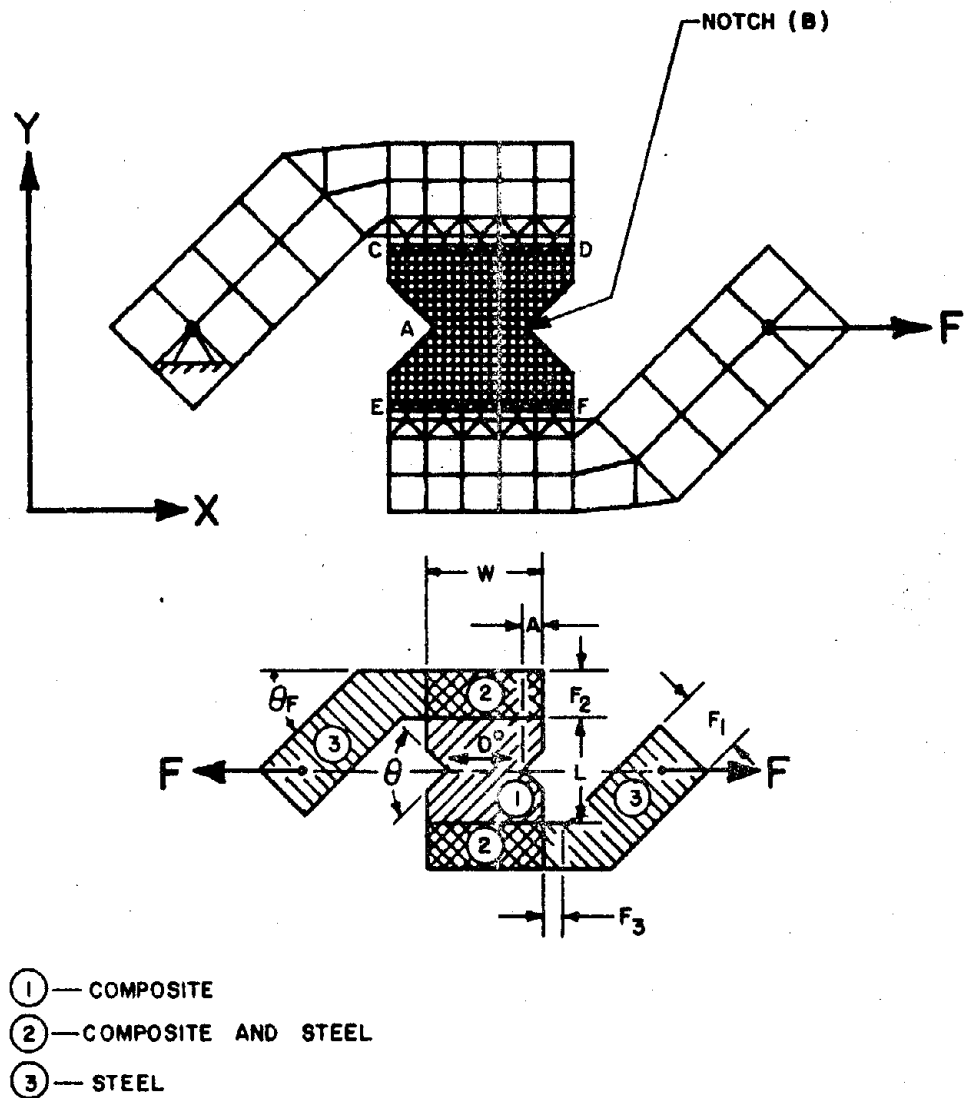


FIGURE 22. FINITE ELEMENT MODEL FOR IOSIPESCU SPECIMEN WITH ELASTIC FIXTURES

6.3.1.1 Isotropic Material

Normalized stress contours for an isotropic specimen (steel) are shown in Fig. 23. A pure uniform shear stress distribution exists along the centerline AB with normalized values ranging from 0.89 at the notch tips A and B to a maximum value of 0.93 at the center of the specimen. It is obvious that these results, which were obtained from a rather coarse finite element mesh, do not satisfy overall force equilibrium exactly since the total shear force transmitted across the test section is not equal to the applied load.

These results can nevertheless be compared to the rigid fixture solution (Fig. 16) in a general manner. With the exception of the lack of quarter symmetry near the elastic fixtures, the shape of the stress contours are very similar. The largest difference occurs near the corners C-F of Fig. 23 where the deformation of the elastic fixtures has the greatest effect on the specimen. Along the centerline AB (with rigid or elastic fixtures) the effects of bending in the fixtures are clearly diminished because of the symmetries that must exist there. This feature of the stress distributions is evident when the shapes of the 0.6 and 0.9 contour lines in Fig. 23c are compared. Therefore, although failure may initiate at the points A-F, this specimen produces a satisfactory stress distribution for determining linear shear response of isotropic materials.

6.3.1.2 The [0] Laminate

The normalized stress contours for a [0] laminate are shown in Fig. 24. The shear stress distribution along the centerline AB is essentially

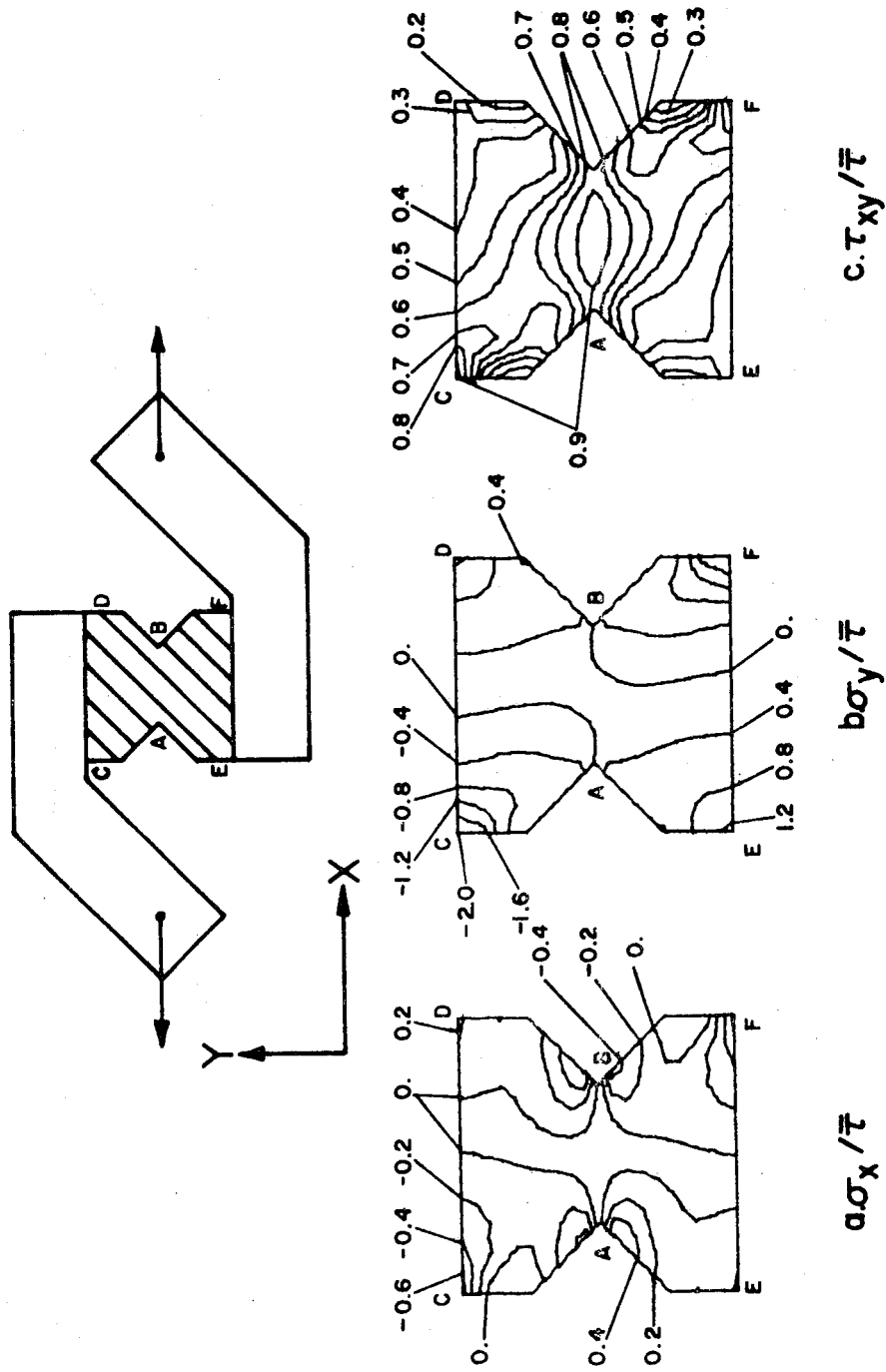


FIGURE 23. NORMALIZED STRESS CONTOURS FOR IOSIPESCU SPECIMEN WITH ISOTROPIC MATERIAL AND ELASTIC FIXTURES

pure, uniform, and maximum at the center of the specimen. The normalized values range from 0.72 at the notch tips A and B to 1.03 at the center of the specimen. Similar to the isotropic specimen, the fixture effects are minimal as a comparison of Figs. 18 and 24 shows. It is also evident from these results that failure is expected to initiate at the notch tips A or B or at the corners C, D, E, or F due to the stress concentrations in these regions.

6.3.2 Thermal Loading

In this section the effects of applying a temperature change of -600°F to a complete stress free specimen (laminate bonded to fixtures) are studied. This loading simulates the elastic behavior resulting from an elevated temperature bond of the fixtures to the specimen. The [0] laminate was used for this analysis with the mesh shown in Fig. 22 ($F = 0$). Contour plots for σ_x , σ_y , and τ_{xy} normalized with respect to their corresponding ultimate stress values, $(\sigma_x)_{ult}$, $(\sigma_y)_{ult}$, and $(\tau_{xy})_{ult}$ are shown in Fig. 25.

The most significant feature of the results is that the thermal stresses are negligible in the test section for all stress components. Normalized σ_y and τ_{xy} stresses are both very high at the corners with maximum values of -2.49 and 1.72, respectively. As expected, the stress in the fiber direction was quite low throughout the specimen with a maximum normalized value of -0.29 at the fixture-specimen interfaces CD and EF. If the specimen was mechanically loaded and the behavior was elastic, a superposition of the stresses depicted in Figs. 24 and 25

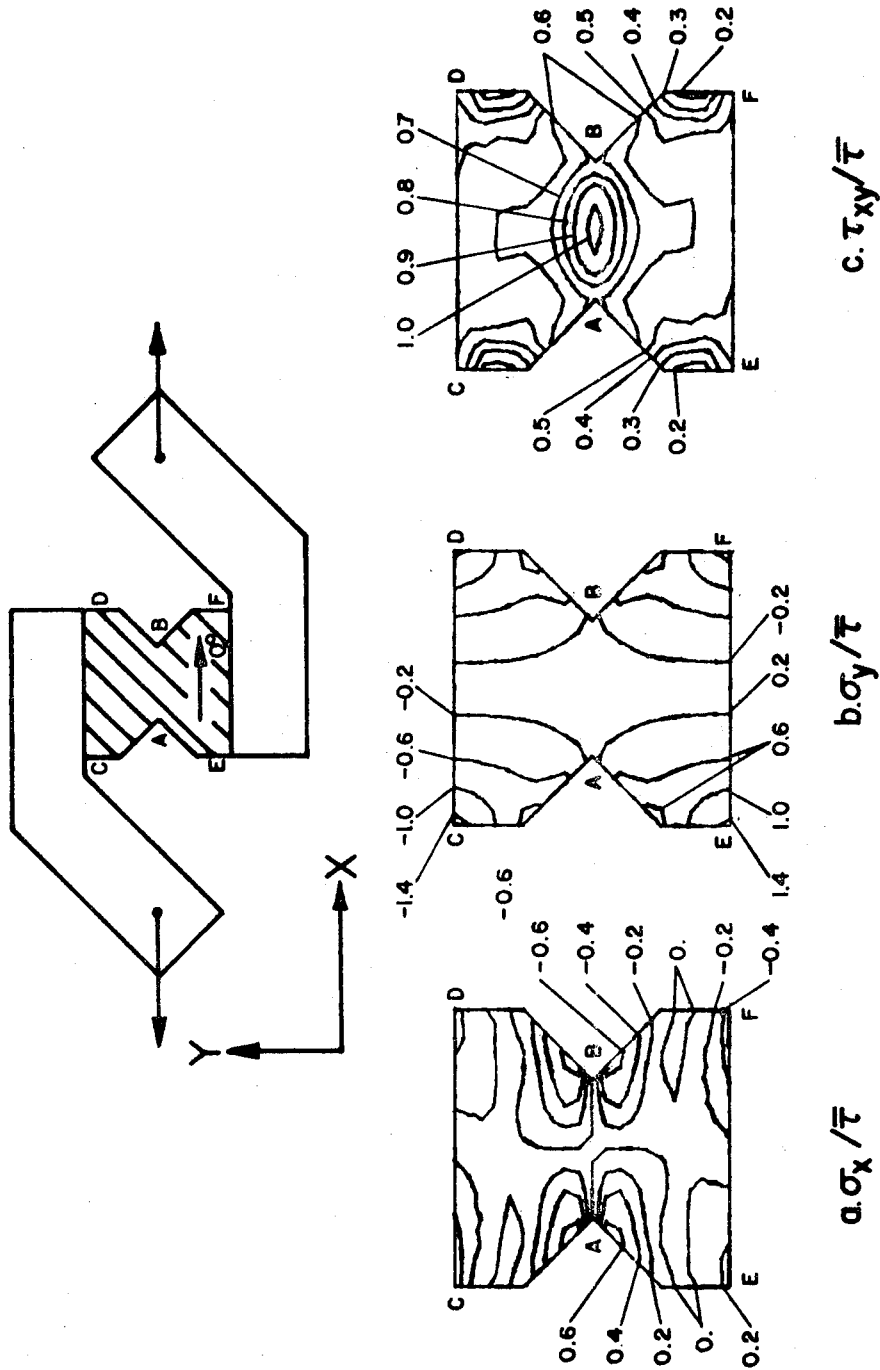


FIGURE 24. NORMALIZED STRESS CONTOURS FOR [0] GRAPHITE-POLYIMIDE IOSIPESCU SPECIMEN WITH ELASTIC FIXTURES

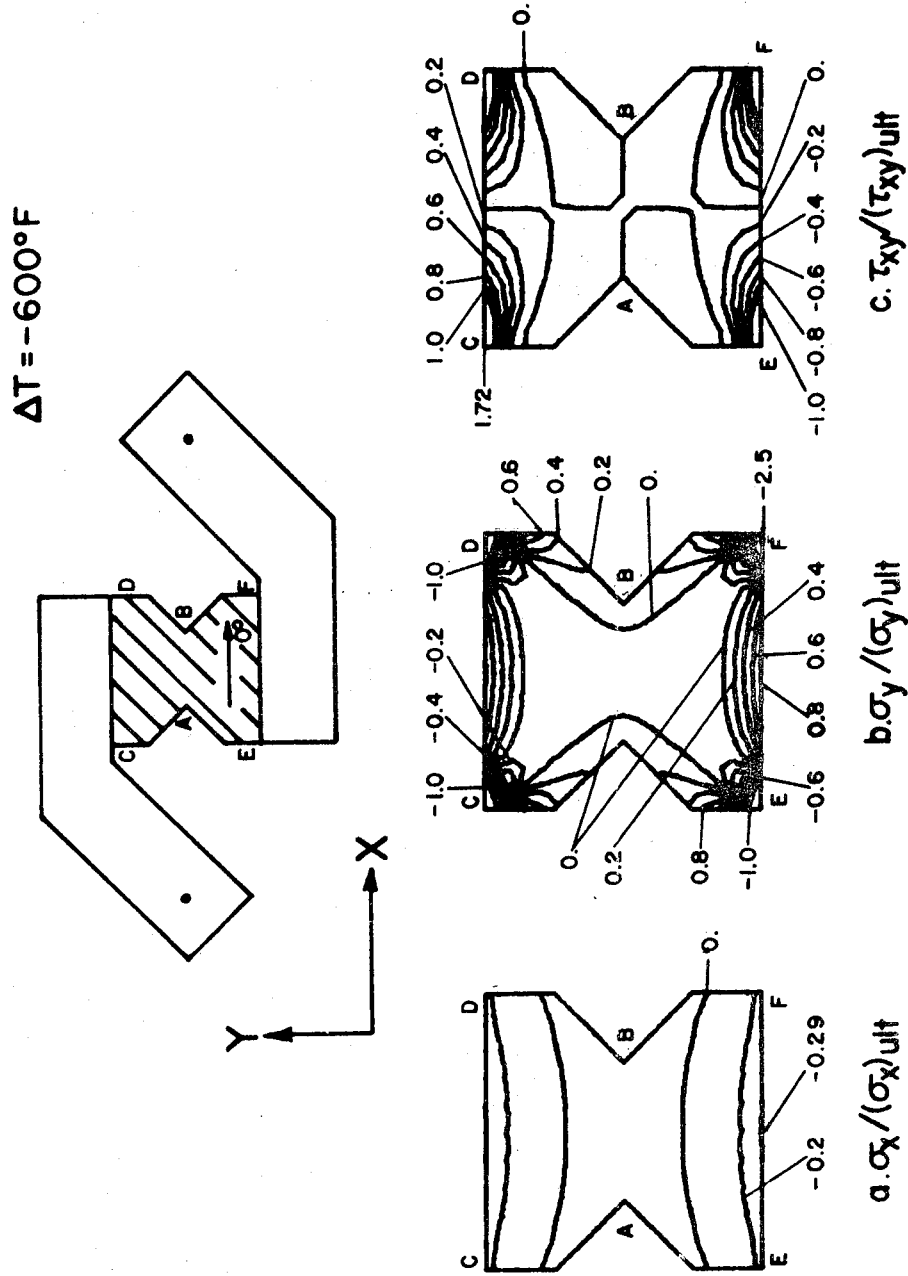


FIGURE 25. NORMALIZED STRESS CONTOURS FOR THERMALLY LOADED [O] GRAPHITE-POLYIMIDE IOSIPESCU SPECIMEN WITH ELASTIC FIXTURES

would give the combined stress distribution. Although the corner stresses at D and E would cancel one another for combined mechanical and thermal loading, the stresses at corners C and F would be additive. For this reason fixtures should be bonded to specimens at the desired test temperature in order to minimize the stress concentration at corners C and F.

6.4 Other Results

6.4.1 Doubler Effects

In addition to the elastic and rigid fixture cases described previously, the effect of doubling the stiffness (doubling the thickness in practice) of the test specimen in the vicinity of the corners was studied. The results showed that other things being equal (dimensions, loads, etc.), doubling the stiffness in the vicinity of the fixture/specimen interface reduced the stress concentrations in this region by approximately 50 percent (Table 2) while the stress distribution in the center of the specimen remained virtually unaltered. These results are significant because they indicate that the high corner stresses can be reduced to reasonable values through the use of doublers without significantly effecting the stress distribution in the test section.

6.4.2 Aspect Ratio Effects

The influence of specimen aspect ratio, $R = L/W$ (Fig. 22), was investigated for $R = 1.0$ and $R = 2.5$. The stresses in the test section of the specimen were not appreciably effected for the elastic and rigid fixture cases studied, however, the corner stresses were significantly

TABLE 2. Effects of Doublers and Aspect Ratios for the Iosipescu Specimen.

[0] Gr/Pi	With Doublers			Without Doublers		
	σ^1	A ¹	C ¹	0	A	C
R = 2.5 A = 0.225 W Rigid Fixtures	σ_x/τ	1.81×10^{-2}	0.60	1.81×10^{-2}	0.48	0.30
	σ_y/τ	1.87×10^{-3}	5.19	1.86×10^{-3}	0.27	2.60
	τ_{xy}/τ	1.10	0.59	1.10	0.61	0.30
		R = 1.0			R = 2.5	
[0] Gr/Pi A = 0.225 W Rigid Fixtures	0	A	C	0	A	C
	σ_x/τ	3.41×10^{-3}	0.25	0.57	3.35×10^{-3}	1.30
	σ_y/τ	2.12×10^{-4}	0.18	3.26	2.38×10^{-4}	6.10
τ_{xy}/τ	1.10	0.48	0.43	1.10	0.48	0.66
		R = 1.0			R = 2.5	
[0] Gr/Pi A = 0.225 W Elastic Fixtures	Center	A ² , B ²	D ² , E ²	C ² , F ²	Center	A, B D, E C, F
	σ_x/τ	-1.13×10^{-3}	-5.08×10^{-4}	0.39	-0.54	-3.07×10^{-5}
	σ_y/τ	3.53×10^{-4}	-4.71×10^{-4}	0.29	-1.52	8.45×10^{-6}
τ_{xy}/τ	1.03	0.72	1.47	0.48	1.04	0.37 0.46

¹See Figure 15.²See Figure 22.

TABLE 3. Graphite-epoxy and Graphite-polyimide Normalized Stresses
for Iosipescu Specimen with Rigid Fixtures ($R = 2.5$).

	Graphite-epoxy			Graphite-polyimide			
	0^I	A^I	C^I	0	A	C	
[0]	σ_x/τ	1.49×10^{-3}	0.39	0.54	1.33×10^{-3}	0.42	0.79
	σ_y/τ	1.07×10^{-4}	0.21	4.49	9.09×10^{-5}	0.24	4.56
	τ_{xy}/τ	1.16	0.47	0.58	1.10	0.53	0.59
[90]	σ_x/τ	6.75×10^{-5}	0.70	4.20×10^{-2}	1.06×10^{-4}	0.71	8.67×10^{-2}
	σ_y/τ	-5.29×10^{-5}	0.72	6.78	-5.52×10^{-3}	0.68	7.02
	τ_{xy}/τ	0.89	1.83	0.41	0.90	1.66	0.47
[0/90] _s	σ_x/τ	6.53×10^{-4}	0.60	7.50×10^{-2}	Not Available		
	σ_y/τ	1.22×10^{-7}	0.41	6.06	Not Available		
	τ_{xy}/τ	1.01	0.93	0.44	Not Available		
[±45] _s	σ_x/τ	1.40×10^{-5}	0.70	3.02	6.66×10^{-6}	0.71	3.29
	σ_y/τ	2.34×10^{-5}	0.56	6.24	2.51×10^{-5}	0.57	6.39
	τ_{xy}/τ	0.93	1.27	2.83	0.93	1.30	3.06
[0/90/±45] _s	σ_x/τ	2.32×10^{-4}	0.61	0.84	2.23×10^{-4}	0.61	0.92
	σ_y/τ	3.22×10^{-5}	0.45	5.20	3.22×10^{-5}	0.45	5.25
	τ_{xy}/τ	0.98	1.04	0.87	0.98	1.04	0.92

¹See Figure 15.

higher for the specimens with $R = 2.5$ (Table 2). These higher stresses were the result of the higher bending moments introduced from the fixtures into the specimen for $R = 2.5$. The effect of different materials (graphite-epoxy and graphite-polyimide) was also studied for $R = 2.5$ (Table 3) using a coarse mesh with rigid fixtures. The stress values for the graphite-epoxy and graphite-polyimide were virtually identical as indicated in the table. With the exception of the $[\pm 45]_S$ laminate, the shear stresses for $R = 2.5$ for these two materials also compare to the shear stresses at the center of the specimen for $R = 1.0$ (Table 2).

6.4.3 Rounded Notch Effects

The effects of rounding the notch tips were studied for both $[0]$ $[90]$ laminates. This was done by adding a "fillet", or round with a radius of $0.0325W$ to the notch tip. The normalized stress distributions along the line $y = 0$ in the vicinity of the notch tip are shown in Figs. 26 and 27 for the $[0]$ and $[90]$ laminates, respectively. For the $[0]$ laminate all components of stress are considerably lower near the free edge with the rounded notch. However, the round causes the shear distribution to become more nonuniform, and as a result the normalized shear stress at the center of the specimen is higher than that of the V-notched specimen (Table 4). As indicated in Fig. 27, rounding the notch for a $[90]$ laminate results in σ_x and τ_{xy} approaching zero near the free edge. However, σ_y remains very high. Since the shear stress distribution for the rounded notch is more uniform, the corresponding normalized shear stress at the center of the specimen is more nearly equal to 1.0. Thus while σ_x and τ_{xy} are always zero at the free edge of

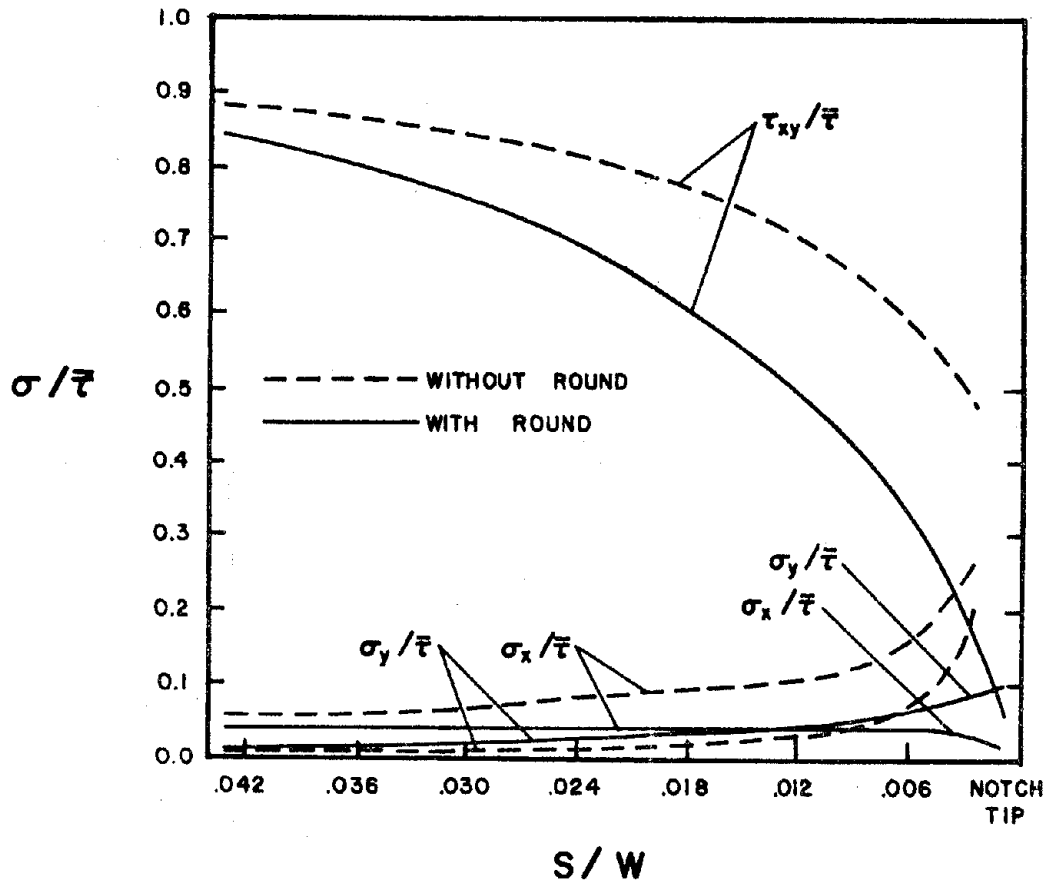
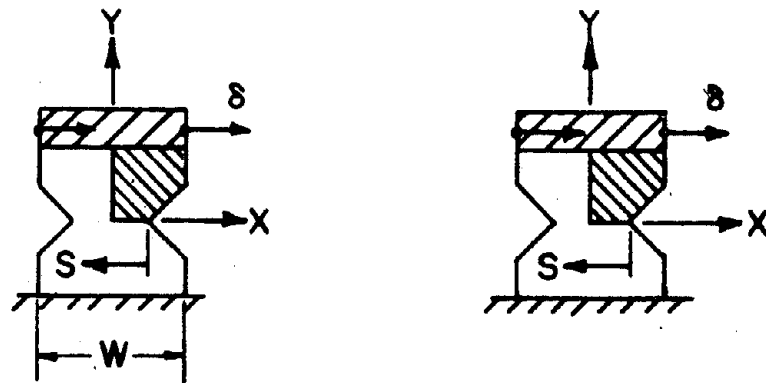


FIGURE 26. ROUNDED NOTCH EFFECTS FOR THE [0] IOSIPESCU SPECIMEN ALONG $Y=0$

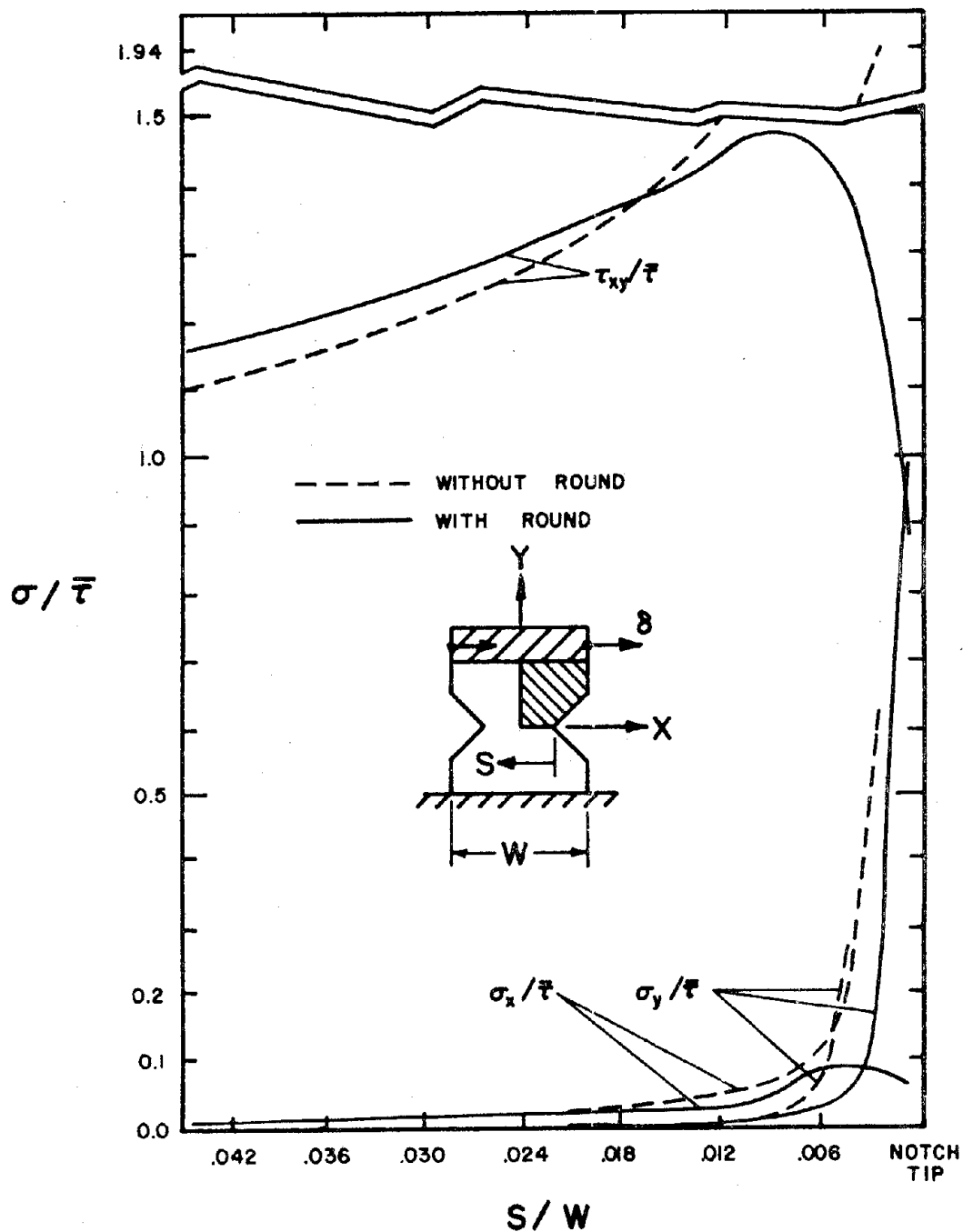


FIGURE 27. ROUNDED NOTCH EFFECTS FOR THE [90] IOSIPESCU SPECIMEN ALONG $Y=0$

TABLE 4. Normalized Stresses for V-notch and Rounded Notch
Iosipescu Specimens with Rigid Fixtures.

	V-notch		Rounded Notch		
	0^I	A^I	0	A	
[0] Gr/Pi	$\sigma_x/\bar{\tau}$	3.41×10^{-3}	0.25	3.40×10^{-3}	1.24×10^{-2}
	$\sigma_y/\bar{\tau}$	2.12×10^{-4}	0.18	2.30×10^{-4}	9.71×10^{-2}
	$\tau_{xy}/\bar{\tau}$	1.10	0.48	1.14	7.28×10^{-2}
[90] Gr/Pi	$\sigma_x/\bar{\tau}$	3.34×10^{-4}	0.56	3.28×10^{-4}	6.69×10^{-2}
	$\sigma_y/\bar{\tau}$	-2.02×10^{-4}	0.62	-1.98×10^{-4}	0.94
	$\tau_{xy}/\bar{\tau}$	0.84	1.94	0.87	0.91

¹See Figure 15.

a rounded notch, the uniformity of the shear stress distribution is a function of the modulus ratio E_x/E_y .

6.5 Summary

While the Iosipescu specimen produces a region of uniform shear stress at the center of the specimen for isotropic and orthotropic materials, the uniformity of the shear stress between the notch tips is highly dependent upon the elastic properties of the laminate. This feature was most evident for the unidirectional laminates. Also, the complex state of stress at the notch tips and corners undoubtedly contributes to failure. This specimen can accurately provide initial shear modulus values for isotropic and orthotropic materials. Bonding suitable doublers to the corners and rounding the notch tips can reduce the stress concentrations in critical areas. Thermal stresses are not significant in the center of the specimen.

7. THE RAIL SHEAR SPECIMEN

7.1 General

As mentioned previously, the rail shear specimen has been used to obtain linear and nonlinear shear stress-strain response for composite laminates at both room temperature and elevated temperatures. For experimental work, it has been assumed that the specimen is subjected to pure, uniform shear stress with the magnitude of the shear stress directly related to the applied load through a simple P/A relationship. The finite element results presented here show to what extent these assumptions are valid. The effects of material properties, thermal loads, and rail configurations for both rigid and elastic rails are presented to more fully understand the elastic behavior of this specimen and to more accurately determine the relationship between the applied load and the stress distribution in the test section.

7.2 Rigid Rail Solutions

7.2.1 Fourier Series Representation

A Fourier series solution was presented [8] as the superposition of two problems with the boundary conditions (Fig. 29) for each problem being:

$$\text{problem 1. } u(x,0) = v(x,0) = v(x,b) = 0$$

$$N_x(0,y) = N_x(a,y) = 0$$

$$u(x,b) = \delta \quad (7.1)$$

$$N_{xy}(0,y) = N_{xy}(a,y) = A_{66} \frac{\delta}{b}$$

$$\text{problem 2. } u(x,0) = u(x,b) = v(x,0) = v(x,b) = 0$$

$$N_x(0,y) = N_x(a,y) = 0 \quad (7.2)$$

$$N_{xy}(0,y) = N_{xy}(a,y) = -A_{66} \frac{\delta}{b},$$

where N_i and A_{66} are defined from equations (3.7) and (3.9). These boundary conditions assume that the actual specimen is perfectly bonded to rigid rails and that uniform rail spacing is maintained during loading. The solution to problem 1 leads to a state of pure shear with the displacements

$$u = \frac{\delta}{b} y ; v = 0. \quad (7.3)$$

The solution to the second problem was assumed to be of the form

$$u = \sum_{m=1}^{\infty} \sum_{n=0}^{\infty} A_{mn} \sin \frac{(2m-1)\pi x}{a} \sin \frac{2n\pi y}{b} \quad (0 < x < a; 0 < y < b) \quad (7.4)$$

$$v = \sum_{m=1}^{\infty} \sum_{n=0}^{\infty} B_{mn} \cos \frac{(2m-1)\pi x}{a} \cos \frac{2n\pi y}{b} \quad (0 < x < a; 0 < y < b)$$

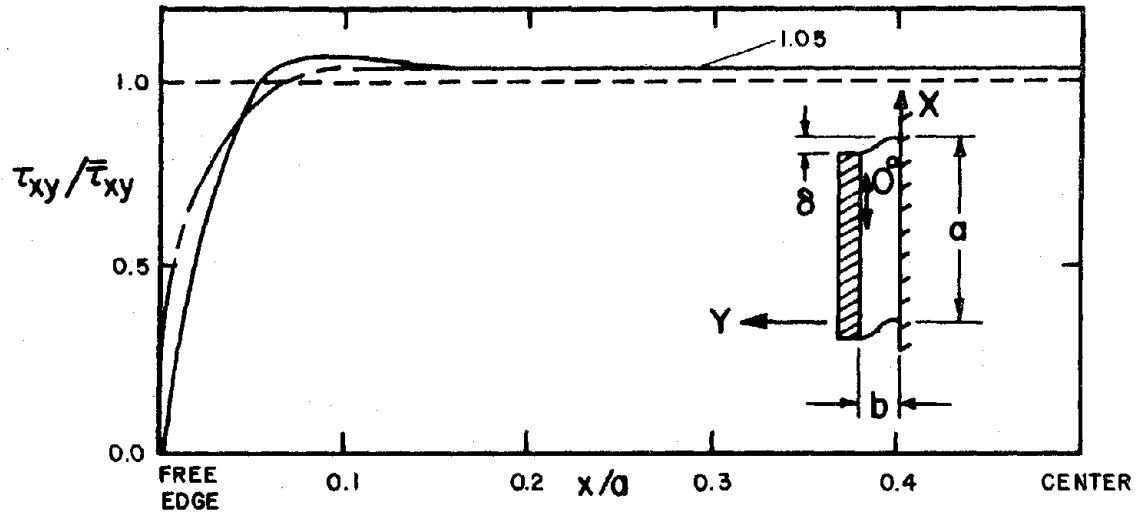
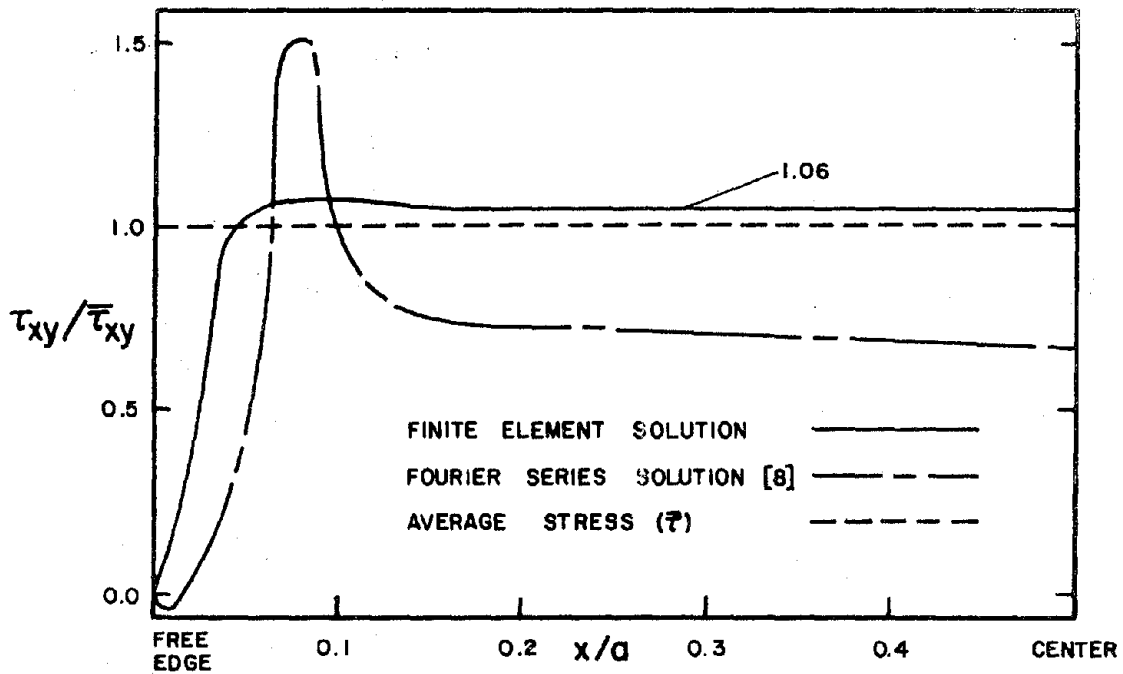
The superposition of the two solutions result in an infinite $m+n$ system of linear equations with unknown Fourier coefficients. Adequate convergence of the infinite series was obtained by truncating the system of equations to 24 terms. The Fourier coefficients were computed and stresses were determined as a function of position.

7.2.2 Comparison of Fourier Series and Finite Element Results

Fourier series solutions are compared to finite element results for $[0/\pm 45]_S$ and $[\pm 45]_S$ Thorne1 50 graphite-epoxy in Fig. 28. The finite element representations used are shown in Fig. 29 along with boundary conditions for the problem. Results were obtained for a specimen aspect ratio $a/b = 12$. Fig. 28 shows the distribution of the shear stress, normalized with respect to the average shear stress, along the centerline of the specimen $y = b/2$.

As indicated in Fig. 28a, the two solutions exhibited very similar results for the $[0/\pm 45]_S$ laminate. The normalized shear stress is uniform over almost 80 percent of the specimen at a value of 1.05. This value is necessarily greater than 1.0 to account for the shear stress approaching zero at the free edge.

The results for the $[\pm 45]_S$ laminate shown in Fig. 28b do not exhibit the same high degree of correlation. The finite element results are very similar to those of the $[0/\pm 45]_S$ laminate with the normalized shear stress uniform over almost 90 percent of the specimen at a value of 1.06. The Fourier series results exhibit a spike with a maximum value of 1.5 a small distance in from the free edge and then exhibit a continuously decreasing stress magnitude toward the center of the specimen. Because of the difference in these results, additional finite element results were obtained using the model shown in Fig. 29b. The results obtained with the refined mesh were so similar to those of the basic mesh that they cannot be distinguished in Fig. 28b. The finite element results are believed to be more accurate than the Fourier series

a. $[0/\pm 45]_s$ LAMINATEb. $[\pm 45]_s$ LAMINATEFIGURE 28. COMPARISON OF RIGID RAIL SOLUTIONS FOR THORNEL 50 GRAPHITE-EPOXY AT $Y=b/2$

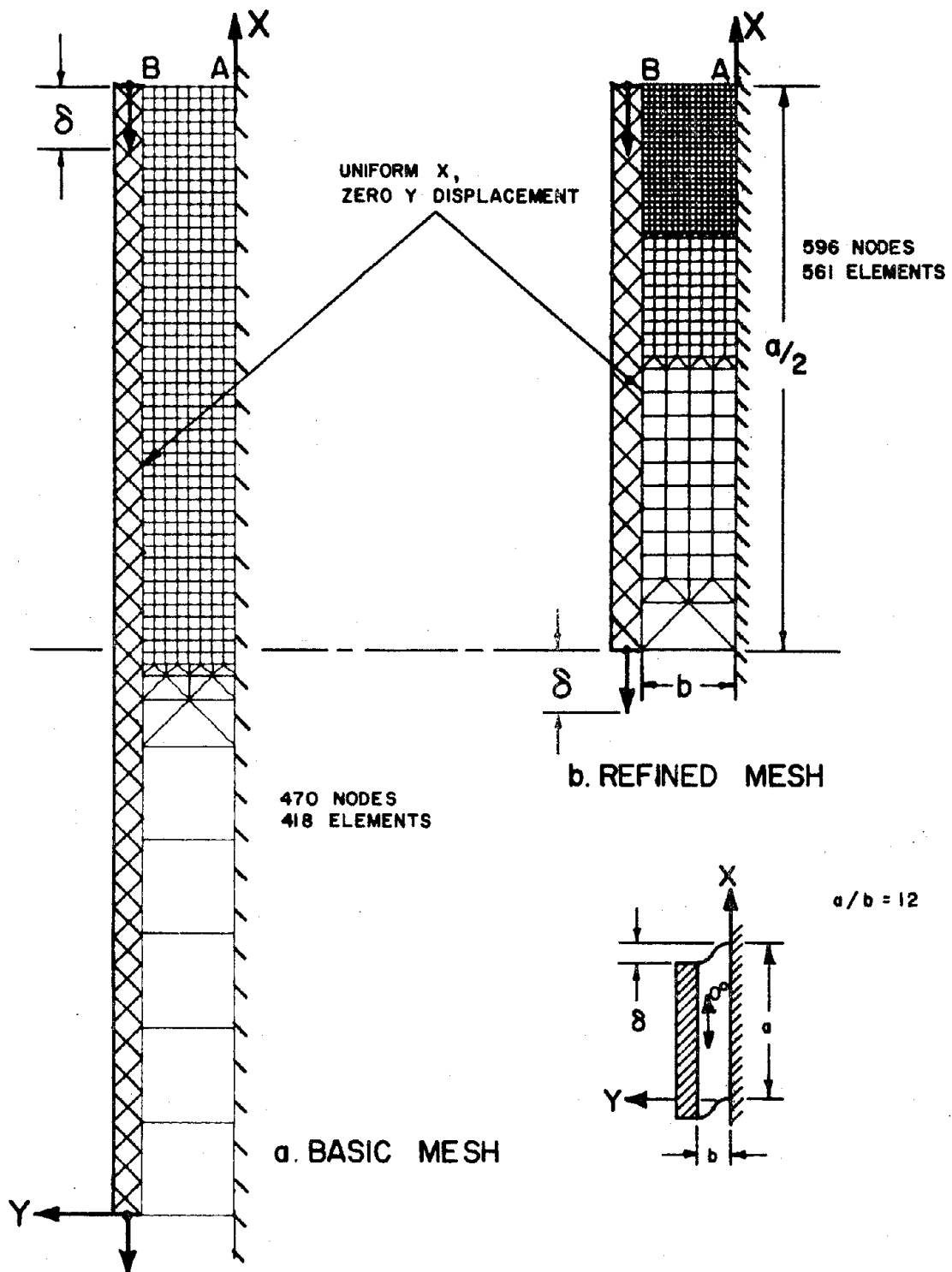


FIGURE 29. FINITE ELEMENT MODELS FOR RAIL SHEAR SPECIMEN WITH RIGID RAILS

results¹ for this $[\pm 45]_S$ laminate due to the proven capabilities of the method, the consistency with the $[0/\pm 45]_S$ laminate, and the more physically appealing stress distribution.

The finite element results indicated that both laminates exhibited high normal stresses in the vicinity of corners, but these normal stresses were negligible over 80 percent of the specimen. Thus, these results indicate that this specimen produces an essentially pure, uniform distribution of shear stress in the test section with the stress magnitude equal 1.05 and 1.06 times the average shear stress $\bar{\tau}$ for $[0/\pm 45]_S$ and $[\pm 45]_S$ laminates, respectively.

7.3 Elastic Rails

7.3.1 Effects of Offset Loading and Tapered Rails

The effects of nontapered and tapered rail configurations loaded along the centerline, and nontapered rails with offset loading for a $[0]$ graphite-polyimide laminate were studied. The finite element mesh for the nontapered rail configuration with axial loading is shown in Fig. 30. The dimensions of the specimen were standardized to: specimen length, $L = 10W$; fixture dimensions, $F_1 = 5.83W$, $F_2 = 3.33W$, $F_3 = 6.67W$, $F_4 = 1.23W$; rail thickness, $T_r = 3.33W$; and composite thickness, $T_c = 0.256W$. Appropriate steel, steel and composite (from lamination theory), and composite properties represented the actual materials in the areas indicated (Fig. 30). The tapered rail configuration was represented by

¹ Personal conversation with Dr. Whitney indicated that his solution appeared to be unstable for the $[\pm 45]_S$ laminate.

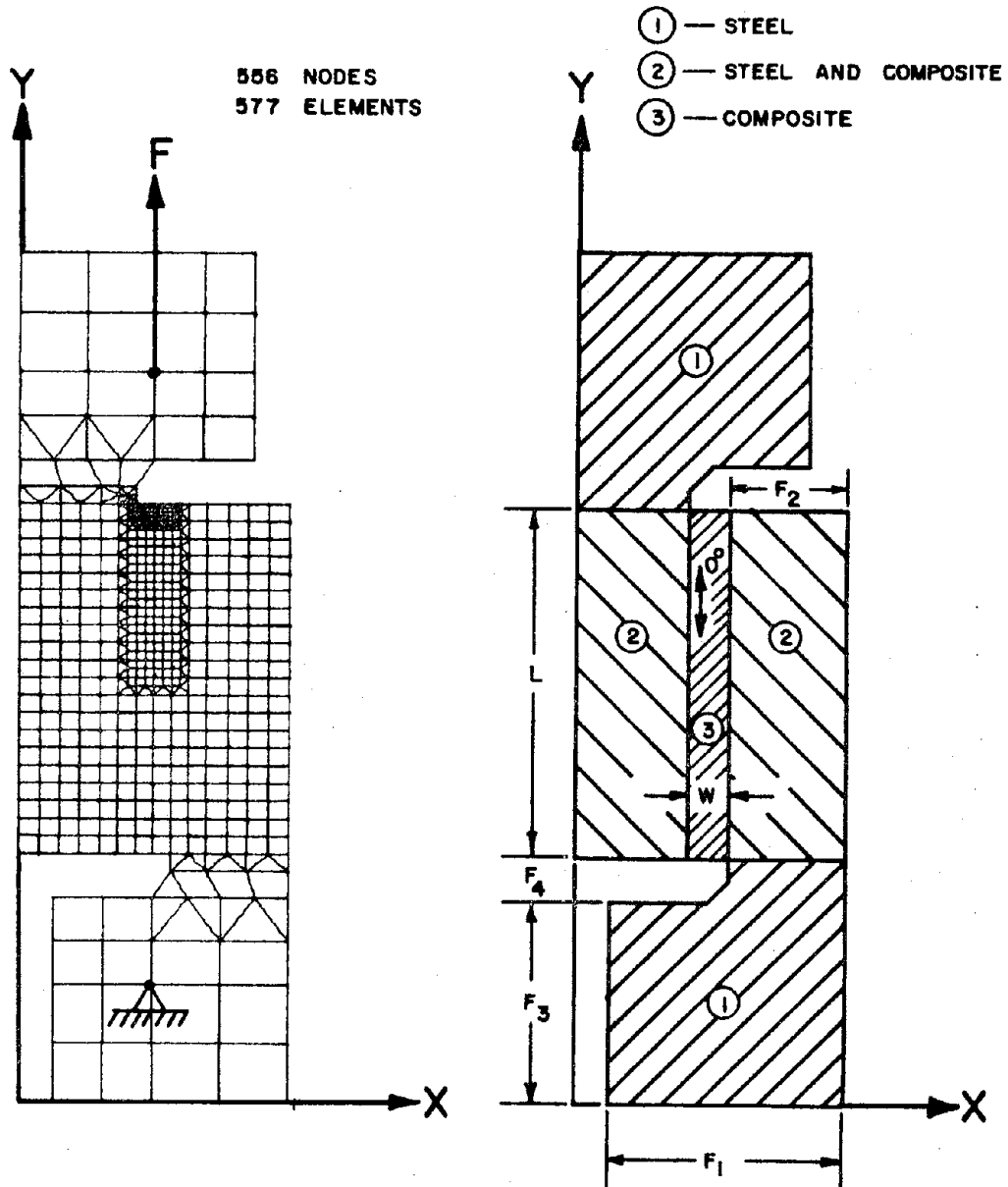


FIGURE 30. AXIALLY LOADED RAIL SHEAR SPECIMEN



FIGURE 31. TAPERED RAIL SHEAR SPECIMEN

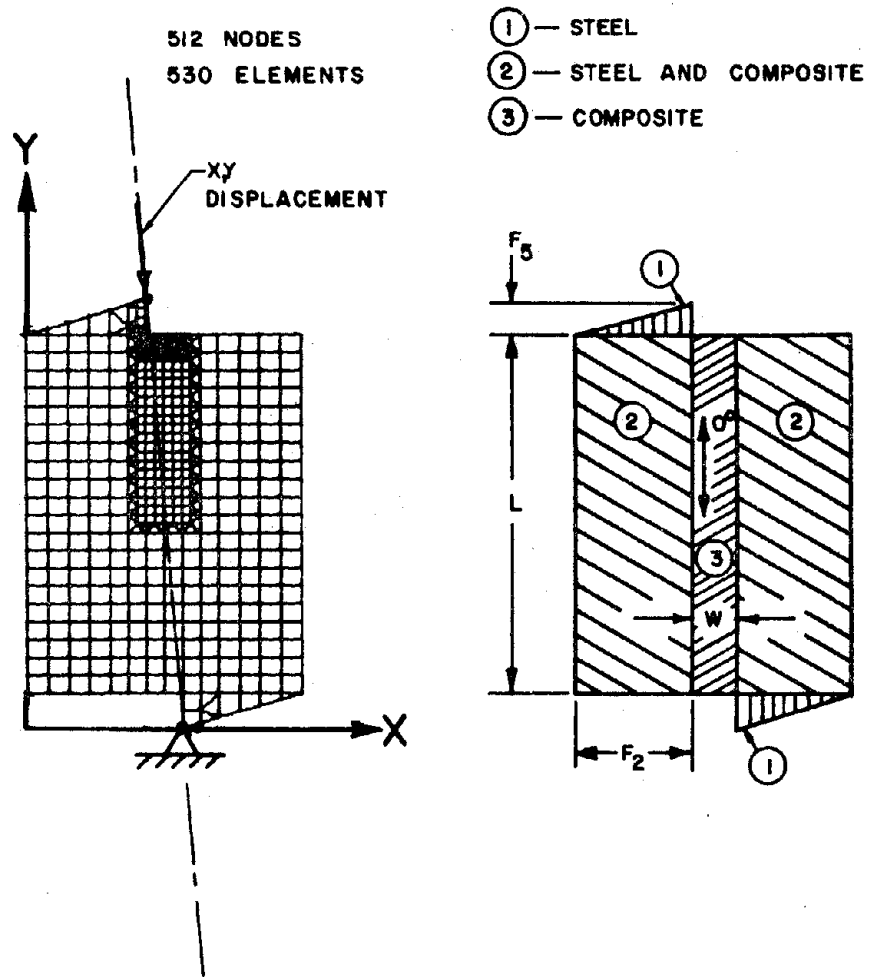


FIGURE 32. OFFSET LOADED RAIL SHEAR SPECIMEN

the same mesh as the nontapered rail configuration and the rail thickness, T_r , was tapered to zero at the free edge of the specimen (Fig. 31). Material properties for the varying rail thickness with uniform composite thickness laminate were obtained from lamination theory at appropriate intervals along the rails. The finite element representation for the shear specimen with offset loading is shown in Fig. 32. The dimensions C , F_2 , T_r , and T_c are the same as those of the nontapered rail (Fig. 30) and in addition $F_5 = W$. The geometry and loading of this specimen are similar to the rail shear specimens used by Whitney et al [8].

The normalized shear stress distributions for the three rail configurations with a [0] laminate (Figs. 33c, 34c, and 35c) indicate a uniform shear stress over most of the specimen. The nontapered rail configuration produces a value of normalized τ_{xy} closest to 1.0 at the center of the specimen. In all cases the maximum shear stress (Table 5) did not occur at the center of the specimen.

The normal stress contour plots indicate that the highest stress concentrations occur in the vicinity of the free edge AB for all rail configurations studied. The σ_x stresses are maximum at the corners A and B. Because of the boundary condition $\sigma_y = 0$ along the free edge AB, the maximum value of σ_y is some distance in from the corner A along the rail-specimen interface AC for the nontapered and tapered rail configurations. For the offset loaded rail configuration σ_y is very low throughout the specimen, and, unlike the axially loaded rail configurations, it

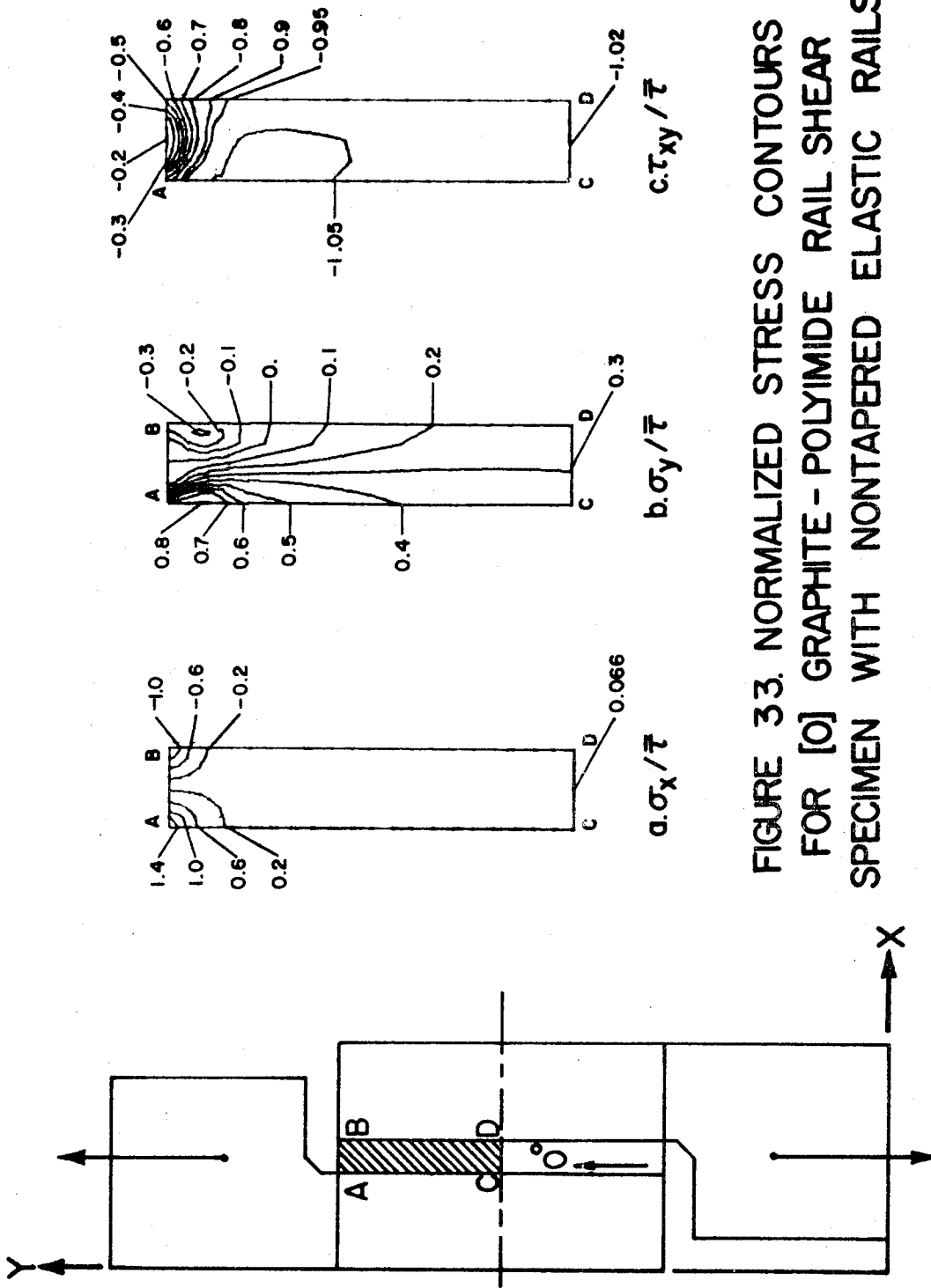


FIGURE 33. NORMALIZED STRESS CONTOURS FOR [0] GRAPHITE-POLYIMIDE RAIL SHEAR SPECIMEN WITH NONTAPERED ELASTIC RAILS

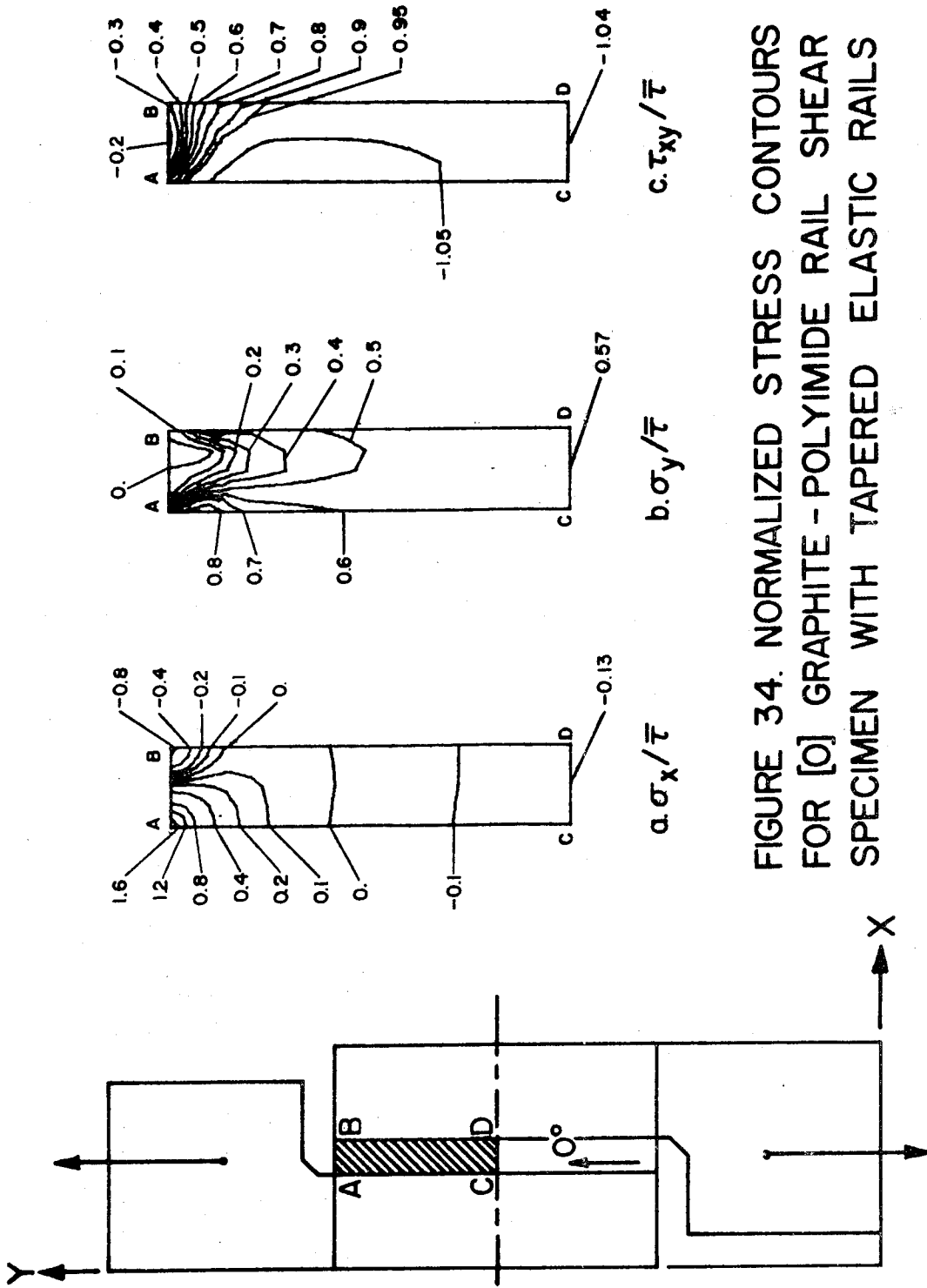


FIGURE 34. NORMALIZED STRESS CONTOURS FOR [0] GRAPHITE - POLYIMIDE RAIL SHEAR SPECIMEN WITH TAPERED ELASTIC RAILS

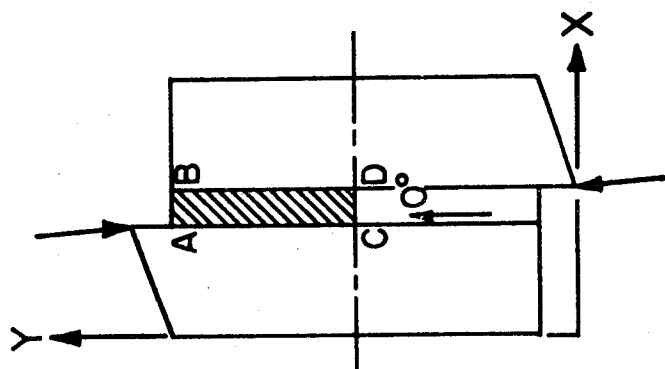
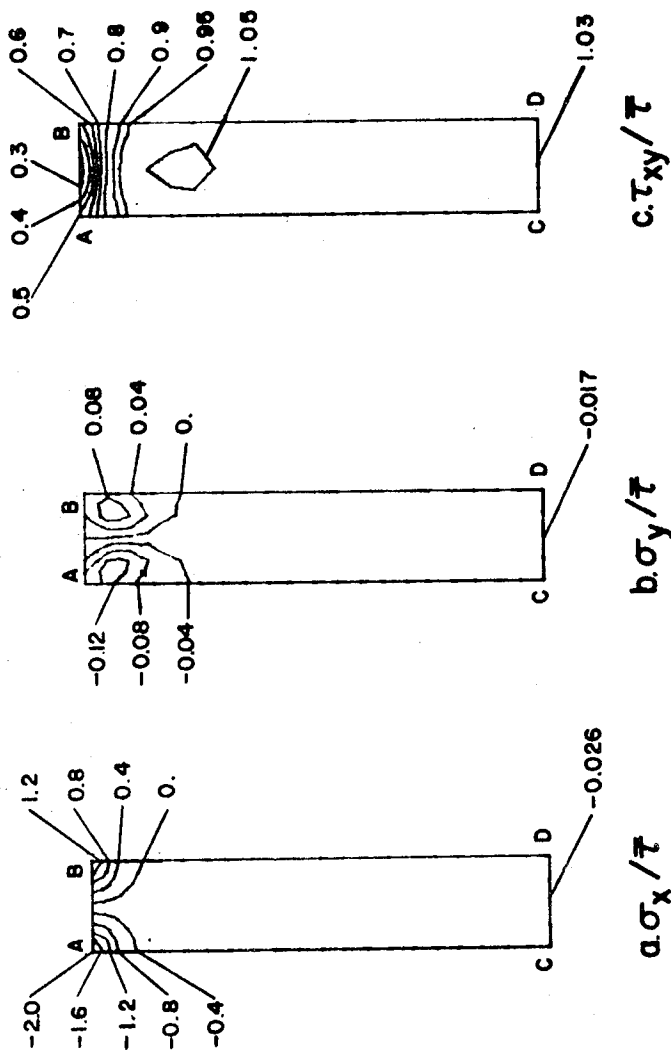


FIGURE 35. NORMALIZED STRESS CONTOURS FOR
 [0] GRAPHITE - POLYIMIDE RAIL SHEAR SPECIMEN
 WITH OFFSET LOADED ELASTIC RAILS

TABLE 5. Normalized Stresses for Graphite-polyimide Rail Shear Specimens
with Elastic Rails.

		Center	A ¹	B ¹	Maximum	
[0]	Non-Tapered Rails	σ_x/τ	-6.67x10 ⁻²	1.77	-1.38	1.77
		σ_y/τ	0.30	0.76	-0.29	0.82
		τ_{xy}/τ	-1.02	-0.74	-0.55	-1.08
	Tapered Rails	σ_x/τ	-0.13	1.91	-0.93	1.91
		σ_y/τ	0.57	0.79	1.68x10 ⁻²	0.87
		τ_{xy}/τ	-1.04	-0.76	-0.29	-1.08
	Offset Loaded Rails	σ_x/τ	-2.56x10 ⁻²	-2.01	1.56	-2.01
		σ_y/τ	-1.74x10 ⁻²	9.72x10 ⁻²	5.20x10 ⁻²	-0.14
		τ_{xy}/τ	1.03	0.52	0.47	1.06
[90]	Tapered Rails	σ_x/τ	-0.85	5.69	-0.33	5.69
		σ_y/τ	9.64x10 ⁻³	0.12	2.61x10 ⁻²	0.12
		τ_{xy}/τ	-0.99	-0.86	-0.52	-1.04

TABLE 5. (continued).

		Center	A ¹	B ¹	Maximum
[±45] _s	$\sigma_x/\bar{\tau}$	-0.53	2.47	-7.10×10^{-2}	2.47
	$\sigma_y/\bar{\tau}$	-0.30	1.39	-3.13×10^{-2}	1.39
	$\tau_{xy}/\bar{\tau}$	-1.01	-1.37	-6.50×10^{-2}	-1.37
Non-Tapered Rails Thermally Loaded	$\sigma_x/(\sigma_x)_{ult}$	-0.34	-5.45	-5.23	-5.45
	$\sigma_y/(\sigma_y)_{ult}$	-0.48	-0.28	-0.27	-0.51
	$\tau_{xy}/(\tau_{xy})_{ult}$	-2.70×10^{-3}	2.21	-2.14	2.28
[0]	$\sigma_x/(\sigma_x)_{ult}$	-0.68	-5.03	-0.15	-5.03
	$\sigma_y/(\sigma_y)_{ult}$	-0.44	0.28	-2.69×10^{-2}	-0.48
	$\tau_{xy}/(\tau_{xy})_{ult}$	-0.12	2.19	-0.73	2.26

¹See Figure 33.

is a maximum away from the rail-specimen interface AC.

A characteristic of all rail shear specimens with elastic rails is the existence of nonzero σ_y normal stresses in the central portion of the specimen. These stresses must be nonzero in this region as a result of the nonzero axial strain present in both the fixture and the specimen as a result of the elastic behavior of the fixture. The effect of rail stiffness on σ_y at the center of the specimen is clearly illustrated by comparing normalized σ_y values for the nontapered and tapered rail configurations (Table 5). Since the tapered rail stiffness at the center of the specimen is half that of the nontapered rail, approximately twice the axial load (and hence stress) is transferred into the specimen with the tapered rails.

7.3.2 Thermal Load Effects

The thermal stresses in a specimen with a [0] graphite-polyimide laminate were determined for a temperature change $\Delta T = -600^\circ\text{F}$ using the finite element mesh shown in Fig. 30 (with $F = 0$). Rail configurations studied included the nontapered and tapered rails described in section 7.3.1. The stress contour plots for σ_x , σ_y , and τ_{xy} normalized with respect to their corresponding ultimate stresses $(\sigma_x)_{ult}$, $(\sigma_y)_{ult}$, and $(\tau_{xy})_{ult}$ (Appendix C) are shown in Figs. 36 and 37.

This linear elastic analysis predicts stress concentrations at the corners A and B with both σ_x and τ_{xy} much greater than their respective ultimate values. While the magnitude of shear stress is zero in the center of the nontapered rail specimen, it is greater than zero in the tapered rail specimen. The nonzero shear stress in the center of the

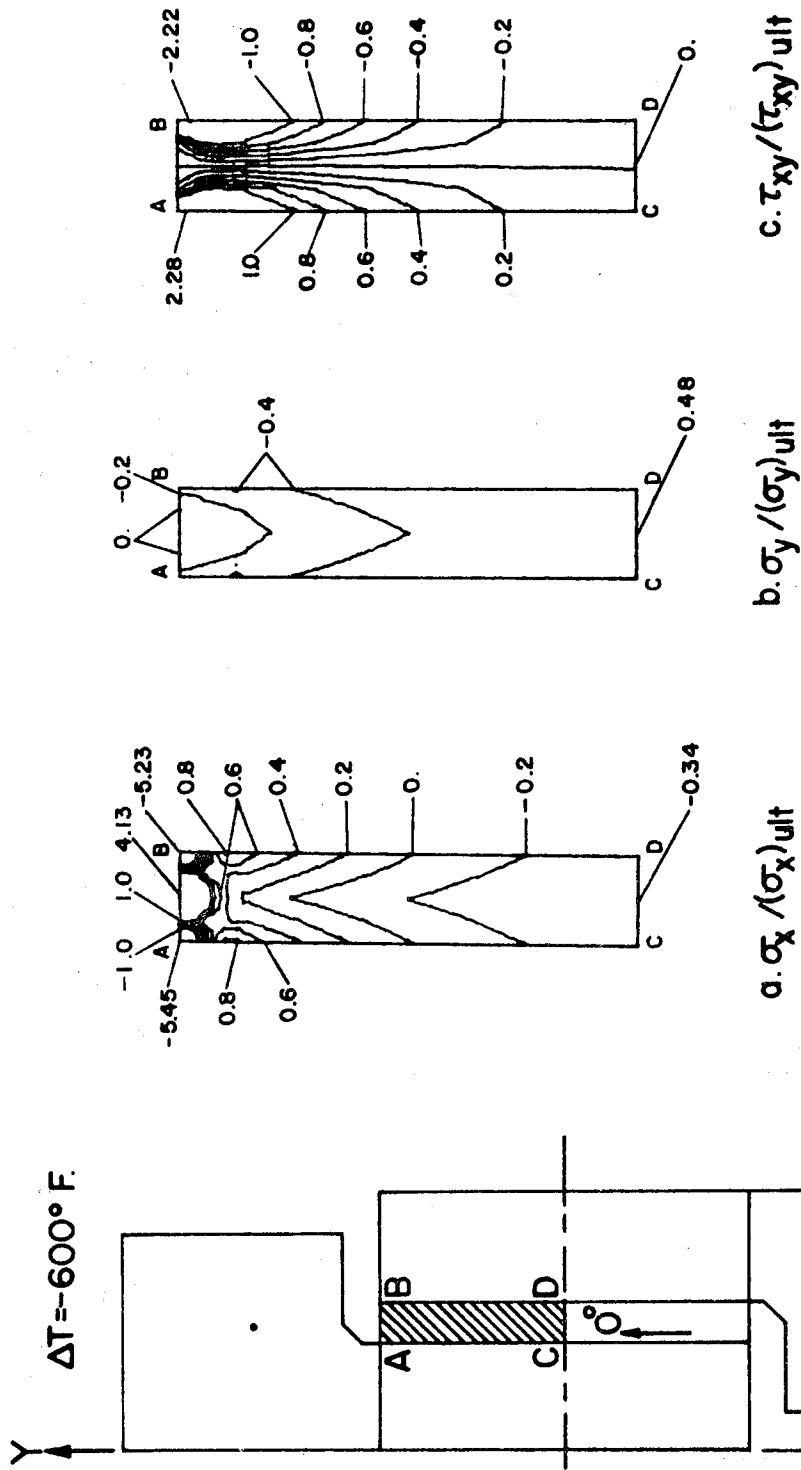


FIGURE 36. NORMALIZED STRESS CONTOURS FOR THERMALLY LOADED [0] GRAPHITE-POLYIMIDE RAIL SHEAR SPECIMEN WITH NONTAPERED RAILS

C 2

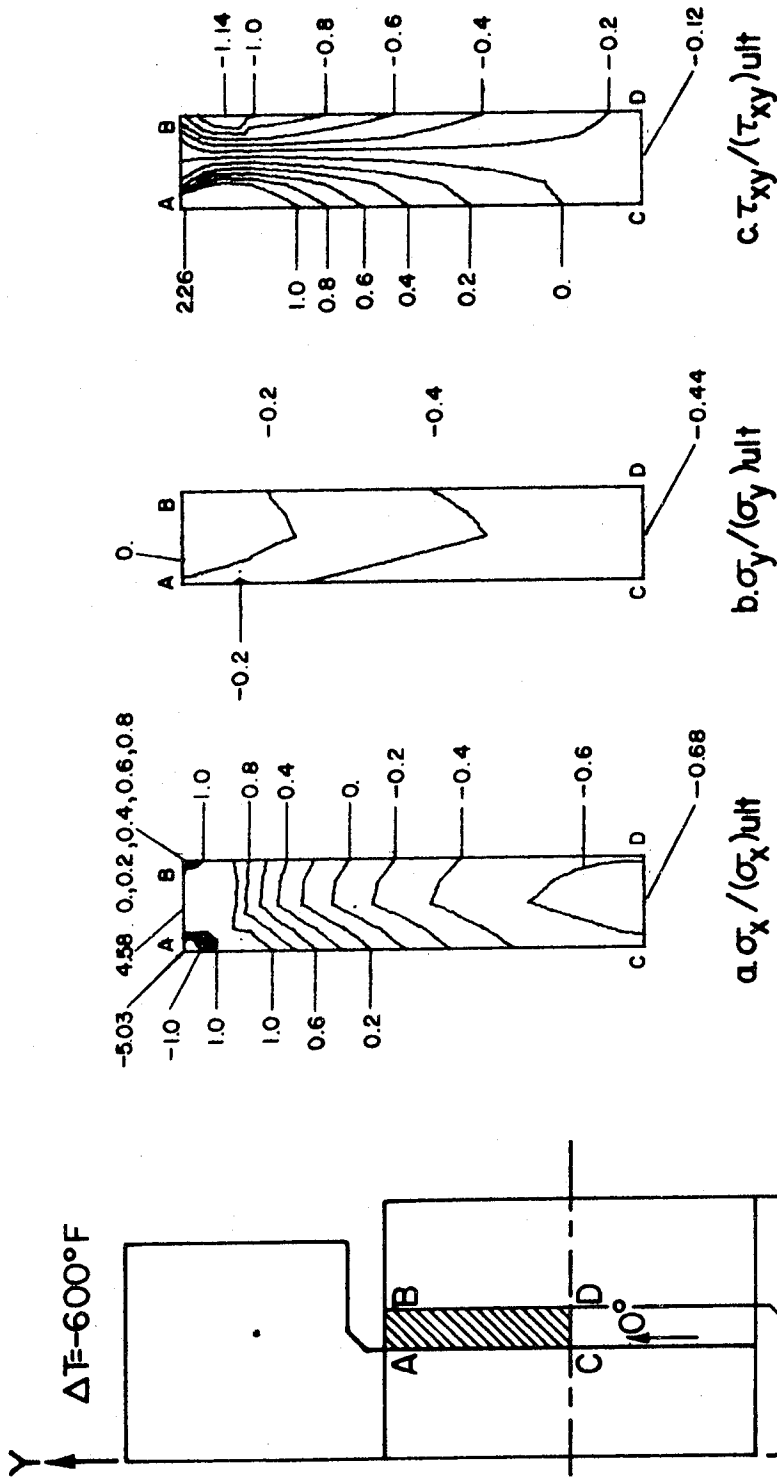


FIGURE 37. NORMALIZED STRESS CONTOURS FOR THERMALLY LOADED [0] GRAPHITE-POLYIMIDE RAIL SHEAR SPECIMEN WITH TAPERED RAILS

tapered rail specimen is attributed to the coarse finite element grid since the shear stress must be zero there to satisfy symmetry conditions. In general the normalized σ_y stresses are considerably lower than σ_x and τ_{xy} , however, σ_y is significant at the center of the specimen.

7.3.3 Other Mechanically Loaded Laminates

Normalized stress contour plots for $[90]$ and $[\pm 45]_S$ graphite-polyimide laminates using the tapered rail configuration are illustrated in Figs. 38 and 39, respectively. The finite element grid described in section 7.3.1 was used for these results.

7.3.3.1 The $[90]$ Laminate

The normalized shear stress distribution for the $[90]$ laminate (Fig. 38c) is nearly ideal in that the normalized shear stress reaches a value of -1.0 very close to the free edge AB and remains very uniform over the entire test section. However, the normal stresses are non-zero in the test section and high stress concentrations are present in the vicinity of corners A and B.

7.3.3.2 The $[\pm 45]_S$ Laminate

The shear stress distribution for the $[\pm 45]_S$ laminate is shown in Fig. 39c. As was the case for the rigid rail results (section 7.2), the tapered elastic rail solution indicates that the magnitude of the normalized shear stress at the center of the specimen is indeed close to -1.0 (Table 5). However, unlike all previous finite element results for both rigid and elastic rails, the maximum normalized shear stress was located at corner A where the value was -1.37 . The contour plots of the normal stresses depict relatively low (but significant) values in the

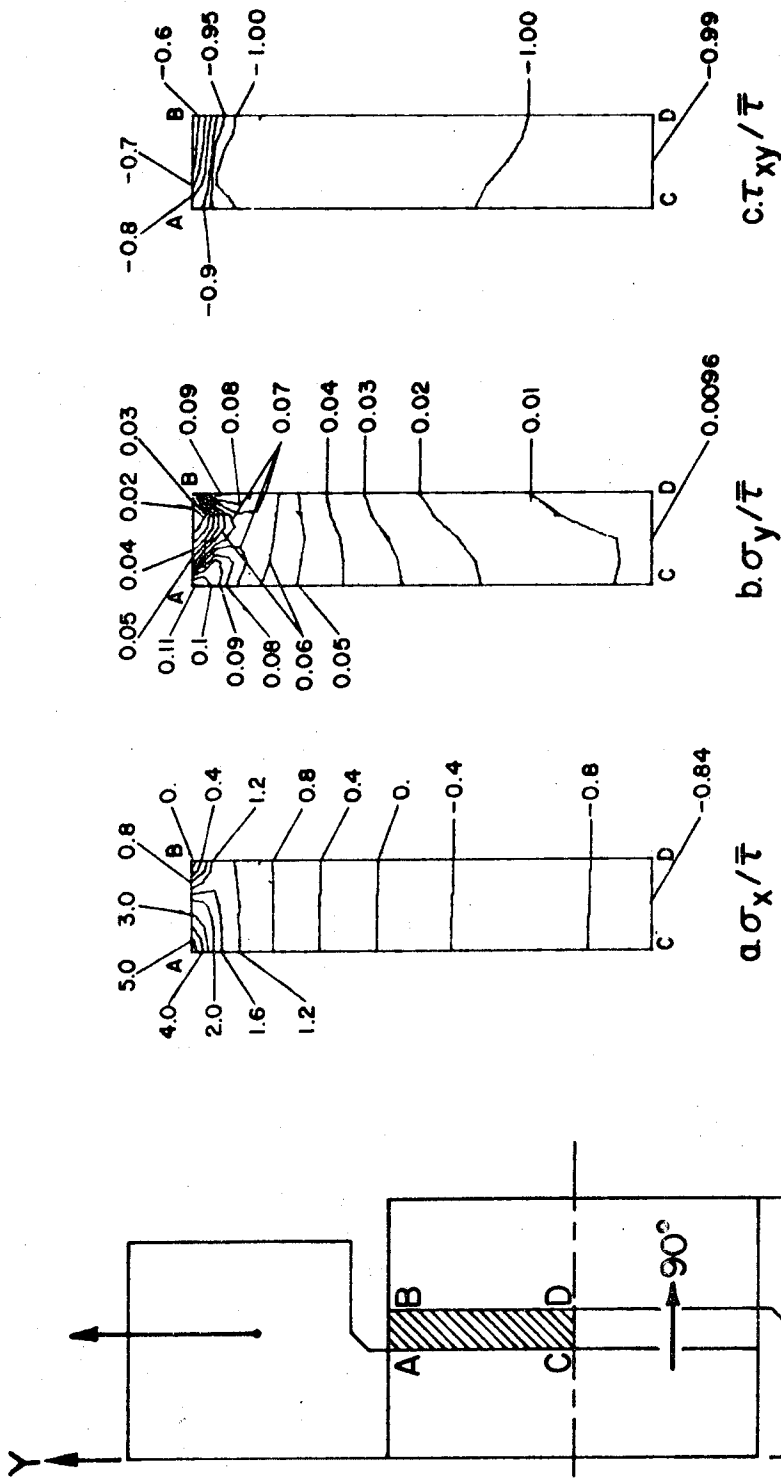


FIGURE 38. NORMALIZED STRESS CONTOURS FOR [90] GRAPHITE-POLYIMIDE RAIL SHEAR SPECIMEN WITH TAPERED RAILS

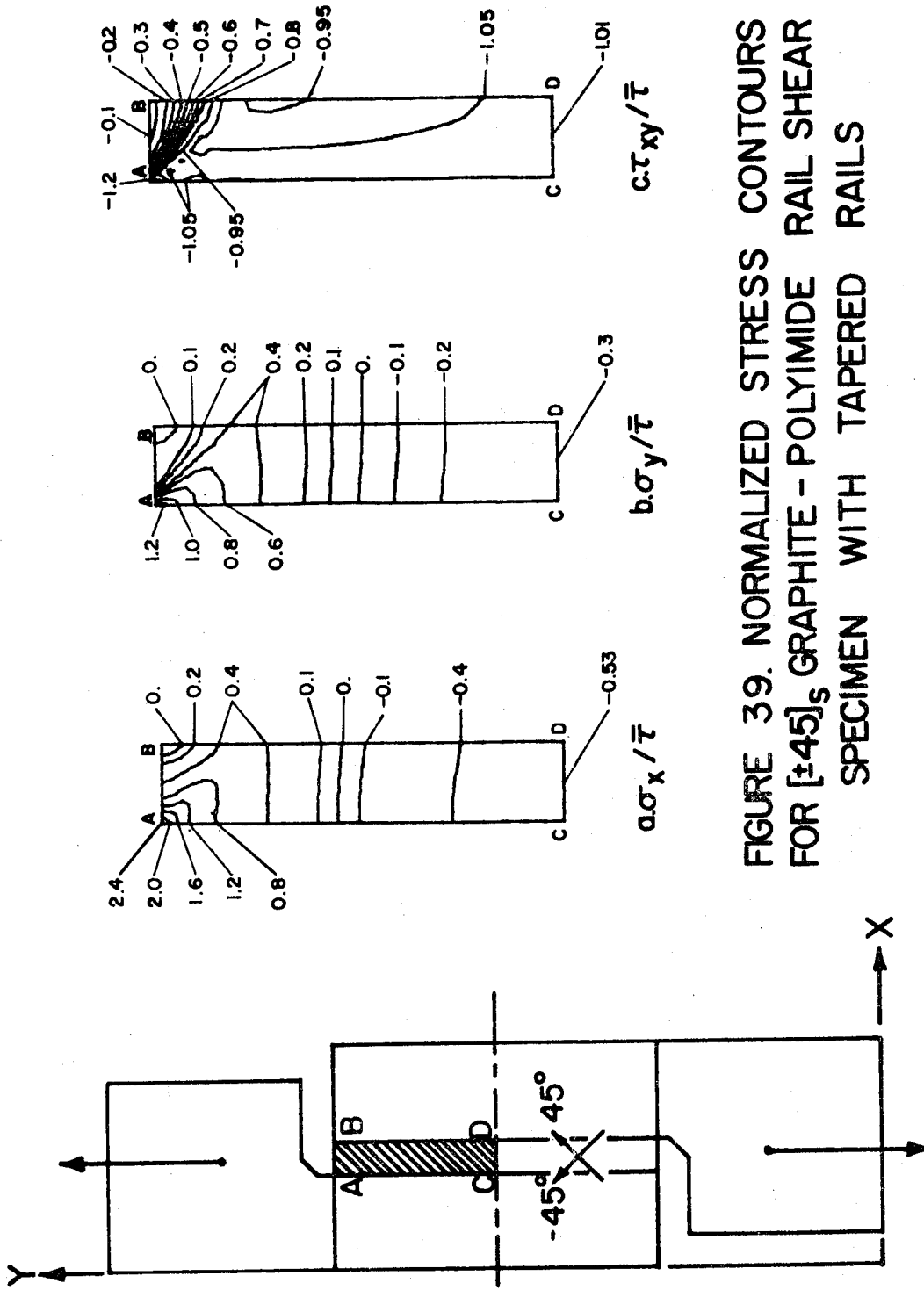


FIGURE 39. NORMALIZED STRESS CONTOURS FOR $[\pm 45]_s$ GRAPHITE - POLYIMIDE RAIL SHEAR SPECIMEN WITH TAPERED RAILS

test section and maximum values in the vicinity of the corners. The distributions of σ_x and σ_y were similar except that σ_y was generally lower in magnitude.

7.4 Summary

The rail configurations investigated produced regions of uniform shear stress over most of the test section for all laminates studied. However, this area of shear stress was often accompanied by significant normal stresses depending upon the stiffness of the rails, the method of load application, and the laminate properties. Significant axial stress was always present in the test section for elastic rails axially loaded. The magnitude of this axial stress was approximately inversely proportional to the stiffness of the rails. The offset loaded rail configuration minimized undesirable normal stresses in the center of the specimen. Stress concentrations in the vicinity of the corners were found in all specimens. Although tapered rails reduce stresses caused by thermal loads, this linear elastic analysis indicates that a non-linear analysis is required for a more accurate solution for a 600° temperature change.

8. CONCLUSIONS

A linear elastic finite element analysis has shown that the cross beam, Iosipescu, and rail shear specimens produce a region of shear stress in the test section. However, effects attributed to laminate properties, core material, and rail configurations significantly influenced the magnitude and the purity of the shear stress at the center of the specimens. In addition, all specimens exhibited stress concentrations in the vicinity of geometric discontinuities.

The rail shear specimen produced a region of uniform shear stress that was not significantly influenced by laminate properties or rail configurations. The axially loaded elastic rails resulted in significant normal stresses at the center of the specimen while the offset loaded elastic rail configuration substantially reduced these stresses. Significant stress concentrations in the vicinity of the free edges were found for all laminates and rail configurations; this was particularly true for the thermally loaded specimens.

The Iosipescu specimen produced uniform, pure shear at the central portion of the specimen for all laminates. Limited studies have shown that the stress concentrations at the notch tips and specimen corners can be substantially reduced by rounding the notch tips and using doublers in the specimen corners. The effects of elastic fixtures and thermal loads were minimal in the test section of this specimen. However, the magnitude of shear stress in the test section of the Iosipescu specimen was dependent upon the properties of the laminate. Although

this specimen is relatively new (and unproven for composites), experience from its use with metals in addition to the analyses in this study indicate that the Iosipescu specimen has potential for future use in testing of composite materials.

The cross beam shear specimen was shown to be a viable specimen for the $[0/90]_s$ laminate. However, the $[\pm 45]_s$ laminate produced a non-uniform shear stress distribution in the test section and this distribution was influenced by the stiffness of the core material. A pure, uniform area of shear stress was not found in the slotted coupon. Therefore, it is not recommended for determining shear response of composites.

In summary, the linear elastic finite element results have indicated that several factors influence the stress distribution present in the test section of each specimen. The rail shear and Iosipescu specimens, despite specific disadvantages, were found to be the most suitable specimens for in-plane shear response of composite laminates.

BIBLIOGRAPHY

1. R. W. Fenn, Jr. and R. B. Clapper, "Evaluation of Test Variables in the Determination of Shear Strength," Proceedings, ASTM, Vol. 56, Philadelphia, 1956, p. 842.
2. W. W. Breindel, C. L. Seale, and R. L. Carlson, "Evaluation of a Single-Shear Specimen for Sheet Material," Proceedings, ASTM, Vol. 58, 1958, p. 862.
3. N. Iosipescu, "New Accurate Procedure for Single Shear Testing of Metals," J. of Materials, ASTM, Vol. 2, Number 3, Sept. 1967, p. 537.
4. R. A. Elkin, G. Fust, and D. P. Hanley, "Characterization of Graphite Fiber/Resin Matrix Composites," Composite Materials: Testing and Design, ASTM STP 460, 1969, p. 321.
5. C. W. Bert, "Experimental Characterization of Composites," Composite Materials (edited by L. J. Broutman and R. H. Krock), Vol. 8, 1974, p. 95.
6. P. H. Petit, "A Simplified Method of Determining the Inplane Shear Stress-Strain Response of Unidirectional Composites," Composite Materials: Testing and Design, ASTM STP 460, 1969, p. 83.
7. M. E. Waddoups, "Characterization and Design of Composites Materials," Composite Materials Workshop (edited by S. W. Tsai, J. C. Halpin, and N. J. Pagano), Technomic Publishing Co., Stamford, Ct., 1968, p. 254.
8. J. M. Whitney, D. L. Stansbarger, and H. B. Howell, "Analysis of the Rail Shear Test - Applications and Limitations," J. of Composite Materials, Vol. 5, Jan. 1971, p. 24.
9. L. Rutherford, C. Bossler, and B. Swain, "Shear Properties of Boron/Epoxy Composites," General Precision Aerospace Research Center, Systems, Inc., Final Report Contract No. 9-69929 to Grumman Aircraft Engineering Corp., Bethpage, New York (1968).
10. Advanced Composites Design Guide, Structures Division, Air Force Flight Dynamics Laboratory, Wright-Patterson Air Force Base, Ohio, section 4.2, Test Methods, December, 1975.
11. D. F. Sims, "In-Plane Shear Stress-Strain Response of Unidirectional Composite Materials," J. of Composite Materials, Vol. 7, January 1973, p. 124.

12. E. L. Bryan, "Photoelastic Evaluation of the Panel Shear Test for Plywood," Symposium on Shear and Torsion Testing, ASTM STP 289, 1961, p. 90.
13. S. Dastin, G. Lubin, J. Munyah, and A. Slobodzinski, "Mechanical Properties and Test Techniques for Reinforced Plastic Laminates," Composite Materials: Testing and Design, ASTM STP 460, Feb., 1969, p. 14.
14. M. W. Hyer and D. O. Douglas, "A Comparison Between Experiment and Theory for a Borsic-Aluminum Picture Frame Shear Test," Technical Report 76-T18, School of Engineering, Old Dominion University, Norfolk, Virginia, Oct., 1976.
15. R. N. Hadcock and J. B. Whiteside, "Special Problems Associated with Boron-Epoxy Mechanical Test Specimens," Composite Materials: Testing and Design, ASTM STP 460, 1969, p. 27.
16. D. O. Douglas, D. E. Holzmacher, Z. C. Lane, and E. A. Thornton, "Studies in Finite Element Analysis of Composite Material Structures," Technical Report 75-M3, School of Engineering, Old Dominion University, Norfolk, Virginia, June, 1975.
17. D. F. Adams and R. L. Thomas, "Test Methods for the Determination of Unidirectional Composite Shear Properties," Advances in Structural Composites, 12th National SAMPE Symposium, Vol. 12, paper AC-5, 1967.
18. B. W. Rosen, "A Simple Procedure for Experimental Determination of the Longitudinal Shear Modulus of Unidirectional Composites," J. of Composite Materials, Vol. 6, October 1972, p. 552.
19. H. T. Hahn, "A Note on Determination of the Shear Stress-Strain Response of Unidirectional Composites," J. of Composite Materials, Vol. 7, July 1973, p. 383.
20. R. R. Rizzo, "More on the Influence of End Constraints on Off-Axis Tensile Tests," J. of Composite Materials, Vol. 3, April 1969, p. 202.
21. G. L. Richards, T. P. Airhart, and J. E. Ashton, "Off-Axis Tensile Coupon Testing," J. of Composite Materials, Vol. 3, July 1969, p. 586.
22. N. J. Pagano and J. C. Halpin, "Influence of End Constraint in the Testing of Anisotropic Bodies," J. of Composite Materials, Vol. 2, January 1968, p. 18.

23. R. B. Pipes and B. W. Cole, "On the Off-Axis Strength Test for Anisotropic Materials," J. of Composite Materials, Vol. 7, April 1973, p. 246.
24. E. M. Wu and R. L. Thomas, "Off-Axis Test of a Composite," Note to the Editor, J. of Composite Materials, Vol. 2, October 1968, p. 523.
25. C. C. Chamis and J. H. Sinclair, "10° Off-axis Tensile Test for Intralaminar Shear Characterization of Fiber Composites," NASA TN D-8215, April, 1976.
26. C. W. Bert, "Static Testing Techniques for Filament-Wound Composite Materials," Composites, January 1974, p. 20.
27. R. R. Rizzo and A. A. Vicario, "A Finite Element Analysis for Stress Distribution in Gripped Tubular Specimens," Composite Materials: Testing and Design (Second Conference), ASTM STP 497, 1972, p. 68.
28. N. L. Hancox, "The Use of a Torsion Machine to Measure the Shear Strength and Modulus of Unidirectional Carbon Fibre Reinforced Plastic Composites," J. of Materials Science 7, 1972, p. 1030.
29. L. B. Greszczuk, "Shear Modulus Determination of Isotropic and Composite Materials," Composite Materials: Testing and Design, ASTM STP 460, 1969, p. 140.
30. S. A. Sattar and D. H. Kellogg, "The Effect of Geometry on the Mode of Failure of Composites in the Short Beam Shear Test," Composite Materials: Testing and Design, ASTM STP 460, 1969, p. 62.
31. C. A. Berg, J. Tirosh, and M. Israeli, "Analysis of Short Beam Bending of Fiber Reinforced Composites," Composite Materials: Testing and Design, ASTM STP 497, 1972, p. 206.
32. R. M. Jones, Mechanics of Composite Materials, Scripta Book Co., Washington, D. C., 1975.
33. C. S. Desai and J. F. Abel, Introduction to the Finite Element Method, Van Nostrand Reinhold Co., New York, 1972.
34. O. C. Zienkiewicz, The Finite Element Method in Engineering Science, McGraw-Hill, London, 1971.
35. E. L. Wilson, K. Bath, and W. P. Doherty, "Direct Solution of Large Systems of Linear Equations," Computers and Structures, Vol. 4, p. 363, 1974.

APPENDIX A.
COMPUTER PROGRAMS

A. COMPUTER PROGRAMS

A.1 Introduction

The present study required three distinct FORTRAN programs to obtain the levels of efficiency and analysis desired. The finite element program described in section A.2 is the basic program. This program performs the finite element solution independently of the other programs. However, for an accurate finite element solution, many intrinsically repetitive node and element cards are required which collectively represent the geometry of the structure. Since repetitive numerical procedures are simplified when programmed, a mesh generation program was developed for the requirements of the study as described in section A.3.

The number of elements in a finite element representation produce a proportional number of stress values which are provided in the form of tabular output by the basic finite element programs. The program described in section A.4 conveniently reduces this data by contour plotting the tabulated stress values.

In practice the finite element mesh is generated first and the resulting node and element card images are written on an indirect access file. Since the node and element card images constitute most of the input to the finite element program (see section A.2) the file is interactively edited to become an input data file for the finite element program. Similarly, the tabulated stress values from the finite element program may be stored on an indirect access file. This file constitutes a large portion of the input for the stress contour plotting program

(see section A.4) and it also is edited to become an input file to the contour plotting program.

A.2 The Finite Element Program

A.2.1 General

The finite element method is a powerful tool for approximating the state of stress in virtually any structure subjected to loads. A requirement for utilizing such a method is the availability of a high speed digital computer and a program to carry out the solution procedure. This section describes such a FORTRAN program.

The use of the finite element method for solutions to structural problems has been well established by Desai and Abel [33], Zienkiewicz [34], and others. This particular program is an extensively modified version of the FORTRAN code by Desai and Abel. The program uses the displacement method for solution (see section 3.2). Both constant strain triangular elements and quadrilateral elements composed of four constant strain triangles are available for either plane stress or plane strain analysis. Capability added to the program by the author includes orthotropic material properties, orthotropic thermal effects, and the implementation of an equation solving subroutine developed by Wilson et al [35]. The improved equation solver allows the program to solve a very large system of linear equations in blocks residing on slow speed storage, as opposed to the more restricted, completely in core solution technique.

The job flow is one pass since linear elastic problems are directly

solved. After material property, node, element, and load information is input, a stiffness matrix for each element is computed. All elemental stiffness matrices are then assembled into a global stiffness matrix, and the load vector is initialized. The unknown displacement vector is determined using Gauss elimination techniques on only non-zero stiffness terms. Once the global displacements are computed, elemental strains are determined. The elemental stresses are then computed from the elemental constitutive matrices and the elemental strains.

A.2.2 Input Description

Column	Contents
Title card (I5,9A8)	
1-5	NPROB = Problem number. If NPROB > 100, stresses are written on unit 2. This option is used with the stress contour plotter (see section A.4). If NPROB = 0, no more problems are run.
6-77	A(I) = Title information
Control card (4I5)	
1-5	NNP = Number of nodes
6-10	NEL = Number of elements
11-15	NMAT = Number of materials
16-20	NOPT = 1 for plane strain analysis = 2 for plane stress analysis

Laminate material property cards (7E10.0)

(for material I)

1-10	EX(I)	= Modulus of elasticity in X direction
11-20	EY(I)	= Modulus of elasticity in Y direction. IF (EY(I).EQ.0.) EY(I) = EX(I)
21-30	PRXY(I)	= Poisson's ratio, ν_{xy} . IF (PRXY(I).EQ.0.) PRXY(I) = EX(I) / (2./GXY(I)-1).
31-40	GXY(I)	= Modulus of rigidity for material I. IF (GXY(I).EQ.0.) GXY(I) = EX(I) / (1.+PRXY(I))/2.
41-50	TH(I)	= Thickness for material I.
51-60	ALPHA(1,I)	= Coefficient of thermal expansion in X direction for material I.
61-70	ALPHA(2,I)	= Coefficient of thermal expansion in Y direction for material I.

Nodal location and mechanical load cards (2I5,4E10.0)

1-5	N	= node number
6-10	KODE(N)	= 0 for ULX(N) and VLY(N) prescribed loads = 1 for ULX(N) prescribed displacement and VLY(N) prescribed load.

		= 2 for ULX(N) prescribed load and VLY(N) prescribed displacement
		= 3 for ULX(N) and VLY(N) prescribed displacements
11-20	X(N)	= X coordinate
21-30	Y(N)	= Y coordinate
31-40	ULX(N)	= X displacement or load
41-50	VLY(N)	= Y displacement or load

Element and thermal load cards(6I5,E10.0)

1-5	M	= Element number
6-10	IE(M,1)	= First node of element
11-15	IE(M,2)	= Second node of element
16-20	IE(M,3)	= Third node of element
21-25	IE(M,4)	= Fourth node of element. For triangular elements, IE(M,3) = IE(M,4)
26-30	IE(M,5)	= Material properties associated with element M
31-40	TEMP(M)	= Change in temperature of element after displacement boundary conditions are imposed. IF (TEMP(M).EQ.0.)TEMP(M) = TEMP(M-1)

Comments

Node and element cards must be in ascending consecutive order. Nodes associated with triangular elements that are not ordered counterclockwise cause a warning message, but are reordered counterclockwise internally. Quadrilateral elements must be ordered counterclockwise. If the mesh generation program (section A.3) is used to supply node and element cards, these cards (or indirect access file) must be altered to include boundary condition (KODE), mechanical load (ULX(N),VLY(N)), elemental material (IE(M,5)), and elemental temperature (TEMP(M)) information. To terminate execution, a blank card is inserted after the last element and thermal load card of the last model. If NPROB is not zero the program expects to read a complete data set for another model.

A.3 The Mesh Generation Program

A.3.1 General

This program generates groups of elements and nodes. In a group, all elements are either identical to one another or have repetitive geometric characteristics. Many groups of elements make up the total model. A group of elements may be located anywhere in X-Y coordinates by several methods. The dimensions, orientation, number of elements, and type of elements for each group are specified by the user. Data for each element group is read sequentially so that data to generate specific element groups may be added or deleted from the entire data set. Specified groups of elements may be scaled, rotated, or repositioned so that element groups frequently needed in different meshes need only be

checked once and can be inserted as needed into different meshes.

Input data to the mesh generator is comprised of four categories. The first category of input is the generation initialization and termination data. The initialization data is at the beginning of the data set and is used only once for the purpose of initializing title information and reference frames. At the end of the data is the card indicating that the mesh generation commands are complete so that the program can perform its final computations.

All other categories of input commands may be used anywhere at any time between the initialization and termination data. The second category of data consists of element group generation data sets. These data sets generate specific groups of elements. An element group generation data set can control every parameter associated with the generation of that particular group, or certain parameters may be passed to it from the preceding group. The third category of input alters the reference frame of one, several, or all groups that constitute the complete model. General capabilities include translation, rotation, and scaling of any desired element groups. The last category of input data has the capacity to reposition nodes. While other input commands operate by element groups, the nodal repositioning commands operate on all nodes that have been previously generated. The only capacity for nodal repositioning in the present version is that of repositioning nodes to lie in a precise circular arc. This avoids the necessity of manually positioning individual nodes that will ultimately lie on some circular arc in the complete model.

A.3.2 Generation Initialization and Termination Data Input

Column	Contents
Title card (10A8)	
1-80	CARD(1) = Title information
Coordinate Initialization Card (6F10.0,2I5)	
1-10	ORIGIN(1) = Absolute X coordinate of initial global and local coordinate system origin
11-20	ORIGIN(2) = Absolute Y coordinate or initial global and local coordinate system origin
21-30	SCALE(1) = X scaling dimension for internal node numbering
31-40	SCALE(2) = Y scaling dimension for internal node numbering
41-50	FACT(1) = X global coordinate scale factor
51-60	FACT(2) = Y global coordinate scale factor
61-65	MSCAN = Node duplication elimination number
66-70	NSV = 0 for numbering nodes by as- cending X then Y location = 1 for numbering nodes by as- cending Y the X location

Comments

The ORIGIN(I) variables initialize the origin of the global coordinates in terms of absolute (final) coordinates. Since the ORIGIN(I) fields have the same purpose as the global origin reset cards, the exact use of these fields are described in section A.3.4.

The node numbers are internally numbered by absolute X and Y location. Such node numbers are determined by the equations

$$\begin{aligned} IX &= X/SCALE(1)*10000.-.5 \\ IY &= Y/SCALE(2)*10000.-.5 \\ \text{IF(NSV.EQ.0)NODE} &= IY*10000+IX \\ \text{IF(NSV.EQ.1)NODE} &= IX*10000+IY \end{aligned}$$

where X,Y are node locations.

NODE is the internal node number. The nodes are internally numbered in this manner for two reasons. Due to roundoff errors caused by reference frame alterations, a previously generated node does not necessarily have the exact coordinate location of another node intended to have the same location. For this reason, duplicate node positions are not eliminated by a check for X-Y absolute coordinate duplication. SCALE(I) must be slightly larger than the expected maximum X-Y node coordinates. NODE is then determined for each node, and any node whose internal IX or IY is equal to or one different from another IX or IY is eliminated. After all nodes and elements have been generated, the NODE numbers are put in ascending order and renumbered 1,2,3,...,NNP, where NNP is the total number of node points. This procedure minimizes

the bandwidth of many meshes since nodes are renumbered by ascending X coordinate then ascending Y coordinate locations (for NSV=0).

The FACT(I) variables initialize the coordinate multiplication factors for all dimensions with respect to any global coordinate system. Since the FACT(I) fields have the same purpose as the coordinate scale reset cards, the exact use of these fields are described in section A.3.4.

The integer MSCAN is used to minimize scanning procedures for duplicate NODE numbers as element groups are processed. For example, if an element group with ten boundary nodes is being added to an existing model whose last ten generated nodes will coincide with these boundary nodes, MSCAN need only be ten. However, if one hundred new nodes are generated between the boundary nodes that have the same location, MSCAN should be at least one hundred and ten. Since all duplicate nodes are eliminated at the time the model is completed, MSCAN can be zero for any model. However, duplicate node information tends to fill up storage arrays rather quickly so the value of this variable should always be overestimated to minimize storage requirements.

Column	Contents
Termination card (I5)	
1-5	KIND = 5. This stops the program from reading additional group generation, reference frame alteration, and nodal repositioning cards. At this point the pro-

gram initiates final processing of the completed mesh. This card may be last in the input deck (or file) or placed between any of the repeatable data sets for mesh debugging purposes

A.3.3 Element Generation Input

Type 1 Rectangular Element Generation Cards

Card 1 (I5,9A8)

1-5	KIND	= 1 for group type 1, rectangular element generation input to follow
6-77	CARD(I)	= Title for element group

Card 2 (3I5,F10.0)

1-5	M	= The number of rectangular elements in the X direction, see figure A-1a
6-10	N	= The number of rectangular elements in the Y direction
11-15	IRC	= The reset code for A(1) and A(2)
16-25	THETA	= The angle of rotation about the local origin

Card 3 (2F10.0,I5)

1-10	A(1) or AX	= Total reset or multiplying factor of A(1)
11-20	A(2) or AY	= Total reset or multiplying factor of A(2)
21-25	JRC	= Reset code for XY(1) and XY(2), the local origin loca- tion in terms of global coor- dinates

Card 4 (2F10.0)

1-10	XY(1) or TEMP(1)	= Total or incremental X local origin location in terms of global coordinates
11-20	XY(2) or TEMP(2)	= Total or incremental Y local origin location in terms of global coordinates

Comments

For the A(I) dimension reset option IRC, the following numbers are admissible

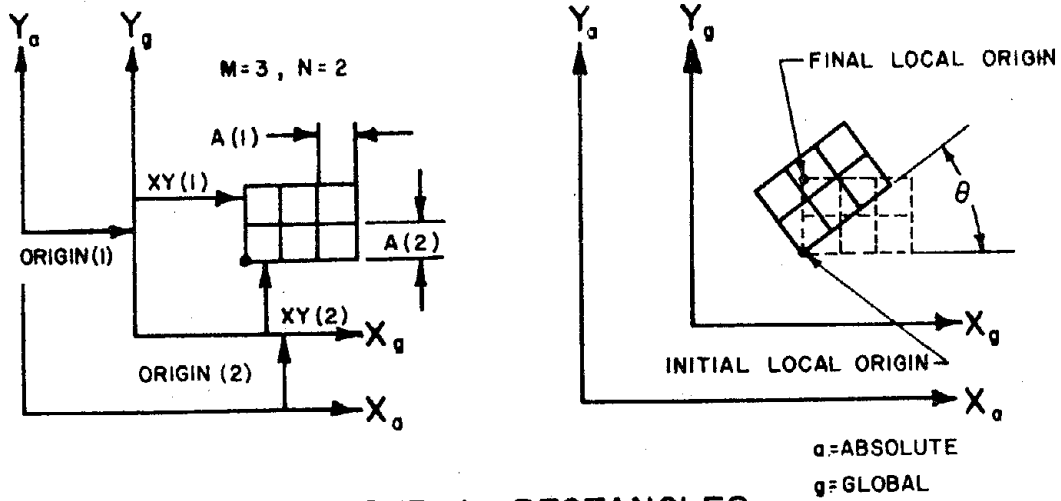
IRC	= 0 for no reset, A(1) and A(2) are used from the previous element group
	= 1 for a scalar reset of A(1), AX is read, $A(1) = AX * A(1) *$ FACT(1)

- = 2 for a scalar reset of A(2),
AY is read, $A(2) = AY * A(2) * FACT(2)$
- = 3 to reset both cases above
- = -1 for a total reset of A(1),
A(1) is read, $A(1) = A(1) * FACT(1)$
- = -2 for a total reset of A(2),
A(2) is read, $A(2) = A(2) * FACT(2)$
- = -3 for a total reset of A(1)
and A(2)

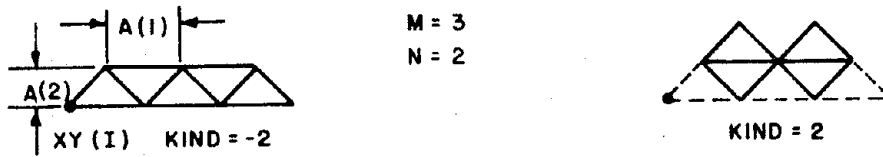
The program omits fields that are not applicable following resets. If IRC = 0, the following field on card 3 becomes (I5). If IRC = 1, the following field on card 3 becomes (F10.0,I5), and similarly for other cases.

For the local origin reset the following options are admissible

- JRC = 0 for the default change in local origin with respect to the global coordinate system
- = 1 for an incremental reset of XY(1), TEMP(1) is read, $XY(1) = XY(1) + TEMP(1) * FACT(1) + ORIGIN(1)$
- = 2 for an incremental reset of XY(2), TEMP(2) is read, $XY(2) =$



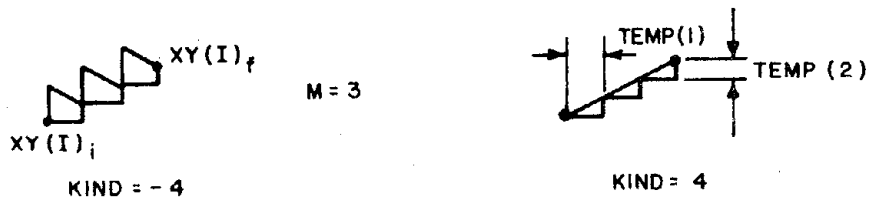
a. GROUP 1 - RECTANGLES



b. GROUP 2 - ISOSCELES TRIANGLES



c. GROUP 3 - TRANSITION "RECTANGLES"



d. GROUP 4 - IRREGULAR ELEMENTS

FIGURE A-1 ELEMENT GROUPS

$XY(2)+TEMP(2)*FACT(2)+ORIGIN(2)$
 = 3 to reset both cases above
 = -1 for a total reset of $XY(1)$,
 $XY(1)$ is read, $XY(1) = XY(1)*$
 $FACT(1)+ORIGIN(1)$
 = -2 for a total reset of $XY(2)$,
 $XY(2)$ is read, $XY(2) = XY(2)*$
 $FACT(2)+ORIGIN(2)$ where $XY(I)$
 become absolute coordinates.
 = -3 for total reset of $XY(1)$
 and $XY(2)$

All element group generation cards may be used anywhere and any number of times after the initialization cards.

Type 2 Isosceles Triangle Element Generation Cards

Card (I5,9A8)

1-5	KIND	= 2 or -2, depending on the generation mode desired for isosceles triangle input, see figure A-1b
6-77	CARD(I)	= Title information for element group

Card 2 (3I5,F10.0)

1-5	M	= The number of isosceles triangles in the X direction
-----	---	--

6-10	N	= The number of isosceles triangles in the Y direction
11-15	IRC	= The reset code for A(I), see type 1 description
16-25	THETA	= The angle of rotation about the local origin

Card 3 (2F10.0,I5)

1-10	A(1) or AX	= Total reset or multiplying factor of A(1)
11-20	A(2) or AY	= Total reset or multiplying factor of A(2)
21-25	JRC	= Reset code for XY(I), the absolute coordinate location for the local origin, see group 1

Card 4 (2F10.0)

1-10	XY(1) or TEMP(1)	= Total or incremental X local origin reset value
11-20	XY(2) or TEMP(2)	= Total or incremental Y local origin reset value, see group 1

Comments

See figure A-1b for isosceles triangle specifications. The

description of cards 3 and 4 are identical to those of element group 1.

Type 3 Transition "Rectangle" Generation Cards

Card 1 (I5,9A8)

1-5	KIND	= 3 or -3, depending on the mode for transition rectangles, see figure A-1c
6-77	CARD(I)	= Title information for element group

Card 2 (2I5,F10.0)

1-5	M	= The number of transition rectangles in the X direction
6-10	IRC	= The reset code for A(I)
11-20	THETA	= The angle of rotation about the local origin

Card 3 (2F10.0,I5)

1-10	A(1) or AX	= Total reset or multiplying factor of A(1)
11-20	A(2) or AY	= Total reset or multiplying factor of A(2)
21-25	JRC	= Reset code for XY(1) and XY(2), the local origin location

Card 4

1-10	XY(1) or TEMP(1)	= Total or incremental X local origin reset value
11-20	XY(2) or TEMP(2)	= Total or incremental Y local origin reset value

Type 4 Irregular Element Generation Cards

Card 1 (I5,9A8)

1-5	KIND	= 4 for irregular triangle generation = -4 for irregular quadrilateral generation
6-77	CARD(I)	= Title information for element group

Card 2 (2I5)

1-5	NELODD	= The number of irregular elements to be generated, see figure A-1d
6-10	JRC	= The local origin reset code

Card 3 (2F10.0)

1-10	XY(1) or TEMP(1)	= Total or incremental X local origin reset value
11-20	XY(2) or TEMP(2)	= Total or incremental Y local origin reset value

Card 4 (6F10.0)

1-10	TEMP(1)	= Change in X coordinate from local origin for second node on element
11-20	TEMP(2)	= Change in Y coordinate from local origin for second node on element
21-30	TEMP(3)	= Same as TEMP(1) for third node
31-40	TEMP(4)	= Same as TEMP(2) for third node
41-50	TEMP(5)	= Same as TEMP(1) for fourth node
51-60	TEMP(6)	= Same as TEMP(2) for fourth node

Card 5 (2F10.0)

1-10	TEMP(1)	= Change in X coordinate of the local origin after each irregular element generation
11-20	TEMP(2)	= Change in Y coordinate of the local origin after each irregular element generation

A.3.4 Reference Frame Alteration Data Sets

Global Origin Reset Cards

Card 1 (I5,9A8)

1-5	KIND	= -1 for global origin reset
6-77	CARD(I)	= Title information

Card 2 (2F10.0)

1-10	ORIGIN(1)	= Location of X global origin in absolute coordinates and initial location of the local coordinate system
------	-----------	---

11-20	ORIGIN(2)	= Location of Y global origin in absolute coordinates and initial location of the local coordinate system
-------	-----------	---

Comments

These cards may be inserted anywhere after the initialization cards and may be used any number of times. The local coordinate position is always initially set to the ORIGIN(I) position. All local origin changes and resets are done with respect to the global coordinate system.

Global Coordinate Scale Factor Reset Cards

Column

Contents

Card 1 (I5,9A8)

1-5	KIND	= 6 for global scale factor reset
6-77	CARD(I)	= Title information for scaled element groups

Card 2 (2F10.0)

1-10	FACT(1)	= Scale factor for global coordinate in X direction
11-20	FACT(2)	= Scale factor for global coordinate in Y direction

Comments

FACT(I) scales all A(I), AX, AY, XY(I), and TEMP(I), input from the element group generation data sets (see section A.3.3).

Input for Rotating Several Element Groups

Column	Contents
Card 1 (I5,9A8)	
1-5	KIND = 8 for element groups following to be rotated
6-77	CARD(I) = Title information
Card 2 (5F10.0)	
1-10	XTH = Rotation in degrees about the X axis at XPIVOT and YPIVOT
11-20	YTH = Rotation in degrees about the Y axis at XPIVOT and YPIVOT
21-30	ZTH = Rotation in degrees about the Z axis at XPIVOT and YPIVOT
31-40	XPIVOT = Global X location for the

point about which nodes are rotated

41-50 YPIVOT = Global Y location for the point about which all nodes are rotated

Card to Terminate Element Groups to be Rotated (I5)

1-5 KIND = -8, to rotate nodes of element groups generated between card 2 and this card

Comments

XPIVOT and YPIVOT are not scaled by FACT(I). Rotation commands may not be nested and for every KIND = 8 there must be a corresponding KIND = -8. All rotations executed with these commands are carried out independently of rotations of individual element groups.

A.3.5 Node Repositioning Data Sets

Column	Contents
Card 1 (I5,9A8)	
1-5	KIND = 7 for node repositioning data to follow
6-77	CARD(I) = Title information
Card 2 (7F10.0)	
1-10	X0 = Absolute X location for the

		center of the circular segment on which repositioned nodes are to lie
11-20	Y0	= Absolute Y location for the center of the circular segment on which repositioned nodes are to lie
21-30	THI	= Initial angle from the X axis for circular segment
31-40	THF	= Final angle from the X axis for circular segment, $THF > THI$
41-50	TDEG	= Tolerance to include nodes lo- cated near angles THI and THF. Nodes that are repositioned lie between the angles $THI-TDEG$ and $THF+TDEG$
51-60	RAD	= Radius of the circular segment about X0, Y0 to which nodes will be repositioned
61-70	TOL	= Tolerance to include nodes located between a radius of $RAD-TOL$ and $RAD+TOL$ to be repositioned along the radius RAD

A.4 The Plotting Program

A.4.1 General

In order to efficiently evaluate finite element meshes and stress fields, it is desirable to have a versatile computer program capable of plotting finite element meshes and stress contour plots either on paper or at an interactive graphics terminal. This section describes such a finite element mesh and stress contour plotting computer program.

The finite element mesh plotting algorithm simply plots the specified elements of the mesh to a specified plot width. Nodes, elements, or both may be numbered. Numbering schemes are chosen by the user.

The stress contour plotting algorithm plots the outline of the mesh and plots lines of constant σ_x , σ_y , and/or τ_{xy} throughout the interior of the mesh outline. The number of stress contours are specified by the user. Stress contour values may be input, internally generated, normalized by input values of stress, or internally normalized. Any stress contour values generated may be punched for future use.

A.4.2 Input Description

Column	Contents	
Control Card (3I5)		
1-5	NNP	= Number of nodes
6-10	NEL	= Number of elements
11-15	NCASE	= Number of plot cases

stress cards, one associated with every element. Node and element cards (or records) are usually generated with the mesh generator and the stress cards are usually generated by the finite element program (NPROB > 100, see section A.2).

Plot Case Cards

Column	Contents	
Title Card (10A8)		
1-80	TITLE(I)	= Title for plot case to follow
Control Card (5F10.0,3I5,6I1)		
1-10	XMIN	= Minimum X dimension for nodes plotted
11-20	XMAX	= Maximum X dimension for nodes plotted
21-30	YMIN	= Minimum Y dimension for nodes plotted
31-40	YMAX	= Maximum Y dimension for nodes plotted
41-50	WIDTH	= Width of the plotted mesh
51-55	NEON	= The labeling index for node numbering on mesh plots
56-60	NEOE	= The labeling index for element numbering on mesh plots
61-65	NCONT	= The number of stress contours

		to be plotted
66	IGRID	= 0 for no grid plot = 1 for grid plot
67	ISIGX	= 0 for no σ_x stress contour plot = 1 for σ_x stress contour plot = 2 for σ_x stress contour plot with all plotted stresses normalized by σ_x normalization elements = 3 for σ_x stress contour plot with all plotted stresses normalized by an input value of stress
68	ISIGY	= Same options as field 67 (ISIGX) for σ_y
69	ITAUXY	= Same options as field 67 (ISIGX) for τ_{xy}
70	ICOVAL	= 0 for elementwise stress contour value generation = 1 for input stress contour values = 2 for stress contour values of constant stress increment generation

71 ICOPUN = 0 for no punched stress contour values
 = 1 for punched stress contour values

Normalizing Stress Card (F10.0)

1-10 AVE(4) = Stress which all others will be normalized by. This card is needed only if ISIGX, ISIGY or ITAUXY is 3.

Stress Normalization Element Cards (I5,F10.0,I2I5)

1-5 ICON = 0 for no more elements to be added
 = +N for every Nth element to be averaged
 = -1 for each following element to be averaged

6-15 FACT = Element's weighting factor

16-80 NOPAIR = Element numbers
 (I,1)

Plotted Element Cards (I4I5)

1-5 ICON = 0 for no more elements to be added
 = +N for every Nth element to be

plotted

= -1 for each following element

to be plotted

6-75

NOPAIR = Element numbers

(I,1)

Contour Stress Value Cards (3E20.0)

1-20

AVE(I,1) = σ_x stress value of contour I

21-40

AVE(I+1,1) = σ_x stress value of contour I+1

41-60

AVE(I+2,1) = σ_x stress value of contour I+2,

repeat cards until NCONT values

are read

1-20

AVE(I,2) = σ_y stress value of contour I

21-40

AVE(I+1,2) = σ_y stress value of contour I+1

41-60

AVE(I+2,2) = σ_y stress value of contour I+2,

repeat cards until NCONT values

are read

1-20

AVE(I,3) = τ_{xy} stress value of contour I

21-40

AVE(I+1,3) = τ_{xy} stress value of contour I+1

41-60

AVE(I+2,3) = τ_{xy} stress value of contour I+2,

repeat cards until NCONT values

are read. If ISIGX, ISIGY,

and/or ITAUXY are 0, their

corresponding stress contour

values are not needed. Contour

stress value cards are only
read for ICOVAL=1.

Comments

All plot case cards are repeated NCASE times. For automatic scaling, XMIN, XMAX, YMIN, and YMAX are zero. The smallest of XMAX-XMIN and YMAX-YMIN is plotted across the plotting drum. For nonzero values of XMIN, XMAX, YMIN, and YMAX the plot will be distorted accordingly. WIDTH is the maximum dimension across the plotting drum for the plotted elements when XMIN, XMAX, YMIN, and YMAX are zero. A poor choice of XMIN, XMAX, YMIN, and YMAX may cause WIDTH to be significantly different from the expected width.

The value of NEON determines which nodes are numbered according to the formula

$$\text{number of labeled node} = 1 + K/\text{NEON} \quad (\text{NEON} \neq 0)$$

$$\text{where } K = 1, 2, 3, \dots, \text{NNP.}$$

No nodes are numbered if NEON = 0. Element numbering is determined in the same manner with NEOE. Element numbers are underlined.

Elementwise stress contour value calculations provide stress contours in the critical, refined mesh areas. For ICOVAL = 0 or 2, the elemental stresses are first put in ascending order in array X. The stress contour values 1 through NCONT-1 are calculated with the equations

$$K = \text{NEL}/\text{NCONT}$$

$$\text{AVE}(I) = (X(I+L)+X(I+1+L)+\dots+X(I+K+L))/K$$

where $L = K*(M-1)$ for $M = 1,2,3,\dots,\text{NCONT}-1$.

The last stress contour value is the average of the stresses at the remaining elements.

Stress contour values of constant stress increments for $\text{ICOVAL} = 2$ are generated with the equations

$$\text{DX} = (X(\text{NEL})-X(1))/(\text{NCONT}+2)$$

$$\text{AVE}(I) = X(1)+\text{DX}*I \text{ for } I = 1,2,3,\dots,\text{NCONT}.$$

The stress normalization cards determine a normalizing σ_x , σ_y , or τ_{xy} stress value from the stresses on one or several elements weighted by FACT . For example, the records

1	2.	1	3	6	8	10
2	1.	11	21			
-1	.5	17	18	35	42	56
0						

would cause the $(\tau_{xy})_{\text{nom}}$ (for $\text{ITAUXY} = 2$) stress value of the indicated element numbers to be weighted as follows

$$A = (\sigma_3+\sigma_4+\sigma_5+\sigma_6+\sigma_7+\sigma_8+\sigma_9+\sigma_{10})/2.$$

$$B = (\sigma_{11}+\sigma_{13}+\sigma_{15}+\sigma_{17}+\sigma_{19}+\sigma_{21})/1.$$

$$C = (\sigma_{17}+\sigma_{18}+\sigma_{35}+\sigma_{42}+\sigma_{56})/0.5$$

$$\text{AVE}(4) = (\tau_{xy})_{\text{nom}} = (A+B+C)/18.,$$

where σ_i are τ_{xy} stresses of the i^{th} element.

If neither ISIGX, ISIGY, nor ITAUXY are equal to 2, these cards are not included. Element numbers on individual cards must be in ascending order.

APPENDIX B
PROGRAM LISTING

- B.1 THE FINITE ELEMENT PROGRAM
- B.2 THE MESH GENERATION PROGRAM
- B.3 THE PLOTTING PROGRAM

Listings of these programs are available upon request.

APPENDIX C.
MATERIAL PROPERTIES

TABLE C. MATERIAL PROPERTIES

Material	E_{11} (msi)	E_{22} (msi)	ν_{12}	G_{12} (msi)	α_1 (μ in/in $^{\circ}$ F)	α_2 (μ in/in $^{\circ}$ F)
Graphite-epoxy	18.5	0.7	0.21	0.83	----	----
Thorne1 50/E-798	19.6	1.2	0.30	0.59	----	----
Graphite-polyimide	17.7	0.99	0.33	0.71	0.19	21.0
Steel	29.0	29.0	0.32	11.0	9.60	9.60

BEST SELLERS

Product Liability: Industry Study, Volumes I and II
PB-265 542/PSK 886 p PC\$24.00/MF\$3.00

An Atlas of Radiation Histopathology
TID-26676/PSK 234 p PC\$7.60/MF\$3.00

**The Medical School Admissions Process. A Review
of the Literature, 1955-76**
PB-263 962/PSK 193 p PC\$9.00/MF\$3.00

Integrated Energy Vocabulary
PB-259 000/PSK 459 p PC\$22.50/MF\$22.50

**Nuclear Air Cleaning Handbook. Design, Construc-
tion, and Testing of High-Efficiency Air Cleaning
Systems for Nuclear Application**
ERDA-76/21/PSK 300 p PC\$9.75/MF\$3.00

**Evaluation of the Air-To-Air Heat Pump for
Residential Space Conditioning**
PB-255 652/PSK 293 p PC\$11.00/MF\$3.00

**Federal Information Processing Standards Register:
Guidelines for Documentation of Computer
Programs and Automated Data Systems. Category:
Software. Subcategory: Documentation**
FIPS-PUB38/PSK 55 p PC\$5.25/MF\$3.00

**Life Cycle Costing Emphasizing Energy Conserva-
tion: Guidelines for Investment Analysis**
ERDA-76/130/PSK 117 p PC\$6.50/MF\$3.00

**Analysis of Projected Vs. Actual Costs for Nuclear
and Coal-Fired Power Plants**
FE-2453-2/PSK 38 p PC\$4.50/MF\$3.00

Quality Criteria for Water
PB-263 943/PSK 537 p PC\$15.50/MF\$3.00

**Passive Solar Heating and Cooling Conference and
Workshop Proceedings May 18-19, 1976,
University of New Mexico, Albuquerque, New
Mexico**
LA-6637-C/PSK 352 p PC\$12.50/MF\$3.00

Predicting the Performance of Solar Energy Systems
AD-A035 608/PSK 45 p PC\$4.50/MF\$3.00

NIOSH Analysis Methods for Set J
PB-263 959/PSK 128 p PC\$7.25/MF\$3.00

**Flat-Plate Solar Collector Handbook: A Survey of
Principles, Technical Data and Evaluation Results**
UCID-17086/PSK 96 p PC\$6.00/MF\$3.00

Coal Preparation Environmental Engineering Manual
PB-262 716/PSK 729 p PC\$21.50/MF\$3.00



Administration

Development of Executive Success
Theodore E. Elsasser.
Naval Postgraduate School Monterey Calif Sep 76, 187p
AD-A035 839/0PSK PC\$9.00/MF\$3.00

Behavior and Society

Interagency Task Force on Product Liability. Insurance Study
McKinsey and Co., Inc., New York. Jan 77, 263p
PB-263 600/9PSK PC\$10.75/MF\$3.00

Biomedical Technology and Engineering

**Economical Multifactor Designs for Human Factors
Engineering Experiments**
Charles W. Simon.
Hughes Aircraft Co Culver City Calif Engineering Equipment
Div Jun 73, 190p
AD-A035 108/0PSK PC\$9.00/MF\$3.00

Building Technology

**Criteria for Selection and Design of Residential Slabs-on-
Ground**
National Research Council, Washington, D.C. Building
Research Advisory Board. 1968, 303p
PB-261 551/6PSK PC\$11.75/MF\$3.00

Business and Economics

Interagency Task Force on Product Liability Legal Study
Research Group, Inc., Charlottesville, Va. Jan 77, 1274p in
7v
PB-263 601/7PSK PC\$34.00/MF\$3.00

Chemistry

Research Program on Hazard Priority Ranking of Manufactured Chemicals (Chemicals 21-40)

S. L. Brown, F. Y. Chan, J. L. Jones, D. H. Liu, and K. E. McCaleb.

Stanford Research Inst., Menlo Park, Calif. Apr 75, 195p
PB-263 162/0PSK PC\$9.00/MF\$3.00

Research Program on Hazard Priority Ranking of Manufactured Chemicals (Chemicals 41-60)

S. L. Brown, F. Y. Chan, J. L. Jones, D. H. Liu, and K. E. McCaleb.

Stanford Research Inst., Menlo Park, Calif. Apr 75, 191p
PB-263 163/8PSK PC\$9.00/MF\$3.00

Research Program on Hazard Priority Ranking of Manufactured Chemicals (Chemicals 61-79)

S. L. Brown, F. Y. Chan, J. L. Jones, D. H. Liu, and K. E. McCaleb.

Stanford Research Inst., Menlo Park, Calif. Apr 75, 198p
PB-263 164/6PSK PC\$9.00/MF\$3.00

Civil Engineering

Asphalt Concrete Overlays of Flexible Pavements. Volume 2. Design Procedures

Austin Research Engineers, Inc., Tex. Jun 75, 96p
PB-263 433/5PSK PC\$6.00/MF\$3.00

Communication

Problems of Space and Terrestrial Microwave Propagation

W. Riedler, and W. Lothaller.

European Space Agency, Paris (France). May 76, 286p
Partly in English and French.

N77-13238/9PSK PC\$11.00/MF\$3.00

Modulation Studies for Direct Satellite Communication of Voice Signals

Hiroshi Akima.

Office of Telecommunications, Boulder, Colo. Inst. for Telecommunication Sciences. Dec 76, 60p

PB-263 888/0PSK PC\$5.25/MF\$3.00

Computers

Windows, Harmonic Analysis and the Discrete Fourier Transform

Fredric J. Harris.

Naval Undersea Center San Diego Calif Sep 76, 70p

AD-A034 956/3PSK PC\$5.25/MF\$3.00

A Semi-Fast Fourier Transform Algorithm Over $GF(2)$ to the m th power)

Dilip V. Sarwate.

Illinois Univ At Urbana-Champaign Coordinated Science Lab Sep 76, 26p

AD-A034 982/9PSK PC\$4.50/MF\$3.00

Test Procedures for Multics Security Enhancements

M. Gasser, S. R. Ames, Jr., and L. J. Chmura.

Mitre Corp Bedford Mass Dec 76, 331p

AD-A034 986/0PSK PC\$12.00/MF\$3.00

Software Visibility for the Program Manager

Alan J. Driscoll.

Defense Systems Management School Fort Belvoir Va Nov 76, 57p

AD-A035 164/3PSK PC\$5.25/MF\$3.00

The Architecture of a Database Computer. Part II. The Design of Structure Memory and its Related Processors

David K. Hsiao, and Krishnamurthi Kannan.

Ohio State Univ Columbus Computer and Information Science Research Center Oct 76, 113p

AD-A035 178/3PSK PC\$6.50/MF\$3.00

Transmission Control Protocol Specification

Jonathan B. Postel, Larry L. Garlick, and Raphael Rom.

Stanford Research Inst Menlo Park Calif Augmentation Research Center Jul 76, 183p

AD-A035 337/5PSK PC\$9.00/MF\$3.00

Terminal-to-Host Protocol Specification

Jonathan B. Postel, Larry L. Garlick, and Raphael Rom.

Stanford Research Inst Menlo Park Calif Augmentation Research Center Jul 76, 178p

AD-A035 338/3PSK PC\$9.00/MF\$3.00

Commercial Data Management Processor Study

J. Cullinane, R. Goldman, T. Meurer, and R. Nawara.

Cullinane Corp Wellesley Mass Dec 75, 84p

AD-A035 790/5PSK PC\$6.00/MF\$3.00

Some Considerations and Models for the Distribution of a Data Base

Joyce Elam, and Joel Stutz.

Texas Univ At Austin Center for Cybernetic Studies May 76, 32p

AD-A035 923/2PSK PC\$4.50/MF\$3.00

Software Acquisition Management Guidebook: Statement of Work Preparation

J. B. Glone, and W. R. Bjerstedt.

Mitre Corp Bedford Mass Jan 77, 104p

AD-A035 924/0PSK PC\$6.50/MF\$3.00

Data Base Management Study

Teledyne Brown Engineering, Huntsville, Ala. Advanced Projects Div. May 76, 62p

N77-15671/9PSK PC\$5.25/MF\$3.00

Computer Science and Technology: Foreign and Domestic Accomplishments in Magnetic Bubble Device Technology

Robert B. J. Warner, and Peter J. Calomeris.

National Bureau of Standards, Washington, D.C. Inst. for Computer Sciences and Technology. Jan 77, 54p

PB-263 123/2PSK PC\$5.25/MF\$3.00

Accessing Individual Records from Personal Data Files Using Non-Unique Identifiers

Gwendolyn B. Moore, John L. Kuhns, Jeffrey L. Trefftz, and Christine A. Montgomery.

Operating Systems, Inc., Woodland, Calif. Feb 77, 206p

PB-263 176/0PSK PC\$9.25/MF\$3.00

Technical Profile of Seven Data Element Dictionary/Directory Systems

Belkis Leong-Hong, and Beatrice Marron.
National Bureau of Standards, Washington, D.C. Feb 77,
49p
PB-263 177/8PSK PC\$4.50/MF\$3.00

A Contribution to Computer Typesetting Techniques, 9 track ASCII

Robert C. Thompson.
National Bureau of Standards, Washington, D.C. Office of
Standard Reference Data. Apr 76, mag tape Source tape is
in ASCII character set. Character set restricts preparation to
9 track one-half inch tape only. Identify recording mode by
specifying density only. Call NTIS Computer Products, if you
have questions. Price includes documentation, PB-251 845.
PB-263 925/0PSK Mag Tape \$300.00; Foreign \$480.00

Electrotechnology

Lightning, Surge, and Transient Protection (A Bibliography with Abstracts)

William E. Reed.
National Technical Information Service, Springfield, Va. Mar
77, 103p
NTIS/PS-77/0099/0PSK PC\$28.00/MF\$25.00

Energy

Site Energy Handbook. Volume I. Methodology for Energy Survey and Appraisal

Energy Research and Development Administration,
Washington, D.C. Div. of Solar Energy. Oct 76, 172p
ERDA-76-131-1PSK PC\$8.00/MF\$3.00

Preparation of a Coal Conversion Systems Technical Data Book. Final Report, October 31, 1974--April 30, 1976

Institute of Gas Technology, Chicago, Ill. 1976, 620p
FE-1730-21/PSK PC\$16.25/MF\$3.00

Diesel Exhaust Emissions (Citations from the NTIS Data Base)

Edward J. Lehmann.
National Technical Information Service, Springfield, Va. Mar
77, 145p
NTIS/PS-77/0104/8PSK PC\$28.00/MF\$25.00

Natural Gas Deregulation Analysis

John Neri, David Nissen, Mark Rodekoher, James Sweeney,
and William Hogan.
Federal Energy Administration, Washington, D.C. Jan 76,
63p
PB-261 599/5PSK PC\$5.25/MF\$3.00

EPA Program Conference Report Fuel Cleaning Program: Coal

Z. S. Altschuler, R. E. Hucko, G. A. Isaacs, P. S. Jacobson,
and J. D. Kilgore.
Environmental Protection Agency, Washington, D.C. Office of
Energy, Minerals and Industry. Oct 76, 127p
PB-262 876/6PSK PC\$7.25/MF\$3.00

Methanol as an Automotive Fuel: A Summary of Research in the M.I.T. Energy Laboratory

Richard G. Donnelly, John B. Heywood, Jules LoRusso,
Frank O'Brien, and Thomas B. Reed.

TAPE OF THE MONTH

COBOL COMPILER VALIDATION SYSTEM

Validates COBOL compilers and ensures their conformance to the Federal Standard prescribed in FIPS PUB 21-1. Consists of:

Audit Routines—Includes tests and procedures to indicate test results.

Executive Routine—Provides a method for resolving implementor names, updating source programs, generating operating system control cards, and compiling audit routines in a particular environment.

Order AD/A-036 173/PPP. \$550 North American continent only. For more information on this and other computer products, call or write the NTIS Computer Products office, (703) 557-4763, 5285 Port Royal Road, Springfield, VA 22161.

Massachusetts Inst. of Tech., Cambridge, Energy Lab. Apr
76, 57p

PB-262 980/6PSK PC\$5.25/MF\$3.00

Energy Management Guide for Light Industry and Commerce. EPIC Energy Management Series

W. J. Kelnhofer, and L. A. Wood.
National Bureau of Standards, Washington, D.C. Office of
Energy Conservation. Dec 76, 31p
PB-263 121/6PSK PC\$4.50/MF\$3.00

Chemical Kinetics of the Gas Phase Combustion of Fuels (A Bibliography on the Rates and Mechanisms of Oxidation of Aliphatic C1 to C10 Hydrocarbons and of Their Oxygenated Derivatives

Francis Westley.
National Bureau of Standards, Washington, D.C. Chemical
Kinetics Information Center. Oct 76, 142p
PB-263 122/4PSK PC\$7.25/MF\$3.00

Assessment of a Single-Family Residence Solar Heating System in a Suburban Development Setting. Project Phoenix

J. D. Phillips.
Colorado Springs Dept. of Public Utilities, Colo. Jul 76,
180p
PB-263 192/7PSK PC\$9.00/MF\$3.00

Barriers to the Use of Wind Energy Machines: The Present Legal/Regulatory Regime and a Preliminary Assessment of Some Legal/Political/Societal Problems

Rita Falk Taubenfeld, and Howard J. Taubenfeld.
Societal Analytics Inst., Inc., Dallas, Tex. Jul 76, 159p
PB-263 576/1PSK PC\$8.00/MF\$3.00

The Correlation of Peak Ground Acceleration Amplitude with Seismic Intensity and Other Physical Parameters
L. J. O'Brien, J. R. Murphy, and J. A. Lahoud.
Computer Sciences Corp., Falls Church, Va. Mar 77, 96p
PB-263 972/2PSK PC\$6.00/MF\$3.00

Cooling Tower Energy Studies - Conservation Techniques Applicable to Existing Installations Plus Comparative Economics and Energy Requirements of Mechanical and Natural Draft Towers
Gordian Associates, Inc., New York. Feb 77, 70p
PB-264 028/2PSK PC\$5.25/MF\$3.00

Environment

Synthetic Fuels from Municipal, Industrial, and Agricultural Wastes (Citations from the NTIS Data Base)
Audrey S. Hundemann, and Edward J. Lehmann.
National Technical Information Service, Springfield, Va. Mar 77, 88p
NTIS/PS-77/0112/1PSK PC\$28.00/MF\$25.00

Dispersion Equation Solutions by Calculator. A Guide for Air Pollution Engineers and Scientists
Richard A. Porter.
Texas Air Control Board, Austin. Nov 75, 69p
PB-262 135/7PSK PC\$5.25/MF\$3.00

The Effect of Gypsum on Lime-Fly Ash Compositions: Literature Review and Annotated Bibliography
L. M. Smith, and A. Kawam.
Gillette Research Inst., Inc., Rockville, Md. May 76, 37p
PB-262 531/7PSK PC\$4.50/MF\$3.00

Effect of a Flyash Conditioning Agent on Power Plant Emissions
L. E. Sparks.
Industrial Environmental Research Lab., Research Triangle Park, N.C. Particulate Technology Branch. Oct 76, 136p
PB-262 602/6PSK PC\$7.25/MF\$3.00

Proceedings: Symposium on Flue Gas Desulfurization-New Orleans, March 1976. Volume II
R. D. Stern, W. H. Ponder, and R. C. Christian.
Industrial Environmental Research Lab., Research Triangle Park, N.C. May 76, 453p
PB-262 722/2PSK PC\$14.50/MF\$3.00

PCB Emissions from Stationary Sources: A Theoretical Study
Herman Knieriem, Jr.
Monsanto Research Corp., Dayton, Ohio. Dayton Lab. Oct 76, 43p
PB-262 850/1PSK PC\$4.50/MF\$3.00

Acute Toxicity of Selected Organic Compounds to Fathead Minnows
Vincent R. Mattson, John W. Arthur, and Charles T. Walbridge.
Environmental Research Lab., Duluth, Minn. Oct 76, 20p
PB-262 897/2PSK PC\$4.00/MF\$3.00

Hazardous Waste Management Facilities in the United States - 1977
Matthew A. Straus.
Environmental Protection Agency, Washington, D.C. Office

of Solid Waste Management Programs. Jan 77, 66p
PB-262 917/8PSK PC\$5.25/MF\$3.00

Evaluation of the General Motors' Double Alkali SO₂ Control System
Edward Interest.
Little (Arthur D.), Inc., Cambridge, Mass. Jan 77, 99p
PB-263 469/9PSK PC\$6.00/MF\$3.00

Tall Stacks and the Atmospheric Environment
Jeremy M. Hales.
Battelle Pacific Northwest Labs., Richland, Wash. Mar 76, 178p
PB-263 561/3PSK PC\$9.00/MF\$3.00

Procedures for Cascade Impactor Calibration and Operation in Process Streams
D. Bruce Harris.
Industrial Environmental Research Lab., Research Triangle Park, N.C. Jan 77, 123p
PB-263 623/1PSK PC\$6.50/MF\$3.00

Public Comments and Task Force Responses Regarding the Environmental Survey of the Reprocessing and Waste Management Portions of the LWR Fuel Cycle. (NUREG-0116)
Nuclear Regulatory Commission, Washington, D.C. Office of Nuclear Material Safety and Safeguards. Mar 77, 427p
PB-264 035/7PSK PC\$14.00/MF\$3.00

Medical Screening Programs for Infants

The proceedings of a 1972 symposium on laboratory screening techniques for newborn and selected high-risk infants are now available from NTIS. The symposium was jointly sponsored by the U.S. and Poland and was attended by representatives of 23 countries—scientists who developed original screening techniques, people from diagnostic centers working on automation of screening methods, and experienced practitioners. Participants shared the findings of new or modified techniques, hoping to improve the effectiveness and stimulate the growth of laboratory and mass screening programs for newborn infants. Subject matter addressed covered laboratory screening techniques applied to dried blood spots, capillary blood, urine samples, and other biological specimens. Participants also discussed the organization and administrative aspects of laboratory and mass screening programs. **Proceedings of the International Symposium on Laboratory Screening Techniques for Inborn Errors of Metabolism in Newborn and Selected High-Risk Infants** lists the names and addresses of all symposium participants and offers a convenient subject index. Order the **Proceedings**, PB-263 027-T/PSK, at \$11.00 per paper copy and \$3.00 per microfiche copy from the National Technical Information Service, 5285 Port Royal Road, Springfield, Va. 22161.



Speed Delivery—Order by Number



Here's how you can get NTIService for YOU!

NTIS brings you the choice new titles of the 5000 announced each month. Each issue of this catalog lets you review a selection of the newest titles in your particular area of interest. This convenient self-mail reply coupon makes it so easy to obtain the reports you select.

You can also speed your order, minimize accounting, record tax-deductible expenses, and reduce chance of error by opening an NTIS Deposit Account. If you haven't already joined the 10,000 satisfied NTIS Deposit Account customers, send for your application today. Just check the box on this order form and your application will be sent by return mail.

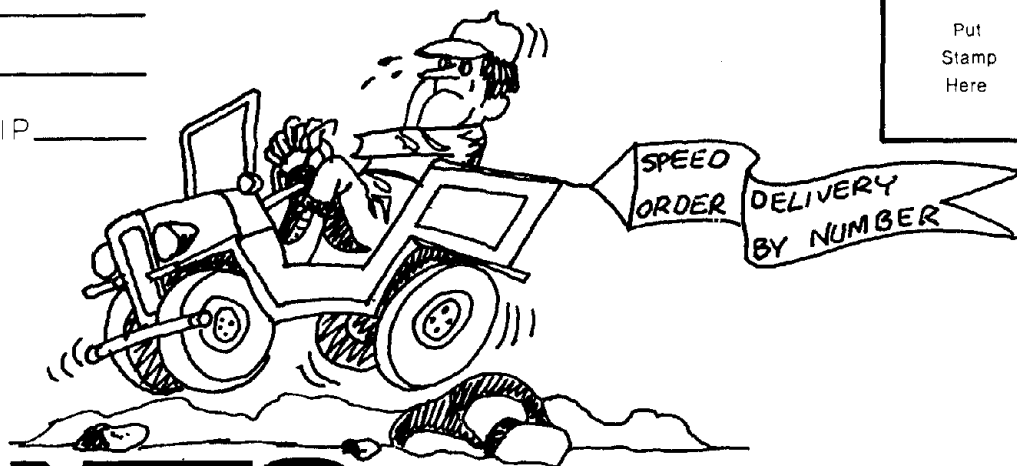
The *Monthly Selections* you see here are just a sampling of the new titles announced by NTIS each month in the *Weekly Government Abstracts*. The WGA newsletters provide a concise overview of important information, newly available, in 26 different fields of interest. Order the free WGA brochure to learn how to keep-up-to-date with the latest Government-sponsored research in your field of interest.

NTIS offers you more than 100 different products and services to meet your needs. If you haven't yet had the opportunity, you can use this order form to send for the NTIS general catalog. It's your pocket-sized guide to the specialized products and services developed to answer your information needs.

You cannot buy . . . or subscribe to . . . these *Monthly Selections*. NTIS supplies this free service to you. It's our way of saying "Thank You."

ZIP _____

Put
Stamp
Here



NTIS

**National Technical Information Service
U.S. DEPARTMENT OF COMMERCE**

Springfield, Va. 22161

Health Planning

Reducing Excess Hospital Capacity

Walter McClure.

InterStudy, Excelsior, Minn. Oct 76, 236p

HRP-0015199/3PSK PC\$9.50/MF\$3.00

Library and Information Sciences

Development of a Model Library Microform Center

Philip J. Gary.

Gary (Philip J.) and Associates, Marina del Rey, Calif.

Micrographic Systems Consulting Services. Aug 76, 56p

PB-263 586/0PSK PC\$5.25/MF\$3.00

Materials Sciences

Detection of Tightly Closed Flaws by Nondestructive Testing (NDT) Methods in Steel and Titanium

W. D. Rummel, R. A. Rathke, P. H. Todd, Jr., T. L. Tedrow, and S. J. Mullen.

Martin Marietta Aerospace, Denver, Colo. Sep 76, 109p

N77-15133/0PSK PC\$6.50/MF\$3.00

Encapsulation by Entrapment

Baruch S. Shasha, William M. Doane, and Charles R. Russell.

Department of Agriculture, Washington, D.C. Filed 19 Oct

76, 42p This Government-owned invention available for U.S. licensing and, possibly, for foreign licensing. Copy of application available NTIS.

PAT-APPL-733 968/PSK PC\$4.50/MF\$3.00

The Electroslag Melting Process

R. H. Nafziger.

Bureau of Mines, Albany, Oreg. Albany Metallurgy Research Center. 1976, 234p

PB-263 219/8PSK PC\$9.50/MF\$3.00

Medicine and Biology

Technical Notes: MEDLARS Indexing Instructions:

Supplements V. Enzyme Key and VI. Fungus Key

Elizabeth J. VanLenten.

National Library of Medicine, Bethesda, Md. Feb 77, 34p

PB-263 335/2PSK PC\$4.50/MF\$3.00

Ocean Technology and Engineering

Standardized Stern Project. Volume I

Charles H. Gross, Jr.

Henry (J. J.) Co., Inc., New York. Sep 76, 59p

PB-262 926/9PSK PC\$5.25/MF\$3.00

Standardized Stern Project. Volume II. Executive Summary

Charles H. Gross, Jr.

Henry (J. J.) Co., Inc., New York. Sep 76, 10p

PB-262 927/7PSK PC\$4.00/MF\$3.00

INVENTION OF THE MONTH

New Improved Method for Synthesis of Methotrexate

Consists of three process improvements in the production of an anticancer agent, antifolate methotrexate—

- Selection of a PH value that minimizes the formulation of pteridines
- Elimination of the sodium acetate or acetate buffer previously used
- Conversion of the sulfite acid addition salt to hydrochloride salt

Results . . . an easier process at about half the current cost . . . with better yields and purer products.

For more information on this and other Government-owned technology, contact George Kudravetz at (703) 557-4733 or write him at NTIS, 5285 Port Royal Road, Springfield, VA 22161.

Transportation

Transportation System Safety Methodology

M. Horodniceanu, F. J. Cantilli, M. Shooman, and I. J. Pignataro.

Polytechnic Inst. of New York, Brooklyn. Nov 76, 147p

PB-262 793/3PSK PC\$7.25/MF\$3.00

Impact of a Suburban Rapid Transit Line of Fuel Consumption and Cost for the Journey-To-Work. Analysis of the Philadelphia-Lindenwold High-Speed Line

David E. Boyce, Khanh Nguyen, Thierry Noyelle, and Kent Webb.

Wharton School of Finance and Commerce, Philadelphia, Pa. Dept. of Regional Science. Dec 75, 74p

PB-263 048/1PSK PC\$5.25/MF\$3.00

Carpool Incentives: Evaluation of Operational Experience

Cambridge Systematics, Inc., Mass. Mar 76, 176p

PB-263 050/7PSK PC\$9.00/MF\$3.00

Aesthetic and Environmental Considerations in the Design of Elevated Transportation Structures

M. L. Silver, and L. S. Bell.

Illinois Univ. at Chicago Circle. Dept. of Materials Engineering. Jun 75, 134p

PB-263 158/8PSK PC\$7.25/MF\$3.00

Federal Support for the Development of Alternative Automotive Power Systems: The General Issue and the Stirling, Diesel, and Electric Cases

Lawrence H. Linden, John B. Heywood, H. D. Jacoby, and Howard Margolis.

Massachusetts Inst. of Tech., Cambridge. Energy Lab. Mar 76, 406p

PB-263 523/3PSK PC\$13.25/MF\$3.00

**National Technical Information Service
U.S. DEPARTMENT OF COMMERCE**

Springfield, Virginia 22161

OFFICIAL BUSINESS

Penalty for Private Use, \$300

POSTAGE AND FEES PAID
U.S. DEPARTMENT OF COMMERCE
COM-211

THIRD CLASS BULK RATE



CUSTOMER MEMO

Dear Friend,

Are you looking for a great gift idea or a special addition to your own library? Send now for the **History of the Star Spangled Banner from 1814 to the Present**. Young and old will enjoy more than 500 pages of fascinating details on the anthem's publication as a poem, adaptation to music, the development of its popularity, inspirational meaning, and more. You can now purchase this attractive, hard cover report written in the spirit of our nation's heritage for just \$6.75.

NTIS has slashed the price from \$13.50 to \$6.75 for a limited time only. Don't let this opportunity pass you by. Act now. Order PB-196 294/PSK for \$6.75.

Ride the Subway to NTIS

Now that the Washington Metrorail System has been expanded, NTIS customers will benefit from more convenient access to our Downtown Bookstore. Located just two short blocks from Metro Center—the heart of the subway system—the Bookstore is just minutes away from many points in and around the city.

Whether you're an out-of-towner traveling the Blue Line from National Airport or Union Station . . . or a local customer riding the Red Line across

town, be sure to visit the NTIS Bookstore for those last-minute orders or rush pick-ups.

Use Code-A-Phone After 5

Another new customer convenience recently added by NTIS is code-a-phone . . . enabling you to place orders, leave messages, or ask questions even after our regular Bookstore hours are over. The very next day of business, an NTIS representative will return your call with news about your order or with an answer to your question. Keep the code-a-phone number—(202) 724-3383—in a handy place at your home and office, and the next time you need something, give us a call.

Sincerely,

Risë L. Burggraff
Editor

P.S. The Premium Service toll-free number was incorrectly announced in an earlier catalog. Please note the following numbers for Premium Service orders. (800) 325-6000; in Missouri, (800) 342-6700.

Parkinson's Disease and Related Disorders—

Worldwide References Available

The National Institute of Neurological and Communicative Disorders and Strokes publication, **Parkinson's Disease and Related Disorders: Citations from the Literature**, is now available by annual subscription from NTIS. Issued monthly, the bibliography provides current, selected, systematically categorized citations from this sizeable body of worldwide biomedical literature.

The National Library of Medicine's MEDLARS program is used for selecting appropriate items. Citations to "core" documents—those primarily clinical in approach and those connecting research directly to a specific disorder are included. These detail Parkinson's disease, Huntington's and Sydenham's choreas, dystonia musculorum deformans, hepatolenticular degeneration, multiple tics, and torticollis.

An annual subscription to **Parkinson's Disease and Related Disorders**, costs \$30. To help keep your specialized medical knowledge current, send your order to National Technical Information Service, 5285 Port Royal Rd., Springfield, Va. 22161.